Probing the Structure and Reactivity of Gaseous Ions

A DISSERTATION
SUBMITTED TO THE FACULTY OF THE GRADUATE SCHOOL
OF THE UNIVERSITY OF MINNESOTA
BY

Matthew Michael Meyer

IN PARTIAL FULFILLMENT OF THE REQUIREMENTS
FOR THE DEGREE OF
DOCTOR OF PHILOSOPHY

Professor Steven R. Kass

Febuary 2010

Acknowledgements

I want to express my gratitude to my advisor Dr. Steven Kass for the opportunity to work with him during my time at Minnesota. I am grateful for his willingness to share not only his vast knowledge of chemistry, but his approach to addressing problems. I also would like to acknowledge professors, John Anthony and Mark Meier for their mentorship while I was at the University of Kentucky that led me to a career in chemistry.

Due to the broad nature of the research contained herein I am grateful for the contributions of the many collaborators I had the opportunity to work with while at Minnesota. In particular, I would like to thank Professors Richard O'Hair, Steven Blanksby, and Mark Johnson for their wiliness to allow me to spend time in their labs. During my course of studies I have also had the opportunities to interacts with a variety of other scientist that have contributed greatly to my development and completing this document, including Dr. Dana Reed, Dr. Mark Juhasz, Dr. Erin Speetzen, Dr. Nicole Eyet and Mr. Kris Murphy.

I am also grateful for the support of my brother and sister through out this process. Lastly, I want to expresses gratitude to my parents for their support in all my pursuits and encouraging my incessant asking why probably since I could talk.

Abstract

Studying ions in the gas phase provides the opportunity to observe their intrinsic structure and reactivity without extraneous perturbations such as solvent effects, aggregation or counterion interactions. This work utilizes various experimental techniques including ion-molecule reactions and IR-action spectroscopy inside an ion cyclotron resonance mass spectrometer, in combination with computational studies, to probe both structures and thermochemical properties. Systems and chemical problems addressed herein include the conjugate bases of carborane superacids, thermodynamic properties of ClO_x and $HClO_x$, lithium acetate enolateanion, lithium acetylide anion, and the development of IR-action spectroscopy at Minnesota.

Table of Contents

List of Tables

List of Figures

Chapter 1.

Investigating the Weak to Evaluate the Strong: An Experimental Determination of the Electron Binding Energy of Carborane Anions and the Gas Phase Acidity of Carborane Acids

Carborane acids are a new class of Lewis acid-free superacids notable for their "strong yet gentle" properties.[1,2] Qualitative measures of their acidity on the mesityl oxide $\Delta\delta$ ^{13}C NMR scale[3] and their anion basicity on the trioctyl-ammonium salt νNH infrared scale[4] place $H(CHB_{11}Cl_{11})$ as the current strongest isolable acid in condensed media.[5,6] DFT calculations support this ranking for the gas phase.[5,7,8] Herein, we address the problem of quantifying the gas-phase deprotonation enthalpy of carborane acids experimentally. We also measure the electron binding energy of the $CHB_{11}Cl_{11}^-$ conjugate base in order to probe the exceptional chemical inertness that accompanies its low basicity. Comparisons are made to the bis(nonafluorobutane-1-sulfonyl)imide ion, $(1\text{-}C_4F_9SO_2)_2N^-$, whose conjugate acid is currently the strongest gas phase acid to be determined experimentally.[9]

Five $CHB_{11}X_6Y_5^-$ carborane anions from the series X = Br, Cl, I and Y = H, Cl, CH_3 were readily generated in a Fourier transform mass spectrometer (FTMS) by electro-spray ionization of aqueous methanolic solutions of the corresponding cesium salts.[10] Each anion was allowed to react with a series of BrØnsted acids of known

strength including CF_3SO_3H (ΔH°_{acid} = 305.4 ± 2.2 kcal mol^{-1})[11] and $(1\text{-}C_4F_9SO_2)_2NH$ (ΔH°_{acid} = 291.1 ± 2.2 kcal mol^{-1}),[9] but no reactions were observed indicating that the proton affinities of all five anions are less than 291.1 ± 2.2 kcal mol^{-1}. These results indicate that the corresponding carborane acids are more acidic than $(1\text{-}C_4F_9SO_2)_2NH$, which is currently the strongest measured acid in the gas phase. To verify these bracketing results and rule out the possibility of a kinetic barrier which could preclude the observation of an exothermic proton transfer reaction, the reverse process between $H(CHB_{11}Cl_{11})$ and the $(1\text{-}C_4F_9SO_2)_2N^-$ anion was examined. The carborane acid was introduced into a FTMS with the aid of a solid probe inlet and was found to readily protonate $(1\text{-}C_4F_9SO_2)_2N^-$ (*m/z* 580) at 298 K to afford $CHB_{11}Cl_{11}^-$ (*m/z* 519). Some $1\text{-}C_4F_9SO_2NH^-$ (*m/z* 298) also was observed (Figure 1.2). Given that proton transfer is observed only in one direction, the lower basicity of the undecachloro carborane anion relative to $(1\text{-}C_4F_9SO_2)_2N^-$ must be of thermodynamic origin. This allows us to confidently assign $\Delta H^\circ_{acid}[H(CHB_{11}Cl_{11})] < 291.1 \pm 2.2$ kcal mol^{-1} which is consistent with B3LYP/6-311+G(d,p)[12] and G3(MP2)[13] predictions at 298 K of 237.6 and 238.3 kcal mol^{-1}, respectively. Protonation is calculated to occur on chlorine, which is in accord with the reported X-ray structure and IR spectrum of the acid.[14] (Figure 1.1)

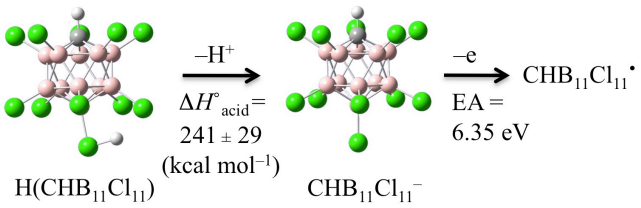

Figure 1.1. Deprotonation of $H(CHB_{11}Cl_{11})$.

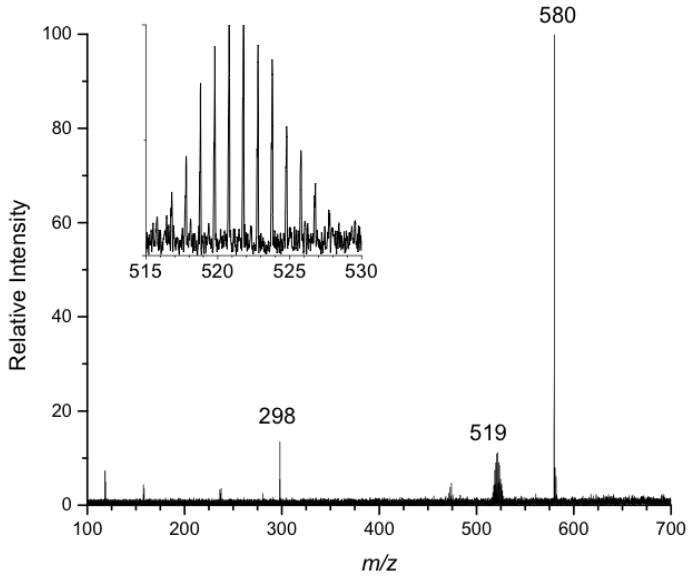

Figure 1.2. Mass spectrum of the reaction of $(1\text{-}C_4F_9SO_2)_2N^-$ (*m/z* 580) with $H(CHB_{11}Cl_{11})$. The inset is an expansion of the $CHB_{11}Cl_{11}^-$ anion (*m/z* 519) that reveals the complex isotopic envelope resulting from a species with 11 B and 11 Cl atoms.

In order to investigate both the basicity and the redox inertness of these remarkable anions, all five carborane anions were reacted with several reference electron transfer reagents with known electron affinities. No reactions were observed with nitrogen dioxide (NO_2, EA = 2.273 ± 0.005 eV), 2-chloroacrylonitrile (CH_2=C(Cl)CN, vertical detachment energy (VDE) = 4.50 eV), molybdenum hexafluoride (MoF_6, EA = 3.82 ± 0.19 eV) and rhenium hexafluoride (ReF_6, EA = >5.14 ± 0.48 eV).[11] These results indicate that the electron binding energies of all five carborane anions are > 5.14 ± 0.48 eV. The value for $CHB_{11}Cl_{11}^-$ was further refined by obtaining its photoelectron spectrum at 157 nm at 70 K (Figure 2).[15] A broad band with a maximum at 7.0 eV was observed and an adiabatic detachment energy (ADE) of 6.35

± 0.02 eV was measured.[16] This is a remarkably large value for a non-solvated, even-electron anion, and is more than 1 eV greater than that for I^-, NO_3^-, $H_2PO_4^-$, FSO_3^-, HSO_4^-, $PhSO_3^-$, and ClO_4^- (EBE = 3.059036 ± 0.000044, 3.937 ± 0.014, 4.57 ± 0.01, 4.71 ± 0.19, and 4.75 ± 0.10, 5.0 ± 0.2, and 5.25 ± 0.1 eV, respectively).[11] It is well reproduced by B3LYP/6-311+G(d,p) and G3(MP2) calculations which give predicted electron affinities of 6.01 and 6.36 eV, respectively. This quantity provides another measure of the remarkable stability of carborane anions and is a direct consequence of σ aromaticity in the delocalized bonding of the CB_{11} cage.[17] Direct equilibrium acidity determinations require a known reference acid within a few kcal mol^{-1} of the compound of interest. However, no such species is available for $H(CHB_{11}Cl_{11})$ so only an upper limit for ΔH°_{acid} is obtain-able. On the other hand, the availability of the electron affinity of $CHB_{11}Cl_{11}^{\cdot}$ makes it possible to evaluate the thermodynamic cycle indicated by Eq. 1.1.

$$\mathbf{\Delta H^\circ_{acid}[H(CHB_{11}Cl_{11})] = BDE[H(CHB_{11}Cl_{11})] + IE(H^{\cdot}) - EA[CHB_{11}Cl_{11}^{\cdot}]} \quad \mathbf{(1.1)}$$

The ionization energy (IE) of hydrogen atom (313.6 kcal mol^{-1}) is well known. If the H–carborane bond dissociation energy (BDE) of the acid were known then $\Delta H^\circ_{acid}[H(CHB_{11}Cl_{11})]$ would be directly available. While the BDE of the carborane acid is unknown, one can reasonably assume that the value is less than that for HCl (BDE < 103 kcal mol^{-1}) because the carborane radical is stabilized by delocalization.[11] A lower limit of 45 kcal mol^{-1} can be assigned by analogy to *tert*-butyl peroxide[18] and the observation that the carborane acid is thermally stable to at least 230 °C.[14] The

resulting 45 – 103 kcal mol^{-1} range for the bond dissociation energy is consistent with the B3LYP/6-311+G(d,p) and G3(MP2) predictions of 62.5 and 70.0 kcal mol^{-1}, and leads to a deprotonation enthalpy for the carborane acid between 212 and 270 kcal mol^{-1} (i.e., $\Delta H^{\circ}_{acid}[H(CHB_{11}Cl_{11})] = 241 \pm 29$ kcal mol^{-1}). Though imprecise, this value is in excellent accord with B3LYP/6-311+G(d,p) and G3(MP2) predictions of 237.6[5,8] and 238.3 kcal mol^{-1}, and clearly indicates that $H(CHB_{11}Cl_{11})$ is the strongest gas-phase acid measured to date. It also bridges the gas-phase acidity and basicity scales for the first time.[19]

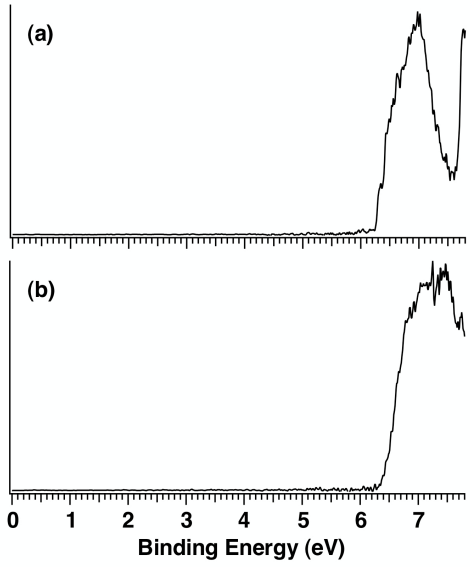

Figure 1.3. Photoelectron spectrum of $CHB_{11}Cl_{11}^-$ (a) and $(1\text{-}C_4F_9SO_2)_2N^-$ (b) at 157 nm (7.866 eV) at 70 K.

The record-breaking carborane deprotonation energy can be accounted for by the extremely high electron binding energy (stability) of its conjugate base, but is this the reason that carborane acids are such potent BrØnsted acids? To address this question, the photoelectron spectrum of the $(1\text{-}C_4F_9SO_2)_2N^-$ anion was obtained (Figure 2). The

spectrum is quite similar to that of $CHB_{11}Cl_{11}^-$ with a maximum at ~7.3 eV and an ADE of 6.5 ± 0.1eV.[15] These values are actually 0.2 – 0.3 eV larger than for the carborane anion even though $H(CHB_{11}Cl_{11})$ is predicted to be 47.2 kcal mol^{-1} more acidic than $(1\text{-}C_4F_9SO_2)_2NH$ (i.e., 238.3 (G3(MP2)) – 291.1 (expt)). Clearly, the stability of the anions as reflected by their ADEs does not account for why the carborane acid is more acidic than the bis(nonafluorobutane-1-sulfonyl)imide although it plays a major role in the high acidity of these compounds. The difference in the bond dissociation energies [BDE $(1\text{-}C_4F_9SO_2)_2N\text{–}H$ = 127.4 ± 3.2 kcal mol^{-1} (expt., this work) vs. $BDE(H\text{–}(CHB_{11}Cl_{11})$ = 70.0 kcal mol^{-1} (G3(MP2))] is the key to the greater acidity of the carborane. If one is to design even stronger BrØnsted acids, one will need to balance both the stability of the anion and the BDE of the acid.

Chapter 1. Experimental Methods

General: $(1\text{-}C_4F_9SO_2)_2NH$ was purchased from Wako chemical and used as obtained. $Cs(CHB_{11}Cl_{11})$, $Cs(CHB_{11}Br_6H_5)$, $Cs(CHB_{11}Cl_6H_5)$, $Cs(CHB_{11}I_6H_5)$, $Cs(CHB_{11}Br_6Me_5)$, and $H(CHB_{11}Cl_{11})$ were prepared as previously described in the literature.[10]

Gas-phase experiments: A dual cell model 2001 Finnigan Fourier transform mass spectrometry was used with a 3 T superconducting magnet and IonSpec (now Varian) electronics including the Omega 8.0 data system. Bis(nonafluorobutane-1-sulfonyl)imide was directly introduced into the analyzer cell of the mass spectrometer and electron ionization (7.5 eV) afforded $C_4F_9SO_2)_2N^-$ (*m/z* 580). This ion was cooled with a pulse of argon and transferred to the source cell where it was allowed to react with $H(CHB_{11}Cl_{11})$. The carborane acid is very sensitive to moisture, so it was placed in a sealed glass capillary which was ruptured against a gate valve in the solid probe at ~0.05 Torr and then was immediately introduced into the main vacuum chamber at $\sim10^{-9}$ Torr; the solid probe was also heated to 150˚ C. In addition, experiments were carried out with an IonSpec ESI FTMS also equipped with a 3 T magnet. Aqueous methanol solutions (30 mM, 3:1 (v/v) CH_3OH/H_2O) of the cesium salts of carborane anions were sprayed into the instrument, and the resulting carborane anions were isolated, cooled with a pulse of argon, and allowed to react with static pressures ($\sim10^{-9} - 10^{-7}$ Torr) of the desired reagents.

Photoelectron Spectroscopy: A 1 mM solution of $Cs(CHB_{11}Cl_{11})$ in 3:1 (v/v) CH_3OH/H_2O was sprayed to generate the $CHB_{11}Cl_{11}^-$ anion. The resulting ions were guided by a series of rf-only quadrupole devices and then bent 90˚ into a temperature-controlled Paul trap where they were accumulated and cooled to 70 K before being

pulsed into the extraction zone of a time-of-flight mass spectrometer.[15] The desired species were mass-selected and decelerated before being detached by a 157 nm (7.866 eV) F_2 excimer laser in the interaction zone of a magnetic-bottle photoelectron analyzer operated at a 20 Hz repetition rate with the ion beam on and off on alternating laser shots for background subtraction. Photoelectrons were collected at nearly 100% efficiency by the magnetic bottle and analyzed in a 5.2 m long electron flight tube. Time-of-flight photoelectron spectra were collected and converted to kinetic energy spectra calibrated with the known spectra of I^- and ClO_2^-. The electron binding energy spectrum reported herein was obtained by subtracting the kinetic energy spectrum from the detachment photon energy. The energy resolution ($\Delta E/E$) of the magnetic-bottle electron analyzer was 2% (i.e., 20 meV for 1 eV electrons).

Computations: All structures were fully optimized with the B3LYP density functional[12] and the 6-311+G(d,p) and aug-cc-pVDZ basis sets. In the latter case, single point energy calculations also were carried out with the aug-cc-pVTZ basis set. Vibrational frequencies were computed for each structure too to confirm that they are energy minima on the potential energy surface and to enable temperature corrections to 298 K. Unscaled frequencies were used for this purpose, and small vibrational modes which contribute more than 1/2(RT) to the thermal energy were replaced by 0.30 kcal mol^{-1}. G3(MP2) energies also were computed as described in the literature.[13] All of the resulting energetics are reported as enthalpies at 298 K in this work. The calculations were carried out using Gaussian 03[a] on workstations at the Minnesota Supercomputer Institute for Advanced Computational Research.

Chapter 2.

Experimental and Theoretical Gas-Phase Acidities, Bond Dissociation Energies, and Heats of Formation of $HClO_x$, x = 1 – 4.

Introduction

Chloric ($HClO_3$) and perchloric acids ($HClO_4$) have long histories going back to their discoveries by Claude-Louis Berthelot and Count Friedrich von Stadion in 1786 and 1815, respectively.[1] Both compounds along with their salts have been extensively studied and have a number of industrial uses ranging from the manufacture of air bags, batteries, and steel to applications in agriculture and medicine. They also have been utilized as potent oxidizers, propellants, and explosives. In addition, $HClO_4$ is a valuable analytical reagent for trace metal determinations.[2]

Further interest in $HClO_x$ and ClO_x, x = 1 – 4, was sparked by Rowland and Molino's landmark report in 1974 on the destruction of stratospheric ozone by man-made chlorofluorocarbons since chlorine oxides were implicated and subsequently found to play an important role in this process.[3] As a result, a wide variety of experimental and computational investigations have been carried out on these species.

Energetic measurements on the larger chlorine oxides and acids (i.e., x = 3 and 4) have proven to be difficult, and as a result the thermochemistry of these species is quite

muddled in the literature. For example, the heat of formation of ClO_4 depends upon the heat of formation of ClO_3, and the currently accepted value for the latter compound does not correspond to an experimental measurement. Laser flash photolysis kinetics was originally used to determine $\Delta H^\circ_f(ClO_3) = 55.6 \pm 4$ kcal mol^{-1} and subsequently this value was revised downward to 51.9 ± 5 kcal mol^{-1}.[4,5] Thereafter, a value of 51 ± 4 kcal mol^{-1} was given without justification for the change and an ab initio prediction of 48 ± 3 kcal mol^{-1} based upon G1 theory at 0 K was adopted by the experimental group.[6,7] More recent G2 calculations give $\Delta H^\circ_f(ClO_3) = 46 \pm 3$ kcal mol^{-1} at 298 K,[8] and this value is often given as the experimentally determined heat of formation. It also has been included in thermochemical reviews such as the JANAF tables and the NASA/JPL publication on chemical kinetics and photochemical data for use in atmospheric studies.[9,10]

In a similar vein, $\Delta H^\circ_f(HClO_4) = -1.5$, -2.3, and 4 ± 4 kcal mol^{-1} have been reported.[6,11,12] The first of these values has been considered to be a group additivity determination, but it actually is derived from the liquid phase heat of formation of perchloric acid and its heat of vaporization. Unfortunately, neither of these two quantities is well established and particular problems were encountered in deriving the former value from the aqueous heat of formation of perchloric acid and its heat of dilution. The heat of dilution was measured by Berthelot in 1882 ($\Delta H^\circ = -20$ kcal mol^{-1}),[13] but he noted that "the experiments were difficult owing to the rapidity with which the acid attracted moisture during weighing, and the violence of the reaction with water when the experiment was carried out."[14] It is for this reason that Goodeve and Marsh,

who measured the aqueous heat of formation of perchloric acid in 1937 (ΔH°_f = -31.6 ± 1.7 kcal mol^{-1}), explicitly refrained from giving the liquid-phase value for the pure compound.[15]

The second of the three values for the heat of formation of perchloric acid given above is based upon the same original data of Berthelot and Goodeve and Marsh, but was given as an estimate.[11] The third and final heat of formation ($\Delta H^\circ_f(HClO_4)$ = 4 ± 4 kcal mol^{-1}), is given in Benson's classic book, Thermochemical Kinetics, and also maybe an estimate but no basis was provided for this quantity.[12]

Chloric acid has not been studied as extensively as perchloric acid, but its heat of formation is not well established either. Colussi provided an estimate of -4.2 kcal mol^{-1} but this value depends upon the heat of formation of perchloric acid.[6] Benson reported a value of 11 ± 4 kcal mol^{-1}, but again no basis was provided for it.[12]

The deprotonation enthalpies of chloric and perchloric acids also have been reported[16,17] and the NIST website gives values of 286.7 ± 5.9 and 288 ± 14 kcal mol^{-1}, respectively.[18] Both of these acidities (we will refer to deprotonation enthalpies as acidities in this work even though others use free energies when using this term) indicate that these compounds are extremely strong acids, which is not surprising given their aqueous pKa's of -3 ($HClO_3$) and -10 ($HClO_4$).[19] The large uncertainties in these quantities make it unclear where these compounds should be placed on the gas-phase acidity scale relative to other strong acids. The absolute values are uncertain too in that the acidity of perchloric acid is based upon lattice energies and heats of solution whereas the acidity for chloric acid was derived from a thermodynamic cycle (eq. 2.1) using BDE(H–$OClO_2$) = 71.1 ± 5.4 kcal mol^{-1}, which is now known to be unreliable.[20]

$$\Delta H^{\circ}_{acid}(HClO_3) = BDE(H–OClO_2) + IP(H) – EA(ClO_3) \quad (2.1)$$

An extensive number of computations have been carried out on ClO_x and $HClO_x$ including highly accurate W4 values, and a wide range of heats of formation have been predicted for these compounds.[3f,7,8,21] Several methodologies which normally are very reliable (e.g., G1 and G2 theory) provide poor atomization energies for some of these compounds. Given that Cl–O bonds suffer from strong electron-electron repulsion effects and inner-shell polarization, adequate computational descriptions of these compounds is a challenge for single reference electron correlation methods including CCSD(T) energies with large basis sets.[21a] As a result, thermochemical data computed using the Gn methods are suspect and may not be as reliable as usual.

In recent publications we explored the top (LiOH) and bottom [$H(CHB_{11}Cl_{11})$] of the gas-phase acidity scale.[22,23] The acidities of chloric and perchloric acids are of interest in this regard and redeterminations of these quantities have been called for on the basis of computational results.[21b,24] It also has been suggested that the conjugate bases of these acids play a role in the atmosphere.[25] Consequently, we report herein the first experimental measurements of the proton affinities for ClO_3^- and ClO_4^-. Given that the adiabatic electron detachment energies of these ions were previously determined by negative ion photoelectron spectroscopy,[26] experimental O–H bond dissociation energies for $HClO_3$ and $HClO_4$ also were obtained. These results are compared to G3,[27] G3B3,[28] and DFT computations using B3LYP[29] and two of the Minnesota 2006 suite of density functionals.[30] All of these methods reasonably reproduce the acidities, electron

affinities, and bond energies, but M06 is the only one to satisfactorily provide the heats of formation via atomization energies. It also is nearly as accurate as W4 calculations despite being enormously more efficient and computationally less demanding.

Results and Discussion

Computing accurate thermochemical values for the ClO_x and $HClO_x$ series of compounds is a challenge for density functional theory and ab initio methods.[21] The Minnesota 2006 suite of density functionals developed by Truhlar and coworkers, however, have proven to be extremely reliable in the initial benchmarking of them.[30] M06 and M06-2X are the two general purpose functionals suitable for main group chemistry, and ClO_x and $HClO_x$ represent a difficult test for these methods. Consequently, geometries were optimized for x = 1 – 4 for both series of compounds with both functionals using aug-cc-pVD(+d)Z, aug-cc-pVT(+d)Z, and aug-cc-pVQ(+d)Z basis sets. The results are summarized in Table 3.1 and they indicate that (a) the M06 and M06-2X bond lengths are very similar with the exception of $HClO_3$ and to a smaller extent $HClO_2$; (b) in general the M06-2X bond lengths are slightly shorter than the M06 values; (c) the aug-cc-pVT(+d)Z and aug-cc-pVQ(+d)Z geometries differ by no more than 0.003 Å for any of these species with either functional and are in good accord with the available experimental data, but the quadrupole zeta bond lengths typically are 0.001-0.002 Å shorter than those obtained with the triple zeta basis set; (d) the aug-cc-pVD(+d)Z bond lengths are systematically too long.[34-38] Computed geometries at the B3LYP/6-31G(d), MP2(full)/6-31G(d), and CCSD(T)/ PVQZ levels also are provided in Table 3.1 since the first two methods provide the structures that are used for the single point energy calculations in G3B3 and G3 theory, respectively, while

the CCSD(T) geometries were used in the very high-level W4 computations carried out by Karton, Parthiban, and Martin.[21a] The B3LYP and MP2 structures are quite poor with Cl–O bond lengths that are ~0.07 Å too long, which is not very surprising given

Table 2.1. Computed M06-2X, M06, B3LYP, MP2, and CCSD(T) Geometries of ClO_x and $HClO_x$, x = 1 – 4.

Cmpd	Basis set[a]	Cl–O Distance			
		Calc.			Expt.
		M06-2X	M06	B3LYP (MP2) [CCSD(T)][b]	
ClO ($C_{\infty V}$)	D(+d)Z	1.580	1.582	1.620 (1.607)	1.570[c]
	T(+d)Z	1.558	1.560		
	Q(+d)Z	1.556	1.559	[1.575]	
ClO_2 (C_{2V})	D(+d)Z	1.483	1.489	1.523 (1.514)	1.470[d]
	T(+d)Z	1.460	1.463		
	Q(+d)Z	1.458	1.461	[1.473]	
ClO_3 (C_{3V})	D(+d)Z	1.460	1.464	1.502 (1.481)	1.485 ± 0.02[e]
	T(+d)Z	1.437	1.437		
	Q(+d)Z	1.435	1.436	[1.445]	
ClO_4 (C_{2V})	D(+d)Z	1.498, 1.420	1.499, 1.424	1.538, 1.458 (1.524, 1.441)	
	T(+d)Z	1.476, 1.402	1.473, 1.401		
	Q(+d)Z	1.474, 1.400	1.472, 1.400		
HOCl (C_S)	D(+d)Z	1.689, 0.968	1.692, 0.969	1.728, 0.975 (1.715, 0.978)	1.689, 0.964[f]
	T(+d)Z	1.673, 0.964	1.675, 0.964		
	Q(+d)Z	1.671, 0.964	1.674, 0.963	[1.694, 0.964]	
HOClO (C_1)	D(+d)Z	1.684, 1.516, 0.971	1.695, 1.514, 0.972	1.757, 1.546, 0.979 (1.753, 1.513, 0.983)	
	T(+d)Z	1.658, 1.496, 0.968	1.668, 1.490, 0.968		
	Q(+d)Z	1.657, 1.494, 0.967	1.667, 1.488, 0.966	[1.694, 1.503, 0.967]	
$HOClO_2$ (C_1)	D(+d)Z	1.685, 1.460, 1.448, 0.976	1.711, 1.462, 1.449, 0.974	1.759, 1.487, 1.484, 0.983 (1.754, 1.466, 1.463, 0.988)	
	T(+d)Z	1.654, 1.438 1.430, 0.974	1.686, 1.434, 1.422, 0.969		
	Q(+d)Z	1.652, 1.436, 1.427, 0.973	1.683, 1.433, 1.421, 0.967	[1.689, 1.444, 1.431, 0.970]	
$HOClO_3$ (C_S)	D(+d)Z	1.644, 1.428, 1.419, 0.974	1.655, 1.430, 1.421, 0.974	1.710, 1.466, 1.455, 0.982 (1.690, 1.450, 1.440, 0.986)	1.641, 1.414, 1.404, 0.98[g]
	T(+d)Z	1.617, 1.410, 1.401, 0.972	1.625, 1.407 1.398, 0.970		
	Q(+d)Z	1.615, 1.408, 1.399, 0.971	1.622, 1.406, 1.397, 0.968	[1.628, 1.412, 1.403, 0.970]	

[a] The basis sets that were used are as follows: D(+d)Z = aug-cc-pVD(+d)Z, T(+d)Z = aug-cc-pVT(+d)Z, and Q(+d)Z = aug-cc-pVQ(+d)Z. [b] B3LYP and MP2(full) geometries were computed with the 6-31G(d) basis set whereas the CCSD(T)/PVQZ structures come from ref 21a. [c] Ref 34. [d] Ref 35. [e] Ref 36. [f] Ref 37. [g] Ref 38.

Table 2.2. Computed M06-2X and M06 Heats of Formation Along with T1 and B1 Diagnostics for ClO_x and $HClO_x$, x = 1 – 4.

Cmpd	DH°_f (298 K)[a]						Diagnostics	
	M06-2X			M06				
	D(+d)Z	T(+d)Z	Q(+d)Z	D(+d)Z	T(+d)Z	Q(+d)Z	T_1[b]	B_1[c]
ClO	28.7	25.7	25.0	27.6	25.0	24.5	0.036	13.4
ClO_2	43.1	31.0	29.7	35.4	24.6	23.9	0.025	17.9
ClO_3	77.5	56.6	54.6	65.3	46.0	44.6	0.024	9.9
ClO_4	101.2	73.9	71.3	86.8	60.2	58.0	0.027	10.6
HOCl	-14.2	-17.3	-17.7	-14.7	-16.1	-16.5	0.011	(8.1)
HOClO	19.3	10.1	9.2	14.0	7.5	7.1	0.023	15.8 (10.5)
$HOClO_2$	27.9	8.8	7.3	16.8	1.2	0.2	0.023	14.8 (7.4)
$HOClO_3$	42.0	13.7	11.4	29.5	4.0	1.8	0.019	4.8 (2.3)

[a] All of the heats of formation are in kcal mol^{-1} and were computed from the atomization energies. Abbreviations are as follows: D(+d)Z = aug-cc-pVD(+d)Z, T(+d)Z = aug-cc-pVT(+d)Z, and Q(+d)Z = aug-cc-pVQ(+d)Z. [b] Computed using M06/aug-cc-pVT(+d)Z geometries. [c] Computed for the Cl–O bond; parenthetical values are for the Cl–OH bond.

the small basis set which is used in the optimizations for the Gn methods. In contrast, the coupled cluster bond lengths reproduce the experimental results, and in the one case where there is a discrepancy (ClO_3), the computed value maybe more accurate.

Heats of formation of the ClO_x and $HClO_x$ compounds were computed at 298 K via their atomization energies. Both M06-2X and M06 were examined with increasingly large basis sets (Table 2.2) because like ab initio methods, the performances of these hybrid meta-generalized gradient approximation (GGA) density functionals are sensitive to the size of the basis set.[30] A systematic decrease with increasingly large

basis sets and a big change of up to 28 kcal mol^{-1} in going from aug-cc-pVD(+d)Z to aug-cc-pVT(+d)Z was found. The differences between the triple and quadrupole zeta basis sets are much smaller but are nontrivial. That is, the heats of formation decrease by 0.4 – 2.6 kcal mol^{-1} with an average change of 1.5 kcal mol^{-1} for the M06-2X data set and 0.4 – 2.2 kcal mol^{-1} with an average difference of 1.1 kcal mol^{-1} for the M06 results. Both of these methods are suitable for many applications, but the M06-2X functional typically performs better for main group chemistry.[30] It does incorporate twice as much Hartree Fock exchange, however, so the M06 functional is more suitable for problems that have multireference character. Consequently, two diagnostic tests (T_1 and B_1) for the importance of nondynamical electron correlation were carried out (Table 2.2).[33,39] Species with $T_1 > 0.02$ and $B_1 > 10.0$ kcal mol^{-1} are considered to have significant multireference character, and this is the case for all of the compounds considered in this work except for HOCl and $HClO_4$. These findings are consistent with the much more detailed analysis carried out by Karton et al.,[21a] and indicate that M06 is more suitable for these compounds than M06-2X.

To assess the reliability of the computed heats of formation, the M06 and M06-2X values obtained with the aug-cc-pVQ(+d)Z basis set were compared to the W4 results of Martin et al.[21a] in Table 2.3 since the latter method has been shown to be extremely reliable and reproduces the ClO_x and $HClO_x$ experimental data.[6,10,40] G3 and G3B3 results also are provided since Gaussian theory is quite popular, generally is very reliable, and has been used to question experimentally determined energetics for some of the species reported in this work. Most strikingly, the M06 heats of formation are on average within 1.3 kcal mol^{-1} of the W4 values, and the maximum difference between

Table 2.3. Computed and Experimental Heats of Formation for ClO_x and $HClO_x$, x = 1 – 4.

Cmpd	DH°_f (298 K)[a]					
	G3	G3B3	M06-2X	M06	W4	expt
ClO	26.7	27.9	25.0	24.5	24.2 ± 0.1	24.29 ± 0.03[b]
ClO_2	28.2	29.4	29.7	23.9	23.7 ± 1.9	22.6 ± 0.3[b,c]
ClO_3	50.3	54.4	54.6	44.6	44.3 ± 0.4	46 ± 3[d]
ClO_4	68.6	68.3	71.3	58.0		
HOCl	-16.6	-15.9	-17.7	-16.5	-18.2 ± 0.1	-17.9 ± 0.3
HOClO	7.8	8.8	9.2	7.1	5.0 ± 0.4	est. 1.0[e]
$HOClO_2$	4.0	5.8	7.3	0.2	-2.6 ± 0.3	est. -4.2[e]
$HOClO_3$	8.2	11.3	11.4	1.8	-0.1 ± 1.0[f]	est. -1.5[e]
Max. Error[g]	8.3	11.4	11.5	2.8		
Avg. Error[g]	4.6	6.5	6.2	1.3		

[a] All of the heats of formation are in kcal mol^{-1} and were computed from atomization energies using the aug-cc-pVQ(+d)Z basis set except for the W4 values for ClO_3 and $HClO_2$ which were obtained via isodesmic reactions. All of the Wn results come from ref 21a. [b] Ref 10. [c] Ref 40. [d] This value is based upon an experimental determination of 51 ± 4 kcal mol^{-1} (ref 6), a modified G1 computation (ref 7), and a G2 prediction (ref 8). [e] Ref 6. [f] This value was obtained using W2.2 theory, see ref 21a for additional details. [g] Errors were computed relative to the Wn results.

the two is just 2.8 kcal mol^{-1}.[41] This is a very impressive finding, particularly, since ClO_x and $HClO_x$ suffer from severe nondynamical correlation effects and M06 calculations are many orders of magnitude faster than W4 computations. G3, G3B3, and M06-2X do not perform well for these compounds, and have average and maximum errors of 4.6 and 8.3 (G3), 6.5 and 11.4 (G3B3), and 6.2 and 11.5 kcal mol^{-1} (M06-2X). These values are significantly outside of the target range for Gaussian-3 theory, but this should not be too surprising given the poor starting geometries obtained using the G3 and G3B3 procedures, and the multi-configurational nature of most of the substrates. Gas-phase acidity measurements have not been carried out on chloric and perchloric acids because the pure compounds are unstable and explosive while their hydrated forms are not volatile enough. The conjugate bases of these acids, however, readily can be generated by electrospray ionization. That is, abundant ion signals for ClO_3^- and ClO_4^- were produced by spraying aqueous methanolic solutions (3:1 CH_3OH/H_2O) of the potassium salts in a FTMS. In separate experiments each of the anions were allowed to react with neutral BrØnsted acids of known strength. Chlorate anion is protonated upon reaction with 2,4,6-trinitrophenol (ΔH°_{acid} = 310.3 ± 2.2 kcal mol^{-1}) and stronger acids, but does not react with methanesulfonic acid ($\Delta H^\circ_{acid}(CH_3SO_3H)$ = 320.9 ± 2.2 kcal mol^{-1}).[18] These results indicate that the proton affinity of ClO_3^- is between 310.3 ± 2.2 and 320.9 ± 2.2 kcal mol^{-1}. To narrow this range, the reaction with 2,4-dinitrophenol (ΔH°_{acid} = 316.1 ± 2.1 kcal mol^{-1}) was examined.[18] Proton transfer was observed to a small extent (~15%), but the major pathway was adduct formation and the overall reaction was relatively inefficient (i.e., k = 1 x 10^{-10} cm^3 $molecule^{-1}$ s^{-1}

and k/k_{ADO} = 5%).[42] This suggests that chloric acid is more acidic than 2,4-dinitrophenol, and in accord with this finding the collision-induced dissociation of the adduct ion led to more ClO_3^- than 2,4-dinitrophenoxide (i.e., a 60 : 40 ratio was observed). Consequently, we assign $\Delta H^\circ_{acid}(HClO_3)$ = 313.2 ± 3.3 kcal mol^{-1}. This bracketing result also is in excellent accord with the value obtained using the Arrhenius equation (313.2 kcal mol^{-1}), where k is the proton transfer rate constant for the reaction with 2,4-dinitrophenol (1.5 x 10^{-11} cm^3 molecule^{-1} s^{-1}), A is the collision-controlled rate constant (k_{ADO} = 2.1 x 10^{-9} cm^3 molecule^{-1} s^{-1}), T = 300 K, and E_a is found to be 2.9 kcal mol^{-1}. Our new and experimentally determined deprotonation enthalpy for chloric acid corresponds to a 26.5 kcal mol^{-1} upward (less acidic) revision in the acidity, and indicates that $HClO_3$ is more acidic than HBr (ΔH°_{acid} = 323.53 ± 0.05 kcal mol^{-1}),[43] less acidic than H_2SO_4 (ΔH°_{acid} = 306.3 ± 3.1 kcal mol^{-1}),[18] and similar in acidity to HI (ΔH°_{acid} = 314.33 ± 0.03 kcal mol^{-1}).[43] The new value also is well-reproduced by M06-2X, G3, and G3B3 predictions of 315.4, 315.6, and 316.5 kcal mol^{-1} but B3LYP and M06 do less well giving acidities of 318.0 and 319.8 kcal mol^{-1}, respectively (Table 2.4).

Table 2.4. Computed and Experimental Heats of Formation for ClO_x and $HClO_x$, x = 1 – 4.

Method[a]		$HOClO_2$[b]			$HOClO_3$[b]	
	DH°_{acid}	$EA(ClO_3)$	BDE (O–H)	DH°_{acid}	$EA(ClO_4)$	BDE (O–H)
M06-2X						
D(+d)Z	316.1	4.25	101.7	298.9	5.42	111.3
T(+d)Z	314.6	4.25	99.9	297.4	5.53	112.3
Q(+d)Z	315.4	4.21	99.4	298.3	5.50	112.0
M06						
D(+d)Z	316.7	4.19	100.7	299.2	5.31	109.4
T(+d)Z	318.7	3.98	96.9	302.5	5.18	108.3
Q(+d)Z	319.8	3.92	96.5	302.4	5.19	108.3
B3LYP	318.0	4.14	98.4	300.8	5.19	105.4
G3	315.6	4.21	98.4	299.4	5.53	112.5
G3B3	316.5	4.23	99.6	300.0	5.36	109.1
expt	313.2 ± 3.3	4.25 ± 0.10[c]	97.6 ± 4.0 (99.0)[d]	299.9 ± 5.7	5.25 ± 0.10[c]	107.4 ± 6.1
		HOCl[b]			HOClO[b]	
M06-2X						
D(+d)Z	354.6	2.29	95.0	333.9	2.37	75.9
T(+d)Z	354.4	2.31	95.1	333.1	2.28	73.1
Q(+d)Z	355.2	2.28	94.8	333.9	2.24	72.6
M06						
D(+d)Z	352.9	2.35	94.4	333.8	2.27	73.5
T(+d)Z	356.4	2.19	93.2	336.7	2.01	69.2
Q(+d)Z	357.6	2.14	93.1	337.7	1.96	68.9
B3LYP	354.9	2.25	91.6	335.4	2.22	71.5
G3	356.4	2.32	95.4	335.2	2.25	72.6
G3B3	357.7	2.28	95.9	336.5	2.19	72.7
expt	355.6 ± 1.1[e]	2.2775 ± 0.0013[f]	94.3 ± 0.3 (94.5)[d]	335.1[z]	2.1451 ± 0.0025[f]	(70.8)[d]

[a] The basis sets that were used are as follows: D(+d)Z = aug-cc-pVD(+d)Z, T(+d)Z = aug-cc-pVT(+d)Z, Q(+d)Z = aug-cc-pVQ(+d)Z, and B3LYP = B3LYP/6-311+G(2df, 2pd). [b] All values in kcal mol^{-1} at 298 K except for the electron affinities which are in eV. [c] Ref 26. [d] Derived from Martin's Wn heats of formation in ref 21a. [e] Ref 18. [f] Refs 26 and 46. [z] Estimated using the experimental electron affinity and the bond dissociation energy derived from Martin's predicted heats of formation.

Perchlorate anion undergoes facile proton transfer reactions with $(CF_3SO_2)_2NH$ (ΔH°_{acid} = 294.4 ± 2.2 kcal mol^{-1})[44] and $(C_4F_9SO_2)_2NH$ (ΔH°_{acid} = ~285.8 ± 2.2 kcal mol^{-1})[45] to afford their conjugate bases, but no reaction is observed with CF_3SO_3H (ΔH°_{acid} = 305.4 ± 2.2 kcal mol^{-1}).[18] These results indicate that the proton affinity of ClO_4^- is between the values for $CF_3SO_3^-$ and $(CF_3SO_2)_2N^-$, and enables us to assign $\Delta H^\circ_{acid}(HClO_4)$ = 299.9 ± 5.7 kcal mol^{-1}. This finding corresponds to a 12 kcal mol^{-1} upward revision to the estimate based upon crystal lattice energies given by Marcus.[17] It also confirms the independent calls for a re-determination of this quantity by Dixon et al. and Vianello and Maksic, which were based upon CCSD(T) and G3 predictions of ~301.2 kcal mol^{-1} and 299.2 kcal mol^{-1}, respectively.[21b,24] All of the computational methods investigated in this work reproduce the acidity as well (Table 2.4) as do the calculations of Otto et al. and Boily.[47]

The electron binding energies of ClO_3^- and ClO_4^- (4.25 ± 0.10 and 5.25 ± 0.10 eV) were experimentally determined by Wang and Wang via photoelectron spectroscopy.[26] These values can be combined with the deprotonation enthalpies obtained in this work to provide the O–H bond dissociation energies for $HClO_3$ and $HClO_4$ via the application of the thermodynamic cycle illustrated for the former case in equation 1. The resulting bond energies are 97.6 ± 4.0 and 107.4 ± 6.1 kcal mol^{-1}, respectively which also are in accord with the computations reported herein as well as the W4 result for $HClO_3$ carried out by Karton et al.[21a]

The $HClO_x$ bond energies and the ClO_x electron affinities do not increase monotonically with x but they do follow the same trend: BDE(H–OClO) > BDE(H–OClO) < BDE(H–$OClO_2$) < BDE(H–$OClO_3$) and EA(ClO) > EA(ClO_2) < EA(ClO_3) < EA(ClO_4). In

contrast, the proton affinities of the ClO_x^- anions systematically increase with x as one would expect. To address these trends, the deprotonation enthalpies of $HClO_x$, x = 1-4, were plotted against the electron affinities of ClO_x since a linear correlation for hetero-substituted HOX acids has previously been noted (Figure 3.1).[48]

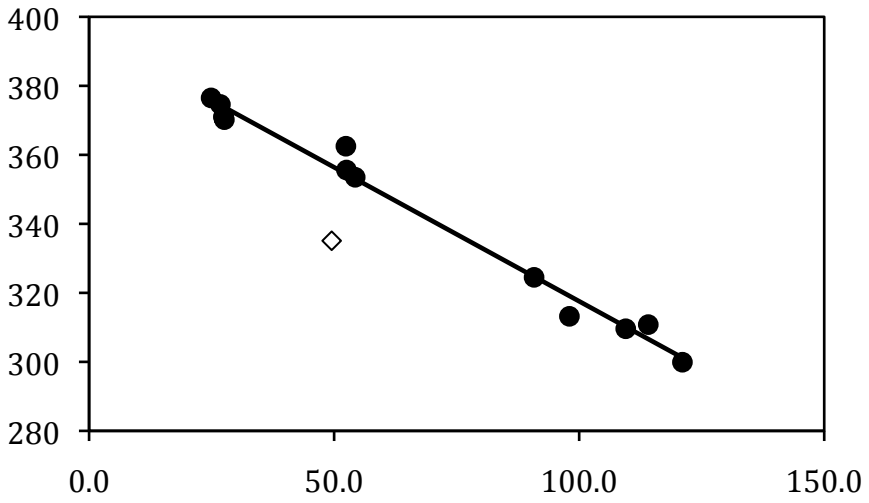

Figure 2.1. Deprotonation enthalpy of XOH versus electron affinity of XO (ΔH°_{acid}(XOH) = -0.777 x EA(XO) + 395.2, r^2 = 0.99). Filled circles are for the data points that were used to derive the line whereas the open diamond ($HClO_2$) was omitted from the least-squares analysis.

That is, the experimental acidities for $HClO_3$ and $HClO_4$ along with a predicted value for $HClO_2$ obtained using the experimental electron affinity for OClO and the W4 O–H BDE for HOClO were added to the previously reported data for HOX acids. All of the compounds including HOCl fall on a line except for $HClO_2$. The simplest explanation for this observation and the nonmonotonic trends in the bond dissociation energies and electron affinities is that OClO is unusually stable relative to the other

ClO_x radicals. This is the case in that OClO does not dimerize or polymerize and is commercially available whereas the other ClO_x radicals are fleeting intermediates which can not be stored at room temperature in a conventional sense.[49] The greater stability of OClO relative to the other chlorine oxides is reflected in its larger computed spin density at chlorine (ClO, 0.27; OClO, 0.39; ClO_3, 0.28, and ClO_4 -0.16 at the M06/aug-cc-pVQ(+d)Z level), which indicates a greater importance of the stabilizing resonance structure **B**. This canonical structure formally has half a bond more than **A** and **A′**. The greater interaction of the unpaired electron on oxygen with the lone pair on chlorine is a result of a better energy match of these two orbitals as indicated by the highest occupied molecular orbital (HOMO) – (HOMO – 1) energy gaps.

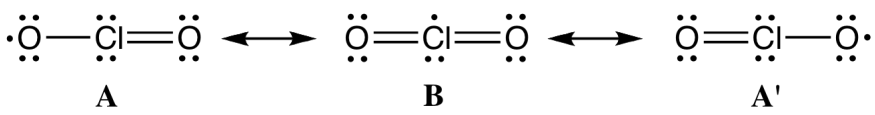

Figure 2.2. Lewis structures for OClO.

Conclusions

Experimental acidities and bond dissociation energies for $HClO_3$ and $HClO_4$ were determined in the gas phase. The latter values can be used with the heats of formation of the acids or chlorine oxides to derive the others when these experimental values become established. Computations also were carried out and heats of formation were calculated via atomization energies. The M06 functional of Truhlar reproduces the highly accurate W4 results of Martin to within 1.3 kcal mol^{-1} on average, despite the known difficulties in accurately calculating these species and the extreme difference

in computational cost. That is, M06 calculations are orders of magnitude faster than W4 computations. Acidities, electron affinities, and bond dissociation energies are generally reproduced by M06-2X, M06, B3LYP, G3, and G3B3 calculations even though the geometries and atomization energies for the last two methods are quite poor. It also appears that M06-2X is preferable over M06 when it comes to computing acidities, electron affinities, and bond energies even though the latter method is much better for calculating the heats of formation.

The proton affinities and electron binding energies of ClO_x^- and the bond dissociation energies of $HClO_x$ span 56, 72, and 37 kcal mol^{-1} range, respectively. Each successive oxidation of chlorine results in an anion, which is less basic, as one would expect, due to increased charge delocalization via resonance stabilization. The EAs and BDEs do not follow this trend in that the values for ClO_2 and $HClO_2$ are anomalously low. This accounts for these two quantities spanning a larger and a smaller range, respectively than for the proton affinities. The simplest explanation for this observation, and the deviation of $HClO_2$ from a plot of ΔH°_{acid} (HOX) vs. EA (XO), is that ClO_2 is unusually stable. In accord with this explanation, ClO_2 is the only room temperature stable radical in the ClO_x series. Computations also indicate that the canonical O=Cl$^{\cdot}$=O resonance structure makes a greater contribution to the structure of ClO_2 than the analogous species do for the other chlorine oxides.

Chapter 2 Experimental Methods

A Fourier transform mass spectrometer (FTMS) equipped with a 3 T superconducting magnet and an Omega ver. 8.0.294 data system was used to carry out the gas phase experiments. The electrospray cart was provided by IonSpec (now Varian) but the inlet system was extensively modified to enable the addition of multiple reagents and the measurement of reaction rates. Both ClO_3^- and ClO_4^- were generated using a Z-Spray (Micromass) ESI source in which 200 μm solutions of $KClO_3$ and $KClO_4$ in a 3 : 1 CH_3OH/H_2O mixture were injected into the system at a flow rate of 10 μL min^{-1}. The resulting $[M - K^+]^-$ ions were stored in a hexapole for a brief time (500 ms) before being transferred into the 6" gold-plated cylindrical cell where they were trapped and cooled with a pulse of argon up to pressures of ~10^{-5} Torr. Both ions were carefully isolated using an arbitrary waveform and subsequent reactions were carried out on the natural abundance of the two chlorine isotopomers (i.e., the ^{35}Cl and ^{37}Cl containing ions were not separated). Neutral acids were introduced into the ICR cell at static pressures with a Granville-Philips (model 203) variable leak valve, and the subsequent reactions were monitored as a function of time by varying the delay between ion isolation and ion detection.

Computations were carried out at the Minnesota Supercomputer Institute for Advanced Computational Research using Gaussian 03 on IBM and SGI workstations.[31] Structures were fully optimized using the M06 and M06-2X density functionals in conjunction with the aug-cc-pVD(+d)Z, aug-cc-pVT(+d)Z, and aug-cc-pVQ(+d)Z basis sets.[30,32] Harmonic vibrational frequencies were computed for each species with both functionals

and all three basis sets. In each case the structures were found to be energy minima on the potential energy surfaces. BLYP and B1LYP optimizations were carried out with the aug-cc-pVT(+d)Z basis set to compute the B1 diagnostic reported by Schultz et al.[33] and B3LYP structures and vibrational frequencies were calculated with the 6-311+G(2df,2pd) basis set. In addition, G3[27] and G3B3[28] energies were computed for all of the species reported in this work as described in the literature. The resulting energetics are reported as enthalpies at 298 K where small vibrational modes which contribute more than ½(RT) to the thermal energy were replaced by 0.296 kcal mol^{-1}.

Chapter 3.

Gas-Phase Synthesis and Reactivity of Lithium Acetate Enolate Anion, $^{-}CH_2CO_2Li$.

Dianions are versatile reagents that are widely used in organic synthesis.[1] They typically are prepared by deprotonation of two hydrogens at carbon, nitrogen, oxygen, or sulfur centers. These reactive intermediates have a long history going back more than one hundred years to Grignard himself, who prepared the dianion of phenylacetic acid.[2] Ivanoff subsequently exploited the dimagnesium salts of carboxylic acids possessing α–hydrogens and developed their reactivity with a variety of electrophiles.[3] Despite the widespread use of Ivanoff reagents and related dilithiated carboxylic acids in organic synthesis, surprisingly little is known about the fundamental properties of these salts.[4] Aggregation and solvation effects complicate studies of these species, and their sensitivity to moisture and oxygen has played a large role in the absence of X-ray crystal structures to date. Theoretical calculations by Schleyer[5a] and Streitwieser,[5b] however, suggest that the monomeric structure of the dilithium salt of acetic acid (**1**) is non-symmetrical with 1,3 and 1,3′ lithium bridges.[6] We previously have shown that the decarboxylation of lithium and other metal complexes of mono and dicarboxylic acids can produce a variety of organometallic ions.[7] In this report the gas-phase preparation and reactivity of lithium acetate enolate anion (**2**, $^{-}CH_2CO_2Li$), a species directly related

Meyer, M. M.; Khairallah, G. N.; Kass, S. R.; O'Hair, R. A. J., Gas-Phase Synthesis and Reactivity of the Lithium Acetate Enolate Anion, -CH2CO2Li. ***Angewandte Chemie-International Edition*** **2009,** 48, (16), 2934- 2936.

The results of high-level computations also are presented as is a comparison of **2** with acetic acid enolate anion (**3**).[8]

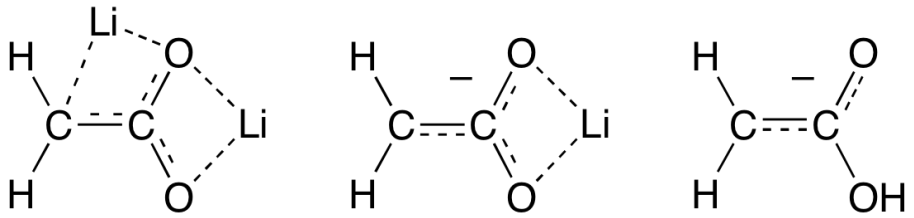

1 **2** **3**

Electrospray ionization of a 3:1 (v/v) water/methanol solution containing malonic acid and lithium hydroxide readily provided the anionic lithium complex of doubly deprotonated malonic acid ($^{-}O_2CCH_2CO_2Li$, *m/z* 109) (Figure 3.1). Collisional-induced dissociation (CID) of this ion resulted in the loss of carbon dioxide to afford lithium acetate enolate anion (*m/z* 65).[9] Its structure was explored by carrying out Becke 3-parameter hybrid exchange and Lee-Yang-Parr correlation density functional calculations (i.e., B3LYP)[10] with the 6-311+G(2df,2pd) basis set. Two low energy anion conformations were located, both of which bind the lithium in a bidendate fashion (Figure 3.2). These structures are directly related to the parent dilithium salt (**1**) via removal of either of the non-equivalent bridging Li^+. The more stable structure (**2a**) has C_{2V} symmetry and both oxygen atoms of the carboxylate interact with the lithium. In contrast, when the lithium coordinates to the α−carbon and one oxygen atom the resulting C_1 structure (**2b**) is predicted at 298 K to be 25.6 kJ mol^{-1} less stable. This energy difference is nearly the same when high-level G3 calculations are used (22.9 kJ

mol^{-1}),[11] which strongly suggests that **2a** is the preferred structure for lithium acetate enolate anion.

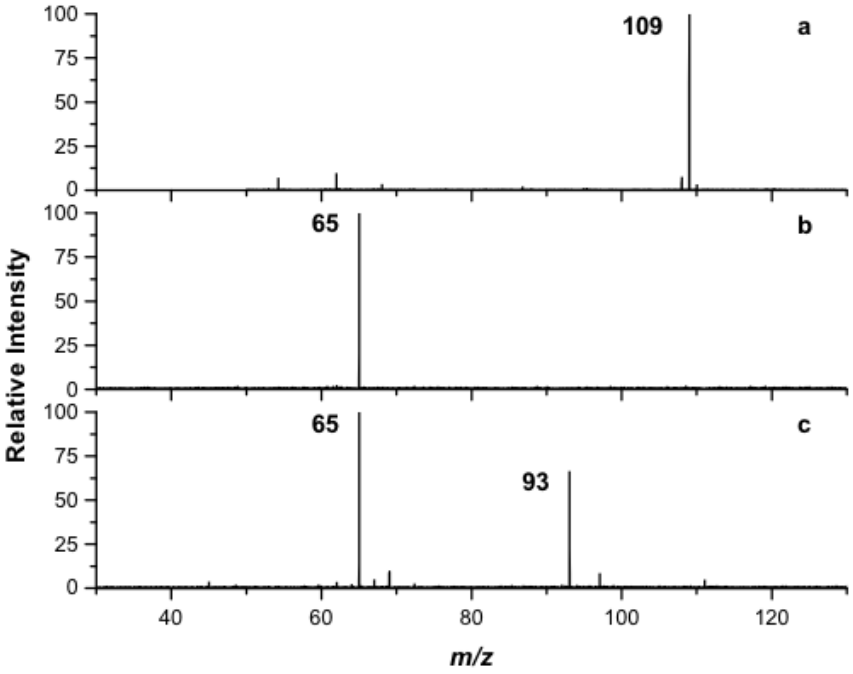

Figure 3.1. (a) Electrospray ionization of malonic acid and lithium hydroxide from a 3:1 (v/v) MeOH/H_2O solution. The *m/z* 109 ion corresponds to $LiO_2CCH_2CO_2^-$. (b) Formation of $^-CH_2CO_2Li$ (*m/z* 65) by CID and its subsequent isolation. (c) Reaction of $^-CH_2CO_2Li$ with EtOH (1.7 x 10^{-8} Torr) for 200 ms. The ion at *m/z* 93 ($HC{\equiv}C{-}O^- \cdots Li^+ \cdots {}^-OEt$) is the only primary reaction product but small amounts of secondary products at *m/z* 69 ($HO^- \cdots Li^+ \cdots {}^-OEt$) and 97 ($EtO^- \cdots Li^+ \cdots {}^-OEt$) also are observed.

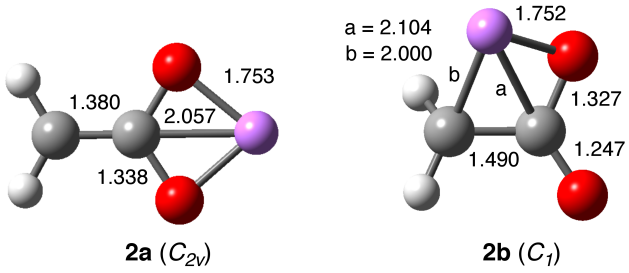

Figure 3.2. B3LYP/6-311+G(2df,2pd) structures of the lithium acetate enolate anion. Bond lengths are in Å.

To further assess the structure of **2**, and since the replacement of H by Li has been shown to dramatically increase the proton affinity (PA) of LiO^- over HO^- while simultaneously decreasing the electron affinity (EA) of $LiO^{\cdot}$ relative to $HO^{\cdot}$,[12] the PA of **2** and the EA of its corresponding radical were measured. This was accomplished by reacting **2** with acids of known strength or electron transfer reagents with known electron affinities [Eqs. (1) and (2)]. More specifically, **2** was found to readily react via proton transfer with acetone, toluene, and pyridazine (ΔH°_{acid} = 1543.1 ± 8.4, 1599.5 ± 5.0, and 1600.0 ± 10.5 kJ mol^{-1}, respectively),[13] but only sluggishly (i.e., the reaction efficiency was less than 5%) with fluorobenzene and furan (ΔH°_{acid} = 1619.6 ± 8.8[14] and 1636.4 ± 1.7 kJ mol^{-1}, respectively). Proton transfer was not observed with pyrazine or deuterium oxide (ΔH°_{acid} = 1642.6 ± 10.5 and 1642.6 ± 0.4 kJ mol^{-1}, respectively) but the former reagent led to an adduct–H_2 ion, and the latter induced two sequential hydrogen-deuterium (H/D) exhanges. These data suggest that the proton affinity of **2** is between that of the conjugate bases of pyridazine and fluorobenzene, so

PA(**2**) = 1610.0 ± 12.1 kJ mol^{-1} was assigned. Calculations indicate that protonation of **2** at carbon is favored over protonation at oxygen by 141 kJ mol^{-1} at the B3LYP/6-311+G(2df,2pd) level. The observed H/D exchange behavior of **2** with D_2O is consistent with this finding. Likewise, the predicted proton affinities of 1610.4 (B3LYP) and 1618.9 (G3) kJ mol^{-1} are in accord with the experimental results.

$$HA \rightarrow A^- + H^+$$
$$\Delta H^\circ_{rxn} = PA(A^-) = \Delta H^\circ_{acid}(HA) \quad (3.1)$$

$$A^- \rightarrow A^\cdot + e^-$$
$$\Delta H^\circ_{rxn} = EA(A^\cdot) \quad (3.2)$$

To determine the electron affinity of the radical corresponding to **2**, the anion was bracketed in a similar manner to the proton affinity measurements, but neutral reagents with known electron affinities were used. Electron transfer was found to readily occur with *p*-fluoronitrobenzene and *m*-fluoronitrobenzene (EA = 1.101 ± 0.048 and 1.210 ± 0.048 eV, respectively),[13] but not with carbon disulfide or sulfur dioxide (EA = 0.58 ± 0.05 and 1.107 ± 0.008 eV, respectively). These results suggest that the electron affinity lies between the values for sulfur dioxide and *m*-fluoronitrobenzene or EA($^\cdot CH_2CO_2Li$) = 1.16 ± 0.06 eV. This quantity can be combined with the proton affinity of **2** to obtain the C–H bond dissociation energy (BDE) of CH_3CO_2Li (410.0 ± 13.4 kJ mol^{-1}) since BDE(HA) = ΔH°_{acid}(HA) - IP($H^\cdot$) + EA($A^\cdot$), where IP($H^\cdot$) is the ionization potential of hydrogen and is well known to be 1312.0 kJ mol^{-1}. Both of these values are in excellent accord with computations which predict EA($^\cdot CH_2CO_2Li$) = 1.07 and 1.06 eV (B3LYP and G3, respectively) and BDE(H–CH_2CO_2Li) = 407.5 and 415.9

kJ mol^{-1} (B3LYP and G3, respectively). These results also reveal that replacement of H with Li increases the proton affinity of **3** (PA = 1540.1 ± 13.0 kJ mol^{-1})[8b,13] by 70 ± 18 kJ mol^{-1} while decreasing the electron affinity of the corresponding radical (EA = 1.80 ± 0.17 eV)[8b,13] by 0.64 ± 0.18 eV or 62 ± 17 kJ mol^{-1}. Consequently, the C–H BDEs for CH_3CO_2H and CH_3CO_2Li are the same within 8 kJ mol^{-1}, which is well within the experimental uncertainty for this quantity.

To gain further insights into the behavior of **2**, its reactions with a variety of compounds were examined. Alcohols react via an addition-water elimination pathway [Eq. (3.3a), R = Me, Et and Fig. (3.1c)] and by proton transfer [Eq. (3.3b)] when more acidic reagents are used (R =$C_6H_5CH_2$ and CF_3CH_2). The former transformation presumably occurs via O-protonation which is facilitated by the presence of the newly formed alkoxide. In accord with this hypothesis, HOD was lost exclusively when deuterated alcohols were used.

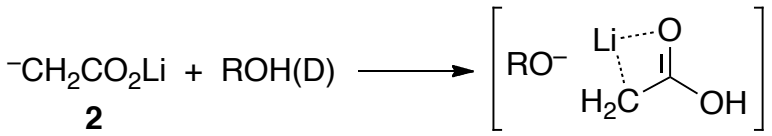

$$\longrightarrow RO^{-}\cdots Li^{+}\cdots{}^{-}O\text{–}C{\equiv}CH + H_2O(HOD) \qquad (3.3a)$$

$$\longrightarrow RO^{-} + CH_3CO_2Li \qquad (3.3b)$$

Several esters (RCO_2R') and a ketone (acetone) also were examined and up to 4 different products were observed as illustrated for methyl propionate [Eq. (3.4)].[15] Both proton transfer and addition-water elimination products were observed [Eqs. (3.4a) and

(3.4b), respectively] just as with the alcohols. Two new reaction channels corresponding to an LiO^- transfer and an E2-type elimination [Eqs. (3.4c) and (3.4d), respectively] were found as well. The former of these also occurred to afford $LiOSO_2^-$ and $LiOCOS^-$ upon the reaction of **2** with SO_2 and COS, respectively; $^-CH_2COSLi$ was also produced in the reaction with COS.

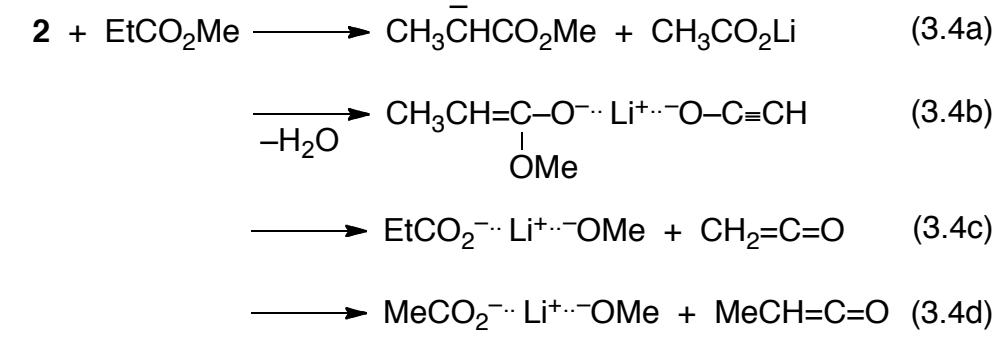

Lastly, nucleophilic aromatic substitution was found to take place with perfluorobenzene and presumably the product is a pentafluorobenzyl anion [Eq. (3.5)].

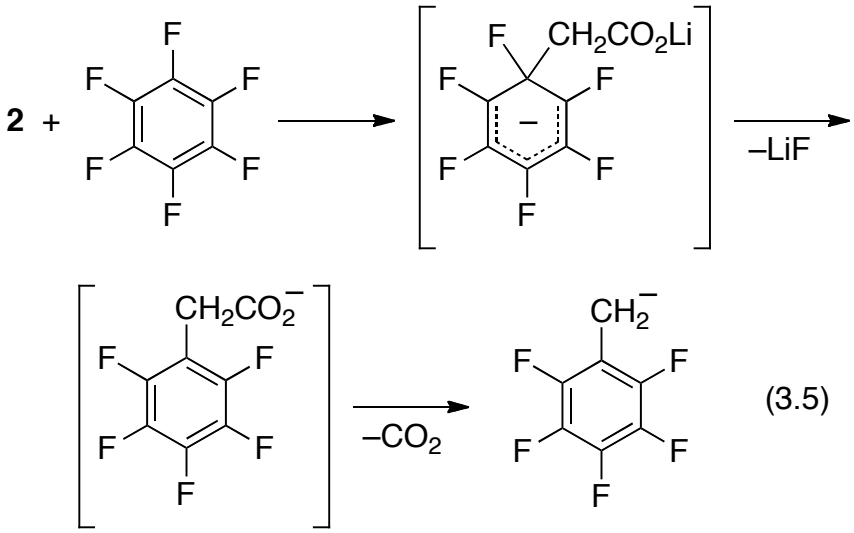

Decarboxylation of appropriate precursors has proven to be a versatile method for the gas-phase generation of textbook organometallic reagents.[7,9] The current work demonstrates that this strategy can be extended to the formation of other reactive intermediates and reagents involved in organic synthesis. Thus, we have shown that anions related to Ivanoff reagents can be prepared and studied in the absence of aggregation and solvent effects.

Chapter 3 Experimental Section

Gas-Phase Experiments. Preliminary experiments were conducted using a modified Finnigan LCQ quadrupole ion trap mass spectrometer equipped with a Finnigan electrospray ionization source.[9a] Electrospray solutions contained malonic acid and lithium hyroxide (both ~0.1 mg mL^{-1}) in a 3:1 (v/v) methanol/water mixture. Subsequent ion-molecule reactions were carried out in a Fourier transform ion-cyclotron mass spectrometer as previously described.[12] In both cases the lithiated salt of malonate dianion was observed at *m/z* 109 upon ESI and subsequently carbon dioxide was expelled by CID to afford **2**.

Computations. Density Functional Theory (DFT) calculations were carried out at the B3LYP/6-311+G(2pf,2pd) level of theory using Gaussian 03[16] at the Minnesota Supercomputer Institute for Advanced Computational Research. Stationary points were characterized by computing vibrational frequencies, and the resulting unscaled values were used for obtaining the zero-point energies and the thermal corrections for the enthalpies to 298 K. Selected species also were computed using G3 theory as described in the literature,[11] and in all instances the energetics reported herein are given as enthalpies at 298 K.

Chapter 4

Gas-Phase Synthesis and Reactivity of Lithium Acetylide Anion, Li–C≡C$^-$

Dianions in the form of their lithium salts are widely used reagents in organic synthesis.[1] These lithium-rich compounds have a long history going back to H. Moissan, who first prepared dilithium acetylide (Li_2C_2, **1**) in 1896 by reacting coal with lithium carbonate in an electric furnace.[2] It also can be directly prepared from the elements and is a commercially available solid with a melting point in excess of 550 ˚C. The non-classical structure of monomeric Li_2C_2 was initially predicted by Apeloig et al.[3] while the structure of the agreggate was determined by X-ray powder patterns.[4] Li_2C_2 is a useful intermediate produced during radiocarbon procedures,[5] and although it is relatively insoluble, it has been found to equilibrate with acetylene to afford lithium acetylide (Li–C≡CH, **1H**) in a synthetically convenient procedure.[6,7] Despite their importance, the investigation of organolithiums in solution is difficult because their reactivity varies with solvent, temperature, and the presences of additives (e.g. HMPA). To eliminate these complications and the effects of aggregation, we previously developed an extensively employed decarboxylation strategy for the regioselective

preparation of radical anions[8,9] and organometallic ions.[10] In this report the gas-phase synthesis and reactivity of lithium acetylide anion (Li–C≡C$^-$, **1A**), a species directly related to Li_2C_2 and a valuable synthetic reagent, is described. The results of G3, G4, and W1 computations among others also are presented.

Electrospray ionization of a basic aqueous methanolic solution of acetylenedicarboxylic in a Fourier transform mass spectrometer (FTMS) produced the lithium salt of acetylenedicarboxylate dianion ($LiO_2C–C≡C–CO_2^-$, *m/z* 119) (Figure 4.1).

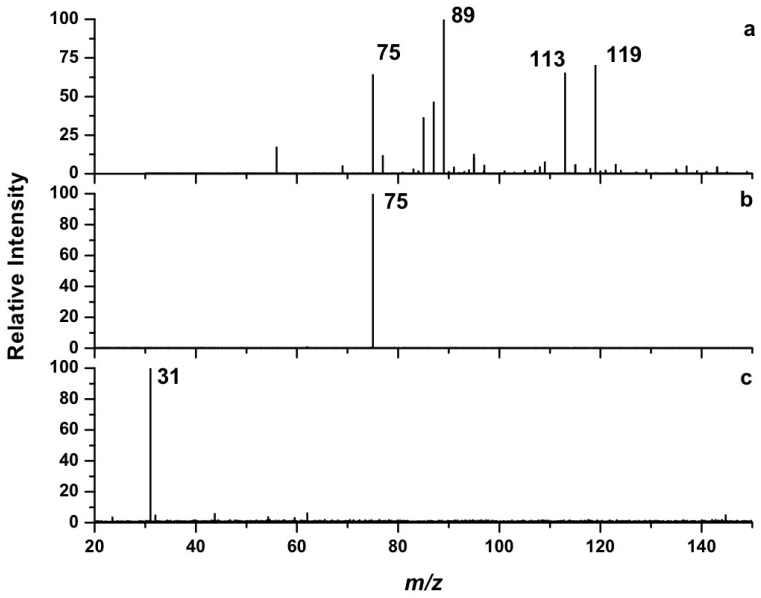

Figure 4.1. (a) Electrospray ionization of acetylenedicarboxylic acid; the *m/z* 113 and 119 ions correspond to $HO_2CC≡CCO_2^-$ and $LiO_2CC≡CCO_2^-$, respectively. (b) Formation and isolation of Li–C≡CCO_2^- (*m/z* 75) by CID. (c) Formation and isolation of Li–C≡C$^-$ (*m/z* 31) by a second CID event.

Fragmentation of this ion by activated collisions resulted in the loss of carbon dioxide to afford the conjugate base of lithium propynoate (Li–C≡C–CO_2^-, *m/z* 75). Cleavage of this ion by a second collision-induced dissociation (CID) pulse led to another decarboxylation, thereby generating the desired lithium acetylide anion [Eq. (4.1); *m/z* 31.0166 (obs), 31.0166 (calc)]. Initial attempts to prepare **1A** resulted in a mixture of the desired ion and CH_3O^-, but this isobaric impurity (*m/z* 31.0188 (expt), 31.0189 (calc)) can readily be resolved given the high resolution capabilities of a FTMS. This contaminant ion was found to arise from the CID of methyl carbonate anion ($CH_3OCO_2^-$, *m/z 75*), which was produced during the electrospray process. It was entirely eliminated, however, by isolating $LiO_2C–C≡C–CO_2^-$ (*m/z* 119) before breaking it apart.

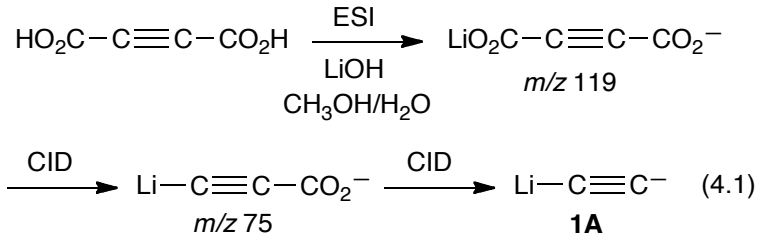

(4.1)

Lithium as a substituent has been found to increase the proton affinity of LiO^- and $^-CH_2CO_2Li$ while decreasing their electron binding energies,[10a,11] so these quantities were examined experimentally and computationally. This was accomplished, in part, by reacting **1A** with a wide variety of acids of known strength. Water (ΔH°_{acid} = 390.27 ± 0.02 kcal mol^{-1})[12] [1 kcal = 4.184 J] reacts as one might expect to afford the acetylide anion presumably through the transient intermediate **2** [Eq. (4.2)].

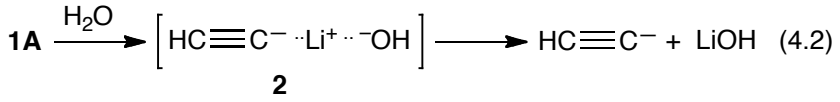

Methanol-d_4 ($\Delta H^\circ_{acid}(CH_3OH)$= 381.9 ± 0.5 kcal mol^{-1}) behaves similarly, but the ion analogous to **2** is detected and methoxide-d_3 serves as a deuteride source leading to the reduction of lithium [Eq. (4.3)]. More acidic alcohols protonate **1A** and ethanol (ΔH°_{acid} = 378.7 ± 0.8 kcal mol^{-1}), like methanol, affords acetylide-lithium ethoxide and acetylide-lithium hydride clusters.

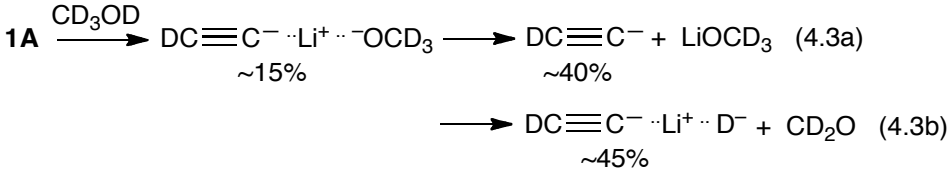

It also reacts via a novel methide-transfer [Eq. (4.4)]. Such a process has been reported by Schröder and Schwarz for the reactions of iron alkoxide cations ($FeOR^+$) with ketones,[13] but to the best of our knowledge has not been described for a negative ion reaction. Amines such as $CH_3CH_2NH_2$, $(CH_3)_2NH$, and $(CH_3)_2CHNH_2$ (ΔH°_{acid}= 399.3 ± 1.1, 396.4 ± 0.9, and 397.2 ± 3.1 kcal mol^{-1}, respectively) also react via hydride- and methide-transfer pathways to give the same ionic products shown in Eqs. 4.4c and 4.4d.

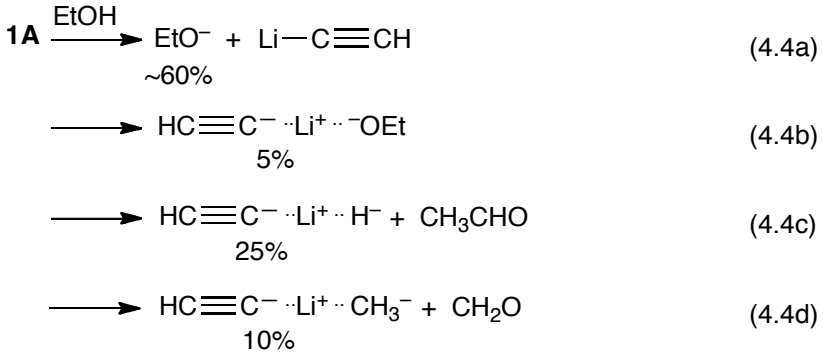

(4.4a)

(4.4b)

(4.4c)

(4.4d)

Fluorobenzene and furan (ΔH°_{acid} 387.2 ± 2.5 and 391.1 ± 0.4 kcal mol^{-1}, respectively) behave in a similar manner, although in the former case fluoride ion is transferred to lithium while in the latter instance lithium-hydrogen exchange takes place [Eqs. (4.5 and 4.6)].[14] In contrast, benzene (ΔH°_{acid}= 401.2 ± 0.2 kcal mol^{-1}) does not react with **1A**, toluene (ΔH°_{acid}= 382.3.2 ± 1.2 kcal mol^{-1}) simply protonates **1A**, and naphthalene (ΔH°_{acid}= 394.2 ± 1.2 kcal mol^{-1}) undergoes addition (44%), addition – H_2 (42%), acetylide formation (7%), and proton transfer (7%).

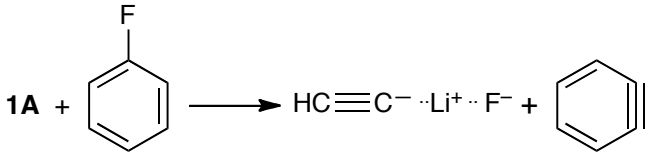

(4.5)

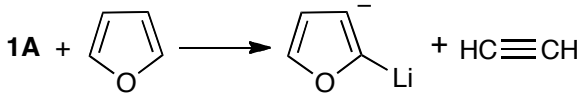

(4.6)

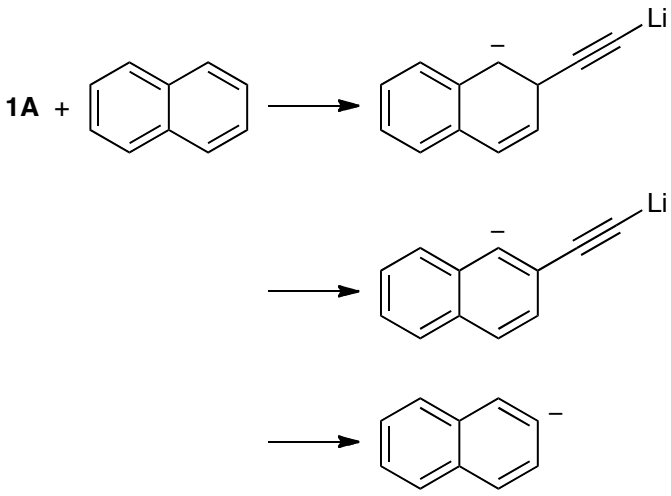

(4.7a)

(4.7b)

(4.7c)

Naphthalene is the weakest acid that was examined that protonated lithium acetylide anion. The overall reaction rate constant was found to be (1.3 ± 0.5) x 10^{-10} cm^3 $molecule^{-1}$ s^{-1}, which corresponds to 7 out of every 100 collisions leading to products given that the collision rate constant (i.e. k_{ADO})[15] is 1.93 x 10^{-9} cm^3 $molecule^{-1}$ s^{-1}. If one assumes that the inefficient proton transfer ($k_{P.T.}$ = (9.1 ± 3.8) x 10^{-12} cm^3 $molecule^{-1}$ s^{-1}, which corresponds to a reaction efficency of 0.5%) is endothermic, then the thermokinetic method[16] can be used to derive the acidity of lithium acetylide. That is, the Arrhenius equation is used to derive the endothermicity of the proton transfer (E_a) by solving Eq. 4.7, where $k_{P.T.}/A$ is 0.5% and T = 300 K. The resulting activation energy is 3.2 ± 0.6 kcal mol^{-1}, which leads to ΔH°_{acid}(**1H**) = 391.0 ± 1.3 kcal mol^{-1}. Substitution of a hydrogen in acetylene for a lithium leads to a 12.7 ± 1.3 kcal mol^{-1} decrease in acidity.

$$\mathbf{E_a = -RTln(}k_{P.T.}/A\mathbf{)} \qquad \mathbf{(4.7)}$$

To probe the acidity of **1H** further, G3,[17] G4,[18] and W1[19] computations were carried out since these methods are well established and known to generally be very accurate. The lowest energy structures for **1H** and **1A** are given in Figure 4.2, and the latter species is found to have a non-classical (bridging) structure as is typical for lithium.[20]

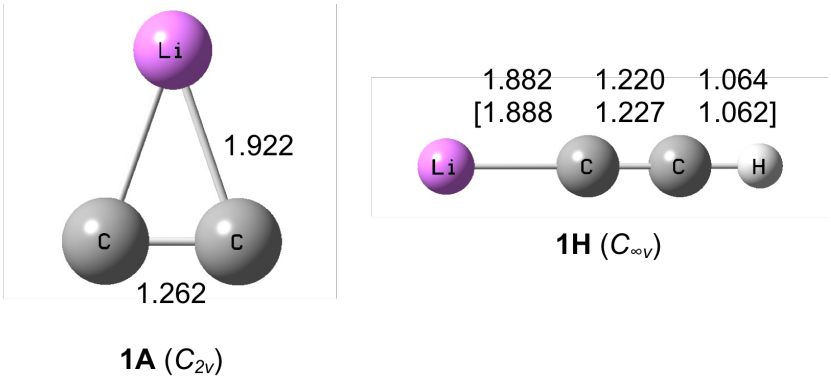

Figure 4.2. B3LYP/cc-pVT(+d)Z structures of lithium acetylide anion (**1A)** and its conjugate acid (**1H**). Bond lengths are in Å, and experimental values from an X-ray crystal structure (ref. 4) are in brackets

The predicted acidities at 298 K for acetylene and lithium acetylide are given in Table 1, and reproduce the experimental measurements to within 1.9 kcal mol^{-1} or less. This provides strong support for our experimental determination.

Table 4.1. Computed energetics for acetylene and lithium acetylide at 298 K.[a]

Cmpd(RH)	ΔH°_{acid}(RH)	EA($R^{\cdot}$)	BDE(RH)
HC≡CH			
G3	378.7	3.00	133.5
W1	378.6	2.94	132.6
expt	378.3 ± 0.1	2.969 ± 0.006	133.32 ± 0.07
LiC≡CH			
G3	389.1	1.73	114.6
G4	389.2	1.76	115.0
W1	390.4	1.69	115.6
expt	391.0 ± 1.3		

[a]Acidities and bond energies are in kcal mol^{-1}, electron affinities are in eV.

The electron affinity of the radical corresponding to **1A** provides another thermodynamic benchmark, but it could not be reliably measured in our apparatus. Reactions with electron transfer reagents were very fast, and the pressure in the reaction region is ~10 times greater than at the ionization gauge used to measure the pressure. Therefore, neutral reagent pressures below our measureable and controllable range (1 x 10^{-9} Torr) were required to slow the reactions down sufficently so that there was time to collisionally cool the reactant ion without it being depleted. Consequently, high-level ab initio methods were employed to compute this quantity. The G3, G4, and W1 electron affinities are given in Table 1 while CCSD(T), BD(T), and CAS-AQCC with the AVQZ basis set are provided in the supporting information. As the average value

(1.66 eV) is nearly the same as the BD(T) and W1 results, it is likely to be very close to the true value. This quantity can be combined with the experimental acidity of **1H** to obtain the homolytic C–H bond energy of LiC≡CH (115.7 kcal mol^{-1}). These results reveal that replacing an acetylene hydrogen by lithium decreases the BDE by 17.6 kcal mol^{-1} and the EA by 30.2 kcal mol^{-1} which is quite different than was observed for CH_3CO_2Li.[10a]

To explore the reactivity of **1A** further, it was reacted with a variety of compounds. Nucleophilic addition followed by the loss of hydrogen was observed with anthracene, styrene, and 3-fluorobenzaldehyde whereas this pathway is precluded with hexafluorobenzene, and consequently LiF was lost, presumably to afford pentafluorophenylacetylide anion (eq. (4.8)).

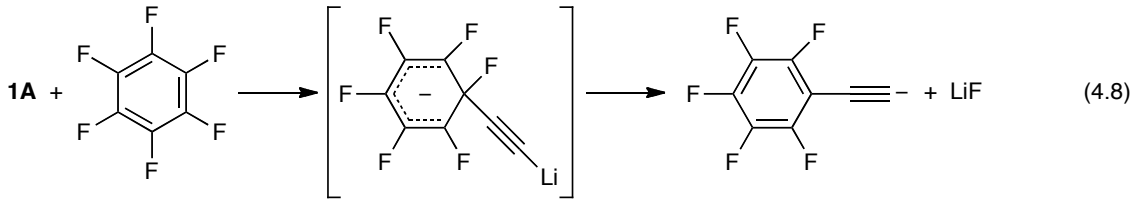

(4.8)

The highly reactive nature of **1A** also is seen in its reaction with carbon disulfide. Two products are formed, one is due to sulfur atom transfer and the other corresponds to addition followed by loss of lithium (eq. (5.9)). B3LYP/aug-cc-pVDZ computations indicate that the intially formed distonic ion is less stable than the cummulene structure $SCCCS^{\bullet-}$ and that there is a low barrier for the isomerization.

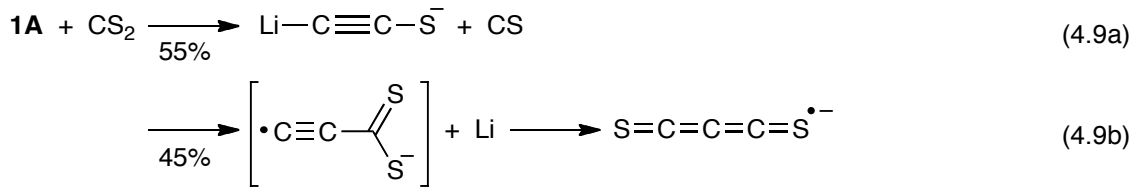

(4.9a)

(4.9b)

Lithiated anions can be generated in the gas phase by the decarboxylation and double decarboxylation of appropriate precursors. This work demonstrates that synthetically useful organolithiums anions can be prepared even in the absence of heteroatoms, and that the reactivity of the monomeric species can be probed in the absence of solvent effects. G3 and W1 computations also indicate that equation 4.1 is exothermic by 2.2 and 2.8 kcal mol^{-1}, respectively, which accounts for Mortier's finding that the disproportionation of lithium acetylide is reversible.

$$Li–C{\equiv}C–Li + HC{\equiv}CH \rightarrow 2\ Li–C{\equiv}CH \qquad (4.10)$$

Experimental Section

Gas-Phase Experiments. These studies were carried out using a FTMS consisting of an IonSpec electrospray ionization (ESI) cart with a 6" gold-plated cylindrical cell and a 3 T superconducting magnet. The inlet system was modified for greater flexibility by incorporating several leak valves, a gas ballast, and an additional pulse valve. Several reagents can be used in succession this way, and kinetic studies can readily be carried out too. Data acquisition and analysis was performed with a PC running the Omega 9 software package. ESI of a 3:1 MeOH/H_2O solution containing acetylenedicarboxylic acid (200 – 500 mM) and a small amount of LiOH was carried out at a flow rate of 10 ml mL^{-1} into a Z-spray (Micromass) ESI source. The resulting anions were extracted into a hexapole to build signal intensity and then were transported into the FTMS cell via a rf-only quadrupole ion guide. A pulse of argon was used to facilitate ion trapping and assist in vibrationally cooling them. Lithium acetylenedicarboxylate (*m/z* 119) was isolated using an arbitrary waveform excitation and subsequently fragmented by two sequential off-resonance excitations to afford $^{-}C{\equiv}CCO_2Li$ (*m/z* 75) and then $LiC{\equiv}C^{-}$ (*m/z* 31). The latter ion was cooled with a pulse of argon, isolated, and then allowed to react with different neutral reagents. Exact masses of all of the ions studied herein were determined to secure their chemical compositions, which was particularly valuable for differentiating species containing two oxygen atoms versus one sulfur atom.

Computations. G3,[17] G4,[18] and W1[19] computations were carried out as described in the literature using Gaussian 03 or 09[21] at the Minnesota Supercomputer Institute for

Advanced Computational Research or the National Computational Infrastructure (NCI) National Facility and the Australian Centre for Advanced Computing and Communications (AC3). Some density functional theory calculations also were carried out using B3LYP[22] and M06-2X[23] along with the aug-cc-pvdz and 6-31G(2df,p) basis sets, and subsequent single point energies were computed at the CCSD(T), BD(T),[24] and CAS-AQCC[25] levels of theory with the aug-cc-pVQZ basis set. All of the resulting energetics are reported as enthalpies at 298 K where small vibrational frequencies contributing more than 0.5RT to the thermal energy were replaced by 0.30 kcal mol^{-1}. Selected Cartesian coordinates and energies are provided in the Supporting Information.

Chapter 5

Enolates in 3-D, a Gas Phase Study of Deprotonated Adamantanone

The deprotonation of carbonyl compounds is a widely used method to generate stabilized anions as intermediates in organic synthesis. Generally, these reactions can be carried out using mild conditions for the deprotonation at the α–position because the charge is delocalized in the resulting enolate. In polycyclic systems where the α–hydrogens are located at a bridgehead position, the acidity will be greatly reduced when the carbon-carbon double bond of the enolate corresponds to an anti-Bredt olefin.[1] Deprotonation in such systems can occur at other sites, but the stabilization of the anion is not as great as for the α–enolate.[2] The resulting homoenolates can be stabilized through space, and have been a subject of long-standing interest both from a theoretical and a practical perspective.[3]

Acyclic systems and larger more flexible bridged species can readily be deprotonated by strong bases such as lithium diisopropylamide (LDA) or lithium tetramethylpiperidide (LTMP) to afford homoenolates. These anionic intermediates subsequently can be trapped in good yields with a variety of electrophiles.[1] In less flexible polycyclic systems such as adamantanone (**1**), only starting material or a small amount of reduced product is recovered.[4] The direct formation of the enolate or homo-

enolate of adamantanone has not been observed, however, some insight into its reactivity has been provided by studying its hydrogen-deuterium (H/D) exchange behavior. That is, three different sites undergo H/D exchange upon reacting **1** with *t*-BuOK in *t*-BuOH at 185 ˚C for 400 hours. The β−equatorial hydrogens exchange 15 times faster than the β−axial hydrogens and twice as fast as those at the α−position. This suggests that the β−equatorial position is the most acidic one in adamantanone,[5] but **1** is not very acidic as it undergoes H/D exchange 100 times slower than camphenilone (**2**). To investigate the enolates of adamantanone further, we report the regiospecific generation of the β− and γ− enolate anions and the acidity of adamantanone in the gas phase. The structures and reactivities of these ions also were probed via ion-molecule reactions and high-level calculations.

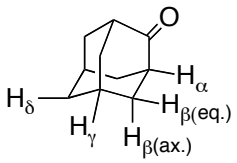

1

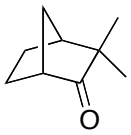

2

The deprotonation of adamantanone was experimentally investigated using a FT-ICR mass spectrometer by reacting **1** with a series of anions of known basicity. Observation of efficient proton transfer indicates that the conjugate acid of the base (BH) is a weaker acid than adamantanone. Slow proton transfer or no proton transfer suggests that adamantanone is more acidic than BH. Amide ($\Delta H^{\circ}_{acid}(NH_3) = 403.4 \pm 0.1$ kcal mol^{-1}) and ethyl amide ($\Delta H^{\circ}_{acid}(CH_3CH_2NH_2) = 399.3 \pm 1.1$ kcal mol^{-1}) were found to readily deprotonate adamantanone, but significant amounts of products (25%

and 40% respectively) corresponded to nucleophilic attack at the carbonyl carbon followed by the loss of water (eqs 5.1 and 5.2). This behavior is analogous to the reactivity of ketones with amines in solution,[6] and both $CH_2{=}N^-$ and 2-azaallyl anion have been previously generated in the gas phase.[8,9]

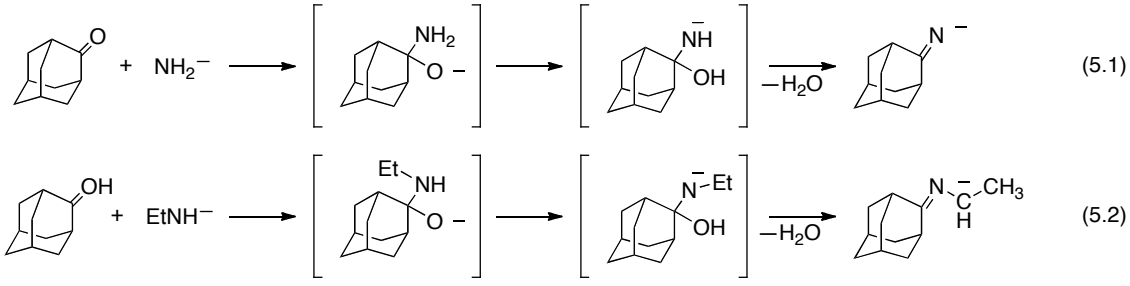

When **1** was reacted with dimethylamide ($\Delta H^\circ_{acid}((CH_3)_2NH) = 396.5 \pm 0.7$ kcal mol^{-1}), proton transfer was observed as the only product and the reaction occurred rapidly ($k = (1.90 \pm 0.13) \times 10^{-9}$ cm^3 molecules^{-1} s^{-1}). In contrast, hydroxide ($\Delta H^\circ_{acid}(H_2O) = 390.7 \pm 0.1$ kcal mol^{-1}), which is a weaker base, only led to an adduct (eq. 5.3), and fragmentation of this ion via collsion-induced dissociation (CID) regenerated the hydroxide ion. These results indicate that adamantanone is more acidic than dimethylamine and less acidic than water, so ΔH°_{acid}(**1**) $= 393.6 \pm 2.9$ kcal mol^{-1}.

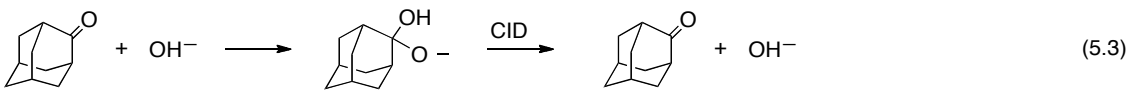

To gain insight into these observations, DFT computations using both the B3LYP and M06-2X functionals were carried out and the acidities of all 5 positions

were predicted. G3 energies were calculated too since this model chemistry has been extensively bench marked and found to be accurate typically to within 2 kcal mol^{-1}. All 3 approaches afford 5 different minima corresponding to the removal of the 5 different hydrogens, and a sixth isomer that corresponds to the cyclization of a β anion. The results are given in Table 1, and predict that the β−axial position is the most site in adamantanone. The preferred structure of the anion, however, is unclear because the energy difference between the cyclic and open β−axial isomer is small, and the favored species depends upon the method that is used. All of the calculations are in good accord with the experimental determination and indicate that the β−equatorial anion is approximately 5 kcal mol^{-1} more basic than the axial ion except for the G3 calculation. In this instance, the geometries of the two ions are similar, but this probably is a reflection of the small (6-31G(d)) basis set, which is used in this method for obtaining the geometries. The M06-2X functional also was used to investigate the interconversion barriers between the three β−anions. Epimerization of the axial to the equatorial anion is predicted to have a barrier of 5.9 kcal mol^{-1} while its isomerization to the cyclized species has a smaller barrier of 3.7 kcal mol^{-1}. No direct pathway was located for the cyclization of the equatorial anion, but these barriers suggest that the β−anions will readily equilibrate between each other.

Table 5.1. Computed B3LYP, M06-2X, and G3 acidities at 298 K for all of the different positions in adamantanone.[a]

Position	$\Delta H^{\circ}_{acid}(1)$[b]			
	B3LYP DZ	**MO6-2X DZ**	**MO6-2X TZ**	**G3**
α	401.1	399.7	400.4	403.7
β–axial	393.9	395.4	396.2	396.8
β–equatorial	398.9	399.8	400.8	397.0
β-cyclic	396.3	393.8	394.1	397.3
γ	396.2	397.7	398.4	400.2
δ	402.0	401.5	402.6	404.4

[a] All values are in kcal mol^{-1}.[b] DZ and TZ stand for aug-cc-pVDZ and maug-cc-pVT(+d)Z, respectively.

To further examine the deprotonation site of adamantanone, the β–anion was regiospecifically generated via the fluoride-induced desilylation of 4-trimethylsilyl-adamantan-2-one[10] (eq. 5.4). The resulting anion was then transferred into a clean reaction cell where it was exposed to variety of neutral reagents to probe its reactivity. Water rapidly protonated **1β** whereas the anlogous reaction with dimethylamine was inefficient ($k = 3.14 \pm 0.14 \times 10^{-10}$ cm^3 $molecule^{-1}$ s^{-1}). Less acidic acids such as ethylamine and ammonia did not undergo proton transfer, but the addition - H_2O products shown in eqs. 1 and 2 were observed. An equilibrium constant can be determined from the forward and reverse reaction rate constants with dimethylamine, and this enables us to assign ΔH°_{acid} (**1**) = 394.1 ± 1.4 kcal mol^{-1}, which is in good accord with the bracketing results.

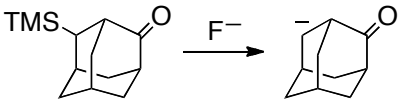

3 1(β) (5.4)

A similar approach was used to bracket the electron affinity of the radical corresponding to **1β**, but instead of using a series of acids of known strength, a series of electron transfer reagents with known electron affinities were employed. Electron transfer was not observed between **1β** and 2-fluorobenzaldehyde (EA = 0.64 ± 0.11 eV) or 2-fluorobenzonitrile (EA = 0.70 ± 0.10 eV), but readily occurred with 4-trifluoromethyl benzonitrile (EA = 0.76 ± 0.09 eV) and perfluorotoluene (EA = 0.86 ± 0.11 eV). This enables us assign EA = 0.73 ± 0.07 eV to the radical corresponding to **1β,** which is in excellent accord with the M06-2X/maug-cc-pVT(+d)Z[9] and G3 predictions of 0.72 eV, but is less well reproduced by B3LYP (Table 2).

Table 5.2. Computed B3LYP, M06-2X, and G3 electron affinities at 298 K for all of the different positions in adamantanone.[a]

Position	EA(**1r**)			
	B3LYP DZ	**M06-2X DZ**	**M06-2X TZ**	**G3**
α	0.59	0.64	0.64	0.65
β-axial	0.48	0.43	0.43	0.75
β-equatorial	0.70	0.62	0.63	0.76
β-cyclic	0.58	0.68	0.72	0.74
γ	0.66	0.58	0.59	0.66
δ	0.40	0.40	0.39	0.62

[a] All values are in eV.[b] DZ and TZ stand for aug-cc-pVDZ and maug-cc-pVT(+d)Z, respectively.

The homolytic bond dissociation energy for adamantanone at the β−position can be derived from the acidity and electron affinity determinations using the thermodynamic cycle: BDE (HA) = ΔH°_{acid} (HA) – IP($H^{\cdot}$) + EA($A^{\cdot}$), where IP($H^{\cdot}$) is the ionization potential of hydrogen atom and is well known to be 313.6 kcal mol^{-1}. Consequently, BDE = 97.3 ± 2.1 kcal mol^{-1} is obtained.

Along with exploring the thermochemistry of **1β**, its general reactivity was examined. In solution enolates are commonly used to make C-C bonds via their reactions with electrophiles. As seen in eq. 5.5a, **1β** reacts with hexafluorobenzene by a nucleophilic aromatic substitution to form a transient intermediate which expels HF to yield the β−substituted homoenolate; this type of transformation is a well-known pathway in the gas-phase for α−enolates. A small amount of pentafluorophenoxide

surprisingly also was observed. This product ion is characteristic of O-reactivity in ion-molecule reactions (eq. 5.5b) which was unanticipated since M06-2X/maug-cc-pVT(+d)Z calculations indicate that protonation at oxygen is 26.3 kcal mol^{-1} less favorable than at carbon.

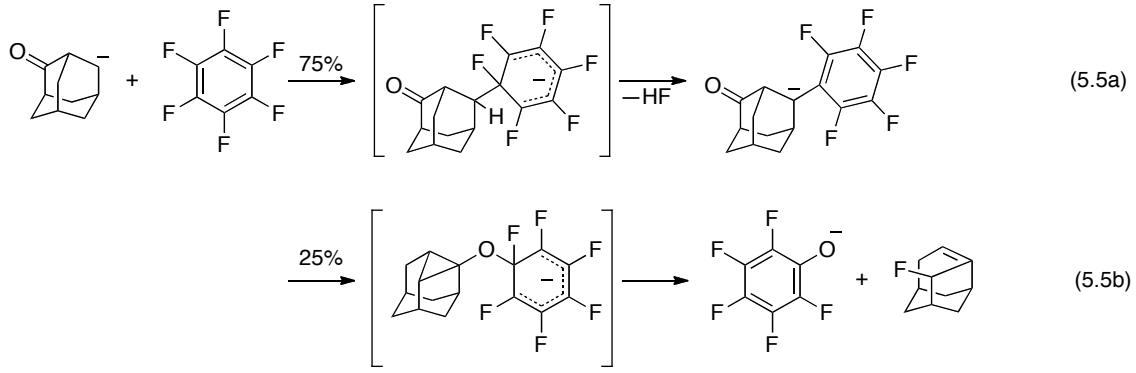

(5.5a)

(5.5b)

When **1β** was reacted with 2-fluorobenzaldehyde, the predominant reaction pathway was proton transfer (60%) but nucleophilic attack at the carbonyl also occurred. The resulting adduct was observed but a subsequent elimination of fluorobenzene led to a cross metathesis product (eqs. 5.6a and 5.6b).

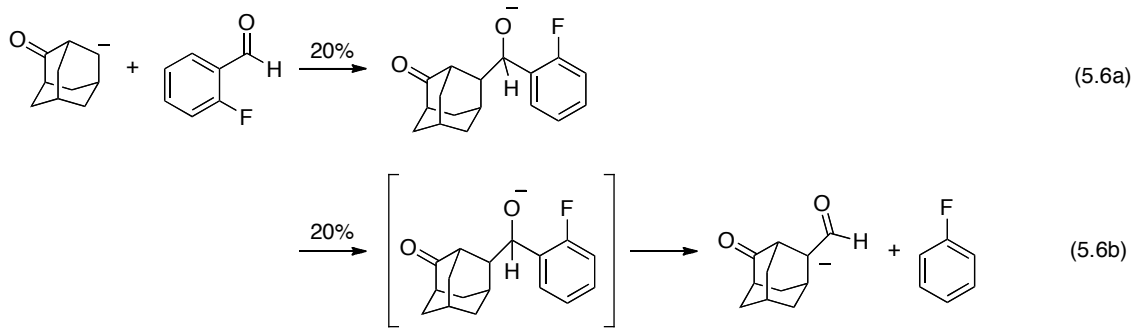

(5.6a)

(5.6b)

The reactivity of **1β** was explored with additional electrophiles such as COS. In this case two products were observed, one of which corresponds to sulfur atom transfer and the other leads to a thiocarboxylate anion (eqs. 5.7a and b).

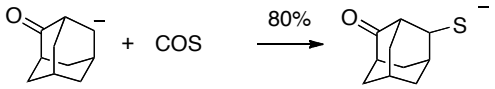

(5.7a)

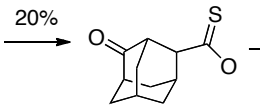

(5.7b)

Deprotonation of adamantanone to afford the γ-anion is not the most favorable pathway, but our calculations indicate that there is a significant long range stabilization. 5-Trimethylsilyladamantan-2-one is the obvious precursor for this ion, but it is not readily available, whereas 5-carboxyadamantan-2-one is known and can be synthesized in two steps from the adamantanone.[11] Therefore, this compound was prepared, and upon electrospray ionization, the corresponding carboxylate was readily generated (eq. 5.8). Collision-induced dissociation of the carboxylate led to the loss of carbon dioxide and the formation of an ion with the correct *m/z* ratio ($C_{10}H_{13}O$, m/z = 149). Proton transfer was found to readily take place with trifluoroethanol ($\Delta H^{\circ}_{acid}(CF_3CH_2OH)$ = 361.7 ± 2.5 kcal mol^{-1}) but no reaction was observed with acetone ($\Delta H^{\circ}_{acid}(CH_3)_2CO$) = 369.1 ± 2.1 kcal mol^{-1}). This suggests a proton affinity of 365.1 ± 4.0 kcal mol^{-1} for the *m/z* 149 ion, but this is much lower than that predicted for the γ-anion and is indicative of an α–enolate.

Calculations at the M06-2X/aug-cc-pVDZ level on the ring opened form of **1γ** give a proton affinity of 363.0 kcal mol^{-1}, which is in accord with the experimental

observations. As for the ring opening barrier (eq. 9), it was computed at the B3LYP/aug-cc-pVDZ , and M06-2X/aug-cc-pVDZ, M06-2X/maug-cc-pVT(+d)Z levels, and found to span from 5.4 (B3LYP) to 7.2 (M06-2X/aug-cc-pVDZ) kcal mol^{-1}. These predictions suggest that **1γ** maybe hard to form, and that the decarboxylation product is the ring-opened α–enolate anion shown in eq. 5.9.

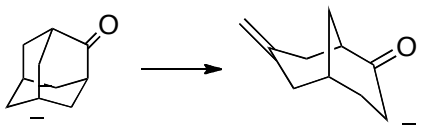

(5.9)

Along with confirming theoretical predictions of the acidity of adamantanone, the experimental results provide interesting insights into the lack reactivity of adamantanone with strong bases in solution. The fluorodesilylation of **3** in condensed media, however, might serve as a synthetically useful approach for introducing substituents at the β position of adamantanone.

Experimental Methods

4-trimethylsilyl-adamantan-2-one (3) was synthesized via 3 steps from adamantanone. Adamantanone was converted to 4-bromoadamantan-2-one,[9] which was then protected with ethylene glycol as the corresponding ketal and subsequently converted to the desired product.[10]

5-carboxyadamantan-2-one was synthesized from adamantanone in two steps via a previously reported procedure.[11]

Gas-phase experiments: A dual cell model 2001 Finnigan Fourier transform mass spectrometry was used with a 3 T superconducting magnet and IonSpec (now Varian) electronics including the Omega 8.0 data system. 2-Adamantanone and 4-trimethylsilyladamantan-2-one[ref] were introduced into the ICR cell at static pressures via a direct inlet metered with a Granville-Philips (model 203) variable leak valve. Amide ion was generated by election impact ionization (7.5 eV) of a pulse of ammonia and was allowed to react with ethylamine, dimethylamine or water to afford their conjugate bases. The resulting ions were subsequently transferred into the second ICR cell where they were isolated, cooled with an argon pulse, and then allowed to react with adamantanone. Deprotonation of a static pressure of **1** was carried out using isolated ethylamide, which was produced by electron impact (7.5 eV) of a pulse of ethylamine. The resulting M–1 ion of adamantanone was transferred into the second reaction cell, cooled with a pulse of argon, and isolated before it was allowed to react with a static pressure of the neutral reagent of interest. Alternatively, fluoride was produced from NF_3 and then allowed to react with 4-trimethylsilyladamantan-2-one.

The resulting M–TMS ion was transferred into the other cell, cooled with a pulse of argon, and isolated before probing its reactivity with different reagents.

The electrospray experiments were carried out with an IonSpec ESI FTMS equipped with a 3 T magnet. Aqueous methanol solutions (30 mM, 3:1 (v/v) CH_3OH/H_2O) of the carboxylic acid were sprayed into the instrument, and the resulting carboxylate anion was fragmented using an sustained off resonance irradiation (SORI). The resulting decarboxylate ion was cooled with a pulse of argon, isolated, and then allowed to react with a static pressure of trifluoroethanol and acetone.

Computations: All structures were fully optimized using the B3LYP and M06-2X density functionals along with aug-cc-pVDZ and maug-cc-pVT(+d)Z (M06-2X only) basis sets. Vibrational frequencies were computed for each structure to confirm that they are energy minima on the potential energy surface, and to enable temperature corrections to 298 K to be made. Unscaled frequencies were used for this purpose, and small vibrational modes which contribute more than 1/2(RT) to the thermal energy were replaced by 0.30 kcal mol^{-1}. G3 energies were computed as described in the literature. All of the resulting energetics are reported as enthalpies at 298 K in this work. The B3LYP calculations were carried out using Gaussian 03 whereas Gaussian 09 was used for the G3 and M06-2X computations. In both cases, workstations at the Minnesota Supercomputer Institute for Advanced Computational Research were employed.

Chapter 6

Mass Spectroscopy

6.1 Introduction

Numerous experimental methods have been developed to study the structure of ions in the gas-phase. The study of these ions has shed insight into a variety of chemical problems including atmospheric chemistry, reactive intermediates, and biological systems. These experiments fall into two general categories – studying fragmentation patterns or studying ion reactivity.[1]

In order to study fragmentation patterns, an external stimulus is used to induce dissociation. Examples of this type of experiment include collisional-induced dissociation (CID), electron capture dissociation (ECD), and infrared multiphoton dissociation (IRMPD). While these techniques are effective at providing information about the connectivity of atoms that make up an ion, they are insensitive to an ion's conformation. They may also provide misleading connectivity information if the ion can readily interconvert between isomers.

The second approach is to use ion-molecule reactions to determine the reactivity and thermodynamic properties of the ion. If the ion is allowed to interact with neutral reagents that behave in a known manner, the indentity of the unknown species often can be inferred by comparison. Additionally, experimentally determined thermodynamic parameters can be compared to DFT computations.[2]

While a more direct approach is desired, this is problematic because columbic repulsion limits the concentration of trapped ions that can be produced. This difficulty can be overcome by the use of action spectroscopy. This technique uses mass spectrometry to indirectly detect a change in population of ions induced by the absorption of light, instead of directly measuring absorbance. Action spectroscopy, therefore, maintains the high sensitivity of a mass spectrometry method, while obtaining new, useful structural information.[3]

Unfortunately, a single photon of infrared light does not typically contain enough energy to induce fragmentation of an ion. A variety of approaches have been developed to circumvent this problem including: tagging,[4] IR-UV-Vis hole burning,[5] and tunable IRMPD.[3] Tagging experiments attach a weakly interacting neutral to the ion of interest; this neutral is lost upon absorption of a photon. In IR-UV-Vis hole burning experiments, IR absorption is measured by the depletion of fragmentation occurring as a result of subsequent UV-Vis absorption. IRMPD uses a high flux of IR radiation facilitating repeated absorption of IR photons followed by intramolecular vibration relaxation (IVR) until the ion it reaches it fragmentation threshold.[6]

Each of these experiments offers its own set of advantages and disadvantages. The main limitation of the use of IRMPD has been the need to use one of the few free electron lasers (FEL) to generate the tunable IR light required for these experiments. Overall, however, the use of IRMPD has the potential be more widely utilized because it does not require an ion to contain a chromophore or be perturbed by the interacting with reporter reagents.

6.2 Bench Top OPO/OPA Lasers

With advancements in non-linear optical (NLO) crystals, it is now possible to generate reasonable quantities of tunable IR light in a bench top system. [7] Unlike early bench top systems, which used gratings to filter a single CO_2 emission wavelength from a broadband CO_2 laser, NLO systems use a single wavelength pump laser that is transformed by one or more NLO crystals to the desired wavelengths of IR light.

When light passes through material that has a noncentrosymmetric structure the interaction of the light with the crystal depends on the relationship of the polarity of the light to the crystal axis. In a 2nd order NLO material, one of the polarizations will behave nonlinearly along a given crystal axis. This polarization is termed the extra-ordinary polarization, whereas the other polarization will behave linearly and is called ordinary polarization.[8] This effect can result in the transformation of light through one of four 2nd order processes. The first process is second harmonic generation (SHG) (Figure 6.1), which involves two photons of the same frequency interacting inside of the crystal to generate a single new photon having a frequency that is double the initial frequency.

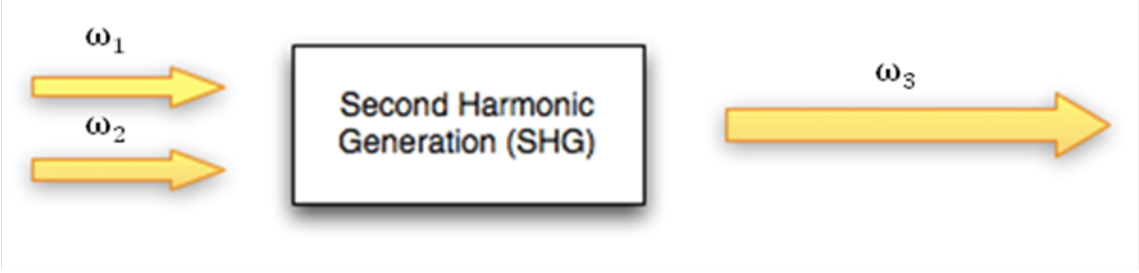

Figure 6.1. Second Harmonic Generation; $\omega_1 = \omega_2$, $2\omega_1 = \omega_3$

A similar process can take place when two photons of different frequency interact in the crystal to form a new photon where the frequency is the sum of the frequencies of the two initial photons (Figure 6.2).

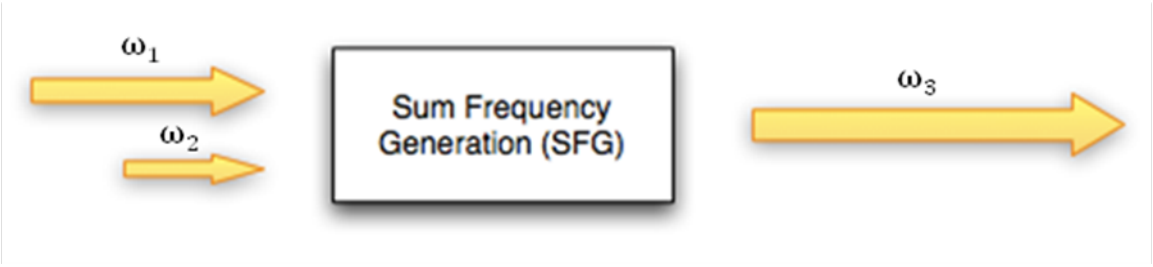

Figure 6.2. Sum Frequency Generation; $\omega_1 \neq \omega_2$, $\omega_1 + \omega_2 = \omega_3$

The third NLO process is called difference frequency generation (DFG). In this process two photons interact in the crystal and the more energetic one, is decomposed into 2 photons. One of the resulting photons is equal in frequency to the smaller of the initial photon frequencies and the second that is the difference in frequency between the two initial photons (Figure 6.3); this lends to an amplification of the smaller intial frequency (ω_2).

Figure 6.3 Difference Frequency Generation; $\omega_1 - \omega_2 = \omega_3 (+ 2\omega_2)$

The last category of NLO processes, known as optical parametric generation (OPG), takes place when a high intensity of photons of a single wavelength interact with the NLO media and a single photon is decomposed into two new photons (Figure 6.4). The frequency of the two photons produced varies as a function of the incident angle of the light or temperature of the crystal. This process is commonly utilized as a method of generating tunable light from a single wavelength.

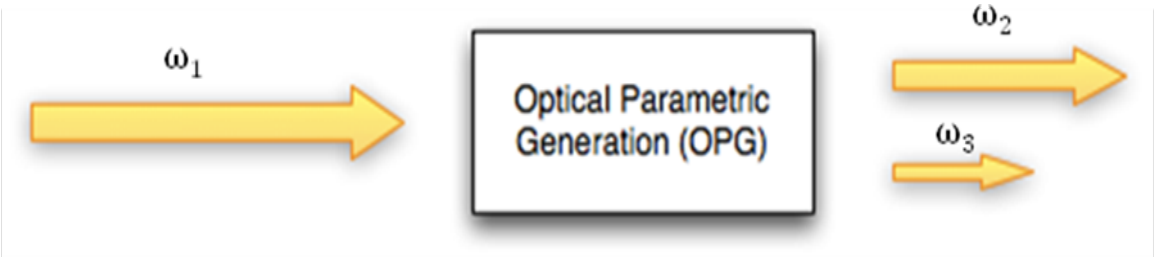

Figure 6.4. Optical Parametric Generation; $\omega_1 = \omega_2 + \omega_3$

Even though these processes have become more general with new advancements in NLO materials, some of the early vocabulary has been retained even though to though its application is no longer obvious. For example, the three different frequencies of light involved in OPG are referred to as the pump, the signal, and the idler. One could envision several meanings for these terms, they simply refer to the frequency of the light in descending order as seen in Figure 6.5.

Figure 6.5. Optical Parametric Generation; $\omega_P > \omega_S > \omega_I$

6.3 Laser Vision OPO\OPA Systems.

The Laser Vision OPO\OPA is a commercially available system that can produce tunable photons (710-885nm [14,085 – 11,299 cm^{-1}] and 1.35 to 5.0 microns [7,407 - 2,000 cm^{-1}]) at a high enough intensity for IRMPD spectroscopy. This system makes use of a combination of 6 nonlinear optical crystals that are broken into 3 different stages. The system is pumped by a Q-switched Nd:YAG laser (Continuum Surelight II) that produces the 1^{st} harmonic (1064 nm), and can produce up to 500 mJ per pulse at 10 Hz. All crystals are positioned such that the e-wave runs parallel to the laser table so that any reflections are trapped within the laser box.

As seen in Figure 6.6, the horizontally polarized pump light (thus defined as e) is brought into the box with 2 steering mirrors. The beam is then split into 2 paths by a beam splitter, which is mounted at an angle of 45^0 and allows 60% of the light to be transmitted and 40% to be reflected. The reflected portion passes through a half wave-plate (HWP) on a rotation mount and then passes into a potassium titanyl phosphate, (KTP) crystal (crystal 1). Within the KTP crystal the light undergoes SHG to yield vertically polarized 532 nm light. The HWP prior to this crystal serves as a method for variable attenuation of the amount of 532 nm light produced. A dichroic mirror reflects the 532 nm light and lets the residue 1064 nm light to pass into the beam dump. **NOTE:** Even if you are not producing 532 nm light, 1064 nm light is still present all the way until the beam dump.

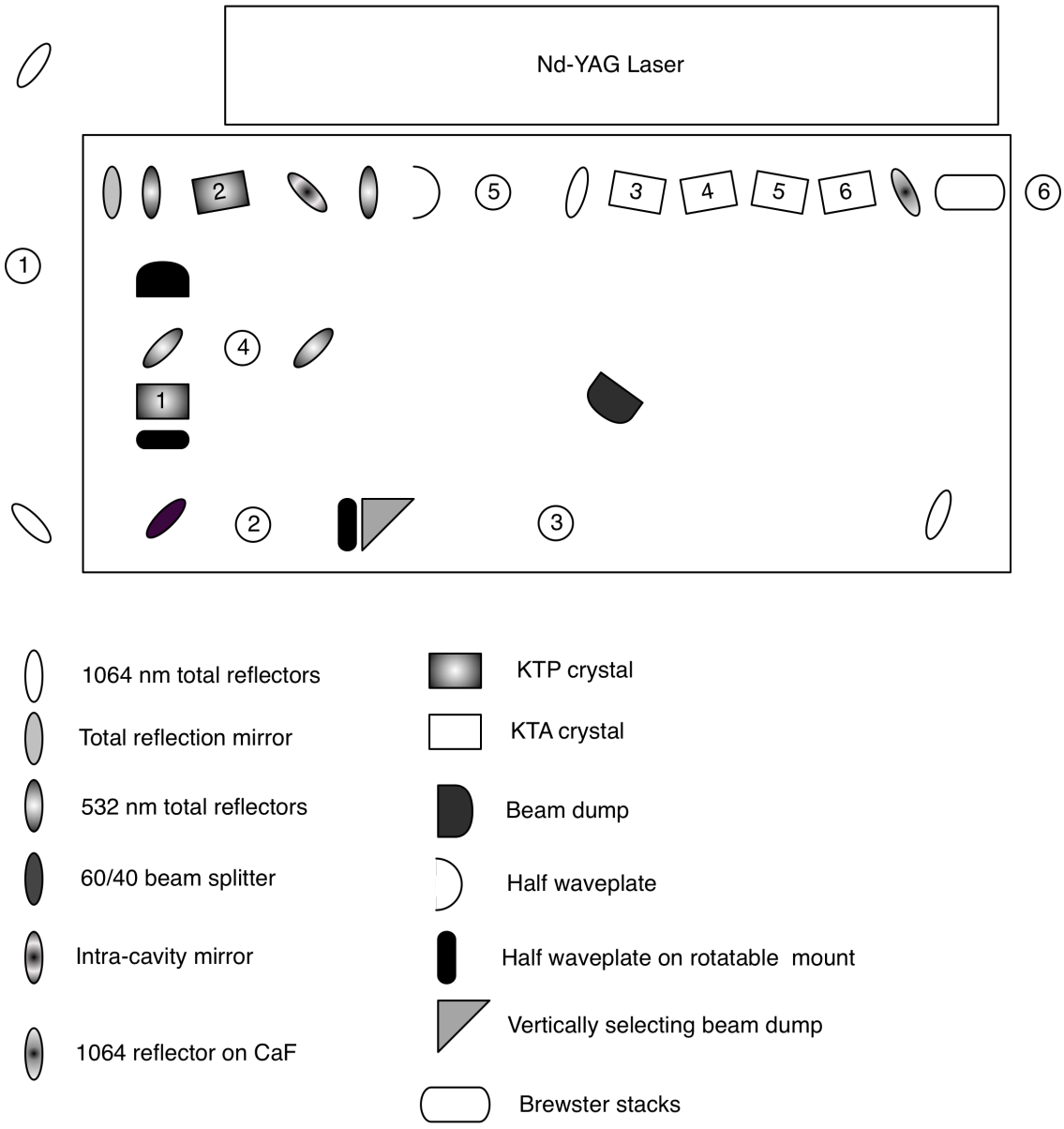

Figure 6.6. Layout of the Laser Vision OPO/OPA System.

Table 6.1. Sample set of power reading with OPO set at 773 nm.

Position	mJ/pulse	
1	480	
2	285	
3	270	
4	95	
5	18	
6	4	OPO only (Near IR with no amplyfication
6	80	Singal and Idler of OPA (Near IR and Mid IR)
6	26	Idler only (Mid IR)

The 532 nm light is then brought into an optical parametric oscillator (OPO) cavity by dichroic mirror that is reflective for 532 nm light mounted at a 45^0 angle to the cavitiy (Figure 5.6). The cavity of the OPO serves to build up enough intensity for crystal 2 (Type II, KTP, 60^0, e,o,o) to undergo OPG (where e,o,o refers to the polarization of the signal, idler, pump). The 532 nm pump produces a signal beam that exits perpendicular to the crystal face that is (e) and is in the visible range. It also produces an idler that is ordinary in the near IR along the trajectory of the oscillator cavity and exits through the output coupler.

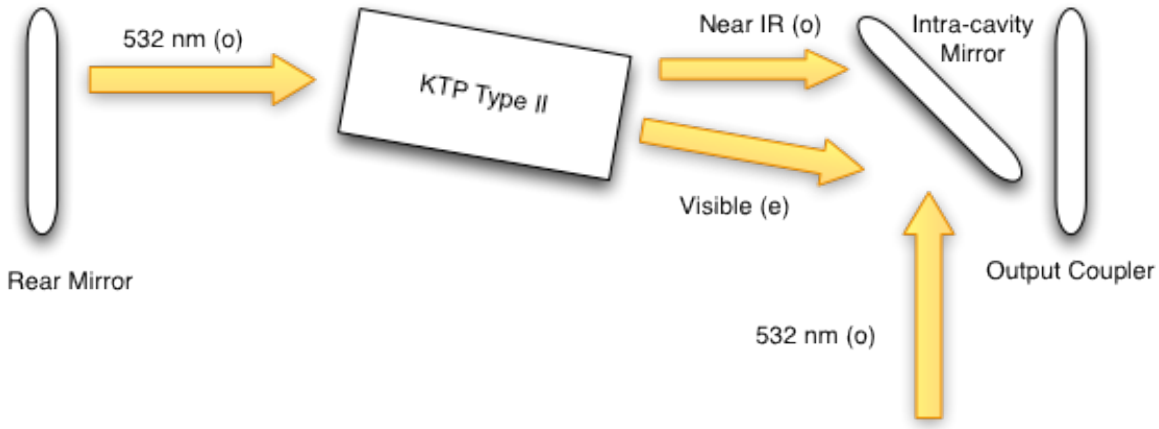

Figure 6.7. Optical Parametric Oscillator; $\omega_1 = \omega_2 + \omega_3$.

The resulting idler light is brought into the third stage of the OPO/OPA and combined with the portion of the 1064 nm light that was transmited through the beam splitter. Both frequencies of light are passed through four potassium titanyle arsenate (KTA) crystals (Crystals 3-6). In order for the 1064 nm photons to interact with the Type II KTA crystals that are (e,o,o), the polarization of the 1064 nm light is reversed by a HWP mounted on a rotation stage, and a polarization filter removes any residual horizontally polarized light. DFG transforms the 1064 nm photon into a near IR and mid IR photon (Figure 6.8).

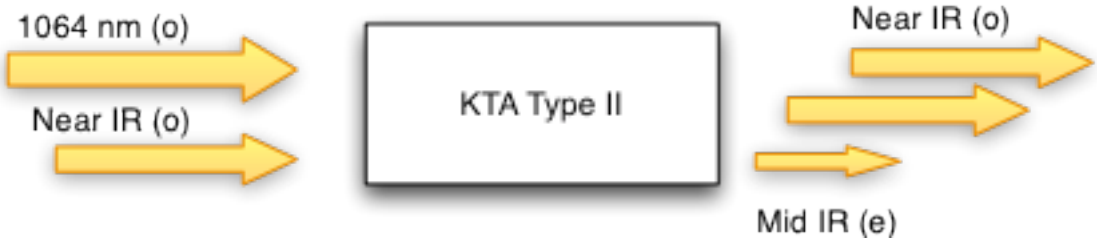

Figure 6.8. Optical Parametric Amplification of Near IR in a KTA crystal.

Once mid-IR photons are produced in the first crystal it can also undergo DFG with the 1064 nm pump to produce both near IR and mid IR. Commonly referred to as Optical Parametric Amplification (OPA) (Figure 6.9).

Figure 6.9. Optical Parametric Amplification of Mid IR in a KTA Crystal.

When these processes are combined across the 4 crystals it should lead to a 41and 40-fold amplification of the power in the near IR mid-IR photons. Unfortunately, as seen in Table 6.1, only a modest increase of power is achieved (~13.5 times) as the efficiency for this process is low. Also, there is a loss of the mid IR light through SFG with 1064 nm light to yield visible light.

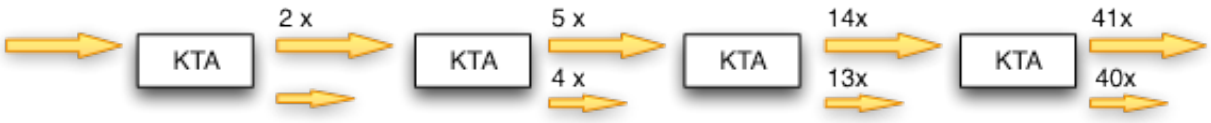

Figure 6.10. Optical Parametric Amplification; $\omega_1 = \omega_2 + \omega_3$.

Crystals 2-6 are mounted on velocity motors that allow them to rotate in the extraordinary plane. As seen in Figure 6.11, the wavelength of the mid-IR photon produced can be changed by angle tuning the OPO. It is important to note that the angle

shown in Figure 6.11 is referenced to the crystal axis not the face of the crystal. The difference is approximately 60^0, and to achieve this exact number the angle must be calibrated.

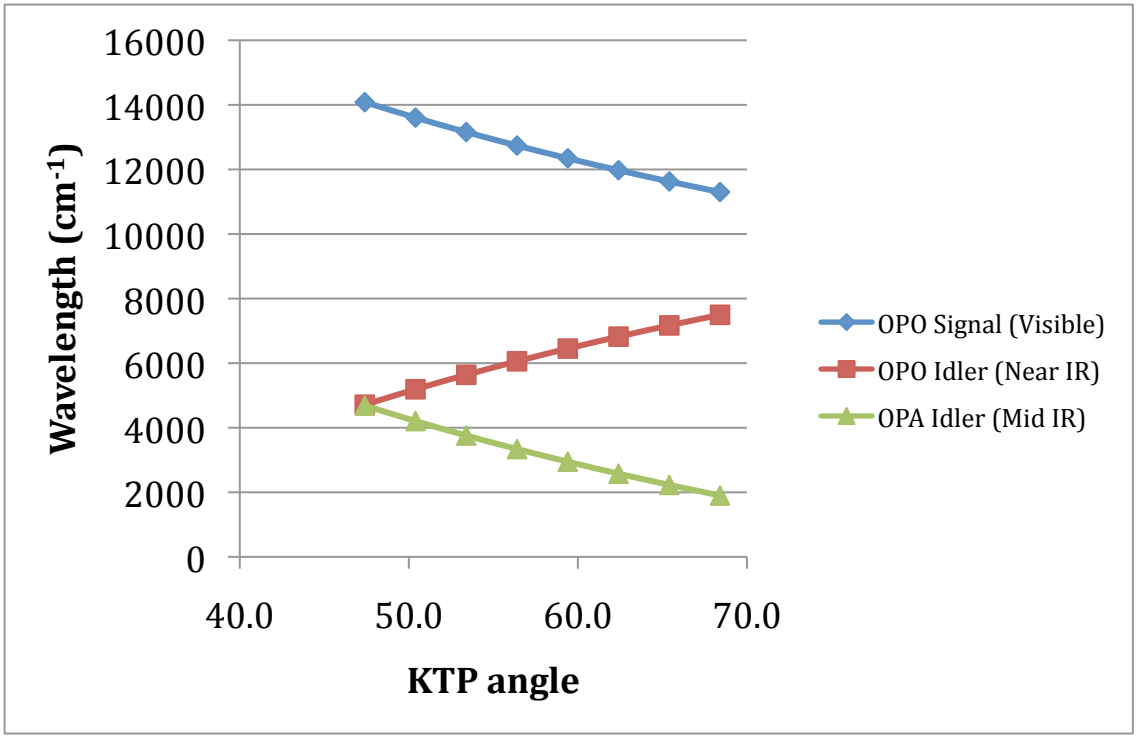

Figure 6.11. Wavelength as a Function of Angle of the KTP Crystal.

In order to achieve phase matching in the OPA, it is necessary to angle tune each of the KTP crystals to the correct acceptance angle. This angle can be found at a given wavelength for each of the crystals by tuning the position of each of the crystals for maximum IR power. Figure 6.12 is a plot of the motor position for each of the crystals vs. OPO wavelength. Each of the these curves can then be fit to a polynomial expansion

and from this it is possible to obtain coefficients for their motions as function OPO wavelength. This allows for the scanning process to be completely automated.

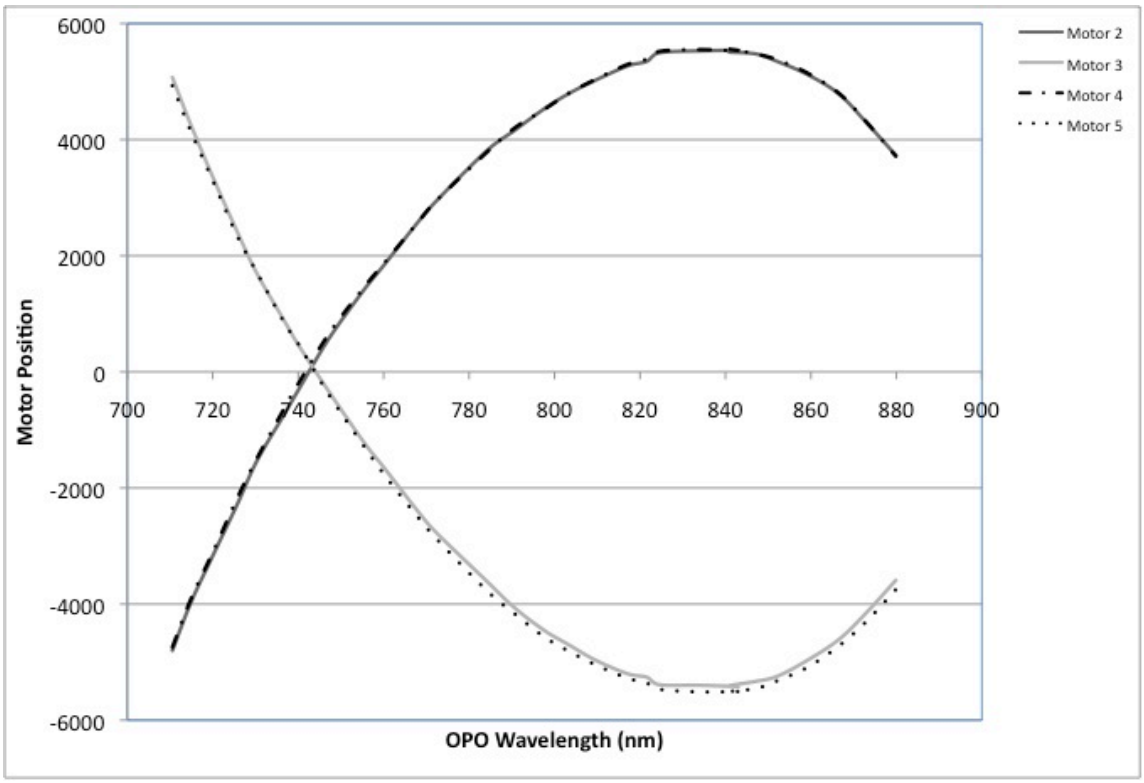

Figure 6.12. Plot of OPA motor positions vs. OPO Wavelength.

The last step in generating IR light for the desired experiment is to remove the undesired component from the output. This is accomplished by passing the beam through several silicon waveplates that are mounted at Brewster's angle, which depending on their orientation will select one polarization over the other.
By selecting for only the (e) polarization, the desired Mid-IR is obtained. Figure 6.13 shows a plot of the power corrected to a per-pulse energy as the wavelength range of interest is scanned.

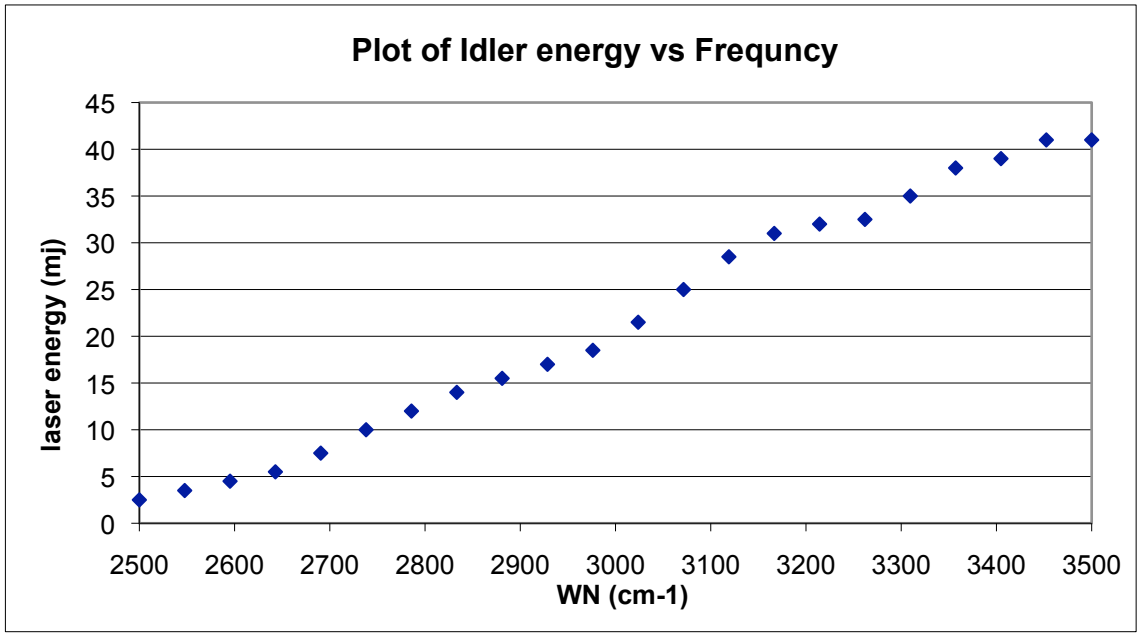

Figure 6.13. Plot of Idler Energy vs. Wavelength (cm^{-1}).

6.4 IRMPD Setup

IRMPD action spectroscopy requires the collection of individual IRMPD mass spectra for a series of wavelengths. These data are then plotted as the percent of fragmentation as a function of wavelength. Acquiring the individual mass spectra is

essentially the same process as used for other FT-MS experiments with the exception that the ions are exposed to IR radiation for fixed periods of time before detection. The irradiation of the ion cloud within our FT-MS requires that the light produced be brought in from the laser by a series steering mirrors and focused (with a 1 m focusing mirror) into the vacuum chamber through CaF_2 window. (Figure 6.14) The timing and duration of the irradiation is control by the addition of a mechanical shutter (EOPC SH10, 15 ms response time). This shutter blocks the lights path to the FTMS cell and only allows it to pass when opened with a 10 V pulse produced at the appropriate time by the mass spectrometer.

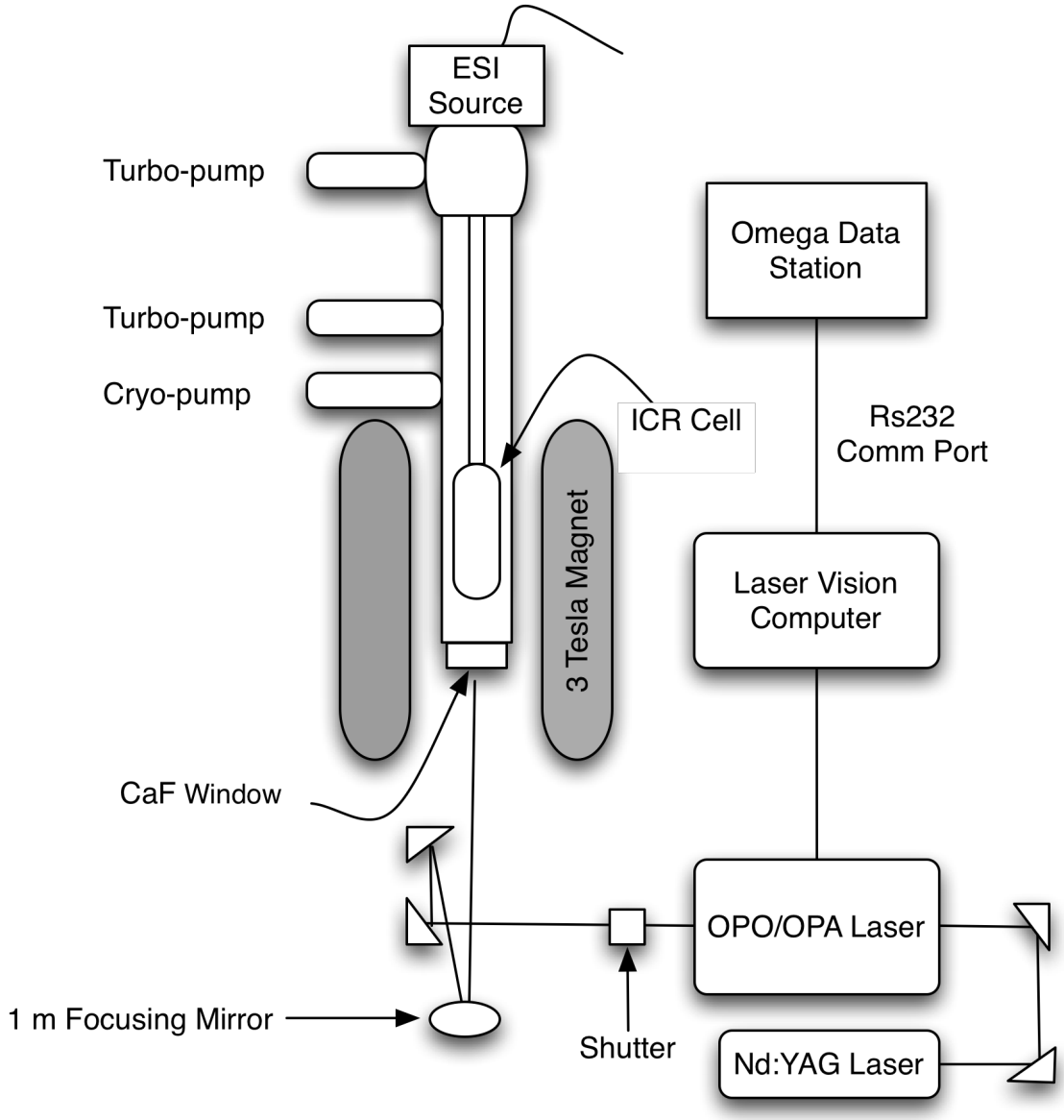

Figure 6.14. Schematic of the IRMPD Setup.

6.5 Automated Data Acquisition

Automating the acquisition of mass spectra by interfacing the FT-MS and Laser Vision control system is necessary due to the amount of data generated during a typical experiment. This process dramatically decreases the amount of time needed to acquire

the composite spectrum, which not only speeds the experiment up but also improves it considerably. That is, the ion signal fluctuates less, the laser power is more constant, and there is less opportunity for the alignment to change all of which tends to lead to to better data. Automation also allows this composite spectrum to be acquired as a chromatogram in the Omega data system, which allows for more detailed, and dramatically faster, data analysis.

To automate the collection of spectra, a software tool was developed to interface the Omega scripting language to the Laser Vision system through an RS-232 connection. Within the Omega software, a script is activated and the desired parameters for spectrum collection are utilized. This script signals the laser to move to a desired wavelength and holds it there until a response from the laser is received. This response then triggers the Omega software to acquire the MS signal data for the aforementioned wavelength. This process is repeated, stepping through the spectral range of the laser system and collecting individual mass spectra at each wavelength. The data are then saved to a chromatogram file for subsequent processing.

The Omega software runs within the Visual Basic environment and can modified via the use the Visual Basic scripting language (VBScript). Though this allows for a variety of modificantion, the modern conveniences of Wscript are not available. This is relevant because direct method to allow for a time delay to listen for the response of the laser is containted in Wscript and is not accessible via VBScript. To overcome this problem, an executable was written as a non-memory intensive way of counting. This executable is called via the external application property of Omega object. It should also be noted that RS-232 communications are controlled through the

MSComm object, which Microsoft does not allow non-developer access, so the NETComm.ocx wrapper is used to call the MSComm object.[9]

6.6 Proton Bound Dimer of Glycine

In one of the seminal works for this technique using FT-ICR, McLafferty et. al. explored the IRMDP spectrum of the proton bound dimer of glycine.[10] Since the spectrum of this ion has been well established, it was chosen as our initial substrate to study. Figure 6.15 shows our results plotted in the same form as McLafferty et al. (-ln(depletion) vs. Wavelength). Here the exposure times are adjusted to 15s(experimentally they were determined at 5 s for 3550 to 3580 cm^{-1} and 60 s for the 3350 cm^{-1}) and the depletion is adjusted for laser power as seen in figure Figure numer needed. These results generally match those of McLafferty et al., but we see a much

higher relative intensity for the dominant peak.

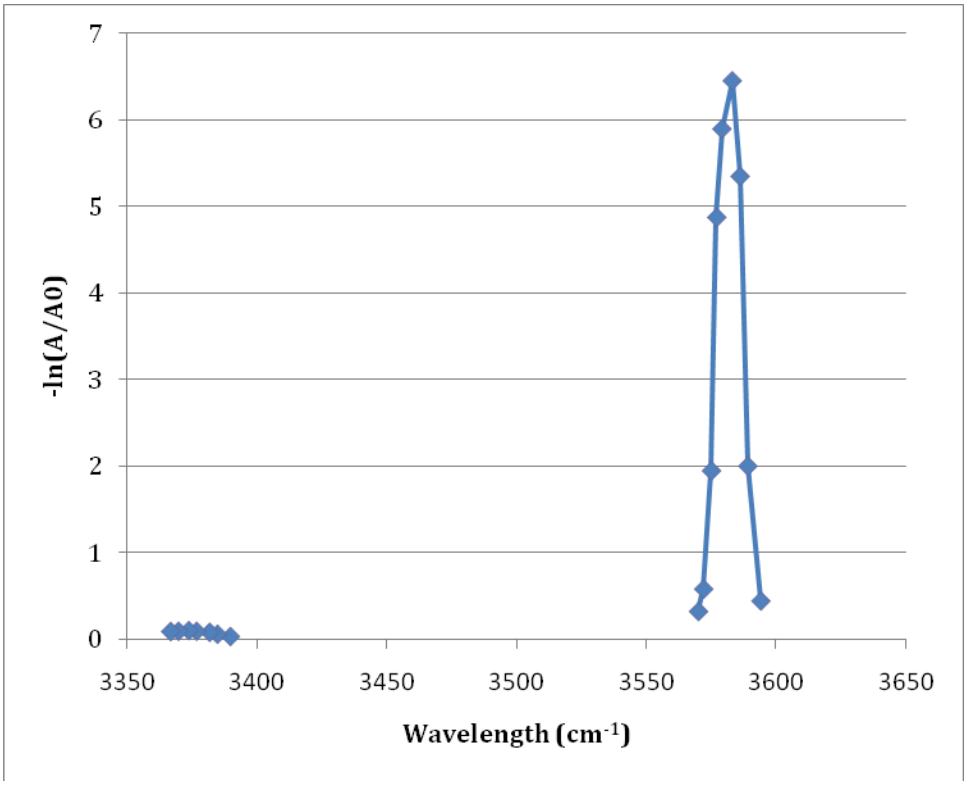

Figure 6.15. IRMPD spectrum of Gly_2H^+.

To examine the effect of relative exposure times, Figure 6.16 shows the depletion of the starting ion as a function of time versus laser pulse at frequency of 3584 cm^{-1}. These plots show a linear response for both 8 and 10 Hz over several half-lives. The fragmentation efficiency was observed to vary greatly depending on the laser cross section with the ion cloud and half-lives as small as 2 s were observed with linearity maintained.

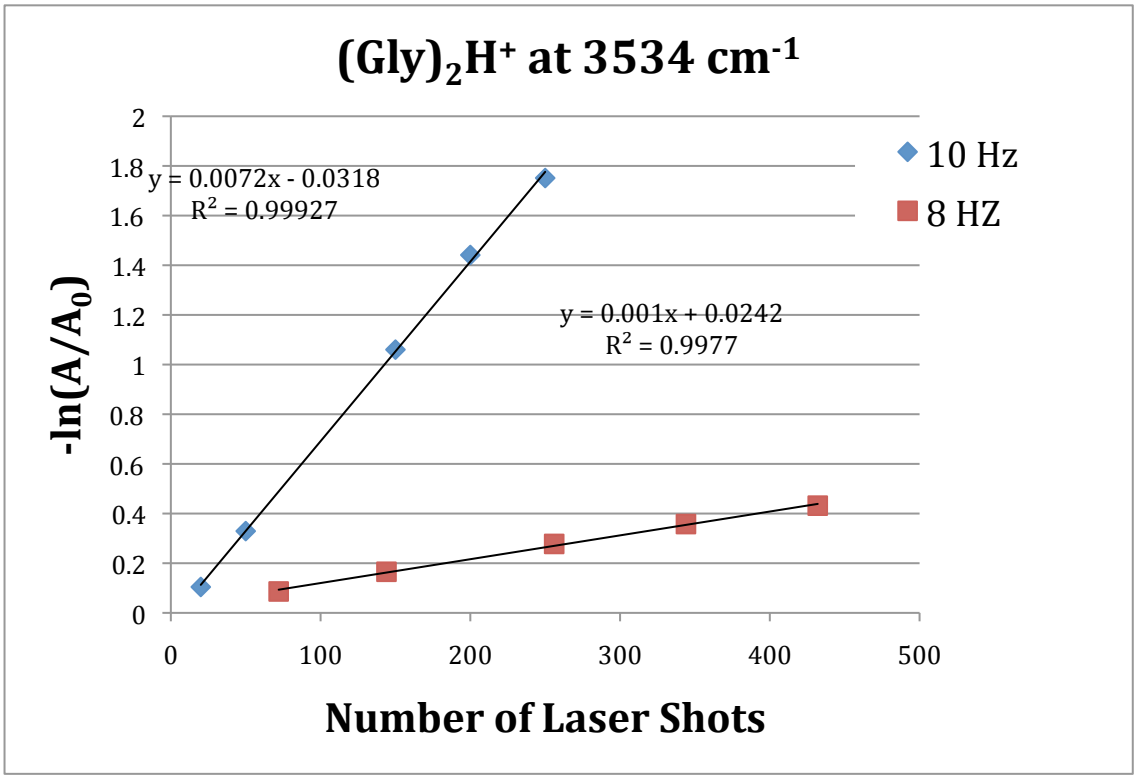

Figure 6.16 Time Dependence of fragmentation of Gly_2H^+ at 3584 cm^{-1}

Future Projects

Initial attempts to look at a variety of covalently bonded substrates were carried out. Though this technique offers the potential to investigate structures of gas-phase ions, there are for a number of potential pitfalls. To date, the majority of studies have been performed on solvated species, or other species that are held together by non-covalent interactions. Since fragmentation is due to multiphoton processes, a small increase in the barrier to fragmentation makes observing fragmentation exponentially harder without a dramatic increase in laser flux. This is especially true at lower frequencies because of the drop in photon energy and laser power. To examine ions

without a clear fragmentation pathway or which are prone to rearrange, it is necessary to develop a method that circumvents the need for a multiphoton process.

References

Chapter 1.

(1) Reed, C. A. *Chem. Commun.* **2005**, 1669-1677.

(2) Reed, C. A. *Accounts Chem. Res.* **2009**, ASAP, DOI**:** 10.1021/ar900159e.

(3) Fărcaşiu, D.; Ghenciu, A. *J. Am. Chem. Soc.* **1993**, *115*, 10901-10908.

(4) Stoyanov, E. S.; Kim, K. C.; Reed, C. A. *J. Am. Chem. Soc.* **2006**, *128*, 8500-8508.

(5) Juhasz, M.; Hoffmann, S.; Stoyanov, E.; Kim, K. C.; Reed, C. A. *Angew. Chem. Int. Ed.* **2004**, *43*, 5352-5355.

(6) A preliminary report has appeared on the synthesis of the acid of a fluorinated carborane which is predicted (ref. 5) to be a stronger acid than the undecachloro derivative: Kuppers, T.; Bernhardt, E.; Eujen, R.; Willner, H.; Lehmann, C. W. *Angew. Chem. Int. Ed.* **2007**, *46*, 6346-6349.

(7) Koppel, I. A.; Burk, P.; Koppel, I.; Leito, I.; Sonoda, T.; Mishima, M. *J. Am. Chem. Soc.* **2000**, *122*, 5114–5124.

(8) Juhasz, M. A. Ph.D. Thesis, University of California – Riverside, 2005.

(9) Koppel, I. A.; Taft, R. W.; Anvia, F.; Zhu, S. Z.; Hu, L. Q.; Sung, K. S.; Desmarteau, D. D.; Yagupolskii, L. M. *J. Am. Chem. Soc*. **1994**, *116*, 3047-3057.

(10) (a) Jelínek, T.; Plešek, J.; Heřmánek, S.; Štíbr, B. *Coll. Czech. Chem. Commun.* **1986**, *51*, 819-829. (b) Xie, Z.; Tsang, C. W.; Sze, E. T. P.; Yang, Q.; Chan, D. T. W.; Mak, T. C. W. *Inorg. Chem.* **1998**, *37*, 6444–6451. (c) Stasko, D.; Reed, C. A. *J. Am. Chem. Soc.* **2002**, *124*, 1148–1149. (d) $H(CHB_{11}Cl_{11})$ was prepared in an identical manner to $H(CHB_{11}H_5Cl_6)$: Reed, C.A.; Kim, K. C.; Bolskar, R. D.; Mueller, L. J. *Science* **2000**, *289*, 101-104.

(11) All thermodynamic data cited herein come from the following source unless otherwise noted: Lias, S. G. "Ionization Energy Evaluation" in *NIST Chemistry WebBook, NIST Standard Reference Database Number 69*, Eds. P.J. Linstrom and W.G. Mallard, June 2005, National Institute of Standards and Technology, Gaithersburg MD, 20899 (http://webbook.nist. gov).

(12) (a) Becke, A. D. *J. Chem. Phys.* **1993**, *98*, 5648-5652. (b) Lee, C. T.; Yang, W. T.; Parr, R. G. *Phys. Rev. B* **1988**, *37*, 785-789.

(13) Curtiss, L. A.; Redfern, P. C.; Raghavachari, K.; Rassolov, V.; Pople, J. A. *J. Chem. Phys*. **1999**, *110*, 4703-4709.

(14) Stoyanov, E. S.; Hoffmann, S. P.; Juhasz, M.; Reed, C. A. *J. Am. Chem. Soc.* **2006**, *128*, 3160-3161.

(15) Wang, X. B.; Wang, L. S. *Rev. Sci, Instrum*. **2008**, *79*, 073108.

(16) Since no vibrational structure was resolved, the ADE was measured by drawing a straight line along the onset of the photoelectron spectrum and adding the instrument resolution to the intersection to the binding energy axis. Thermal broadening is largely eliminated at 70 K and a clear threshold is evident for $CHB_{11}Cl_{11}^-$.

(17) Reed, C. A. *Acc. Chem. Res*. **1998**, *31*, 133-139.

(18) The lower limit for the BDE was obtained by using the A factor for the thermal decomposition of *tert*-butyl peroxide and assuming that its fragmentation rate at 150 ˚C is the same as that for the carborane at 230 ˚C. For details on the pyrolysis of the peroxide, see: Shaw, D. H.; Pritchard, H. O. *Can. J. Chem*. **1968**, *46*, 2721-2724.

(19) (a) Burk, P.; Koppel, I.; Trummal, A.; Koppel, I. A. *J. Phys. Org. Chem*. **2008**, *21*, 571-574. (b) Gal, J. F.; Maria, P. C.; Raczynska, E. D. *J. Mass Spectrom*. **2001**, *36*, 699-716.

Chapter 2

(1) Hines, J. I. D., *Inorganic Chemistry With The Elements of Physical and Theoretical Chemistry*, 2nd ed.; John Wiley: New York, 1908; pp 1-349.

(2) (a) Schumacher, J. C., *Perchlorates. Their Properties, Manufacture and Uses;* Reinhold Publishing, NY, 1960, pp 1-243. (b) Schilt, A. A., *Perchloric Acid and Perchlorates*; G. Frederick Smith Chemical Co.: Columbus, OH, 1979, pp 1-189. (c) Mendiratta, S. K., Dotson, R. L., Booker, R. T., Perchloric acid and Perchlorates. In *Kirk-Othmer Encyclopedia of Chemical Technology*, 5th ed.; Kroschwitz, J. I., Ed.; John Wiley and Sons: New York, 2006, Vol. 18, pp 274-287. (d) Petrisor, I. G.; Wells, J. T. Issues Environ. Sci. Tech. **2008**, *26*, 105-129.

(3) (a) Molina, M. J.; Rowland, F. S. *Nature* **1974**, *249*, 810-812. (b) Finlayson-Pitts, B. J.; Pitts, J. N., Jr. *Atmospheric Chemistry: Fundamentals and Experimental Techniques*; Wiley Interscience: New York, 1986, pp 1 –1098. (c) Barrett, J. W.; Solomon, P. M.; de Zafra, R. L.; Jaramillo, M.; Emmons, L.; Parrish, A. *Nature* **1988**, *336*, 455-458. (d) Sander, S. P.; Friedl, R.; Yung, Y. L. *Science* **1989**, *2454*, 1095-1098. (e) Vaida, V.; Solomon, S.; Richard, E. C.; Rul, E.; Jeffereson, A. *Nature* **1989**, *342*, 405-408 . (f) Francisco, J. S.; Sander, S. P. J. Phys. Chem. **1996**, *100*, 573-579.

(4) Colussi, A. J. *J. Phy. Chem*. **1990**, *94*, 8922-8926.

(5) Colussi, A. J.; Sander, S. P.; Friedl, R. R. *J. Phy. Chem*. **1992**, *96*, 4442-4445.

(6) Colussi, A. J.; Grela, M. A. *J. Phy. Chem*. **1993**, *97*, 3775-3779.

(7) Rathmann, T.; Schindler, R. N. *Chem. Phys. Letters* **1992**, *190*, 539-542.

(8) Rauk, A.; Tschuikow-Roux, E.; Chen, Y.; McGrath, M. P.; Radom, L. *J. Phy. Chem*. **1993**, *97*, 7947-7954.

(9) The following reference clearly indicates that the recommended value for $DH^{\circ}_{f}(ClO_3)$ is based upon experiment and theory. Chase, Jr., M. W. 1998, NIST–JANAF Thermochemical Tables, Fourth Ed., J. Phys. Chem. Ref. Data, Monograph 9, Part I.

(10) Sander, S. P.; Friedl, R. R.; Golden, D. M.; Kurylo, M. J.; Moortgat, G. K.; Keller-Rudek, H.; Wine, P. H.; Ravishankara, A. R.; Kolb, C. E.; Molina, M. J.; Finlayson-Pitts, B. J.; Huie, R. E.; Orkin, V. L. (2006) *Chemical kinetics and photochemical data for use in atmospheric studies, evaluation no. 15*, JPL Publication 06-2, Jet Propulsion Laboratory, Pasadena, http://jpldataeval.jpl.nasa.gov

(11) Schultz, R. D.; Dekker, A. O. *Proceedings of the 6th Symposium (International) on Combustion;* Reinhold: New York, 1956, 618-626.

(12) Benson, S. W., *Thermochemical Kinetics*; 2nd ed.; John Wiley: New York, 1976; pp 1-320.

(13) Berthelot, M. *Compt. Rend*. **1881**, *93*, 240, 291.

(14) This quotation was taken from ref 15, and the results also have been questioned in the following: Bidinosti, D. R.; Biermann, W. J. *Can. J. Chem*. **1956**, *34*, 1591-1595.

(15) Goodeve, C. F.; Marsh, A. E. L. *J. Chem. Soc.* **1937**, 1816-1819.

(16) Alekseev, V. I.; Fedorova, L. I.; Baluev, A. V. *Russ. Chem. Bull.* **1983**, *32,* 980-986.

(17) Marcus, Y. *J. Chem. Soc., Faraday Trans. 1,* **1987**, *83*, 339-349.

(18) Bartmess, J. E. *NIST Chemistry WebBook, NIST Standard Reference Database Number 6;* Mallard, W. G., Linstrom, P. J., eds.; National Institute of Standards and Technology: Gaithersburg, MD 20899 (http://webbook.nist.gov).

(19) Reger, D. L.; Goode, S. R.; Ball, D. W. *Chemistry: Principles and Practice*, 3rd ed.; Brook Cole: CA, 2010; pg 664.

(20) This bond energy was derived from an old value of $DH^{\circ}_{f}(ClO_3)$ = 30.1 kcal mol^{-1}, which is inconsistent with more recent determinations (see refs. 4-6), and Benson's estimate for the heat of formation of chloric acid (11 ± 4 kcal mol^{-1}). Also, see: (a) Figini, R. V.; Coloccia, E.; Schumacher, H. J. *Z. Physik. Chem.* (Frankfurt) **1958**, *14*, 32-48. (b) Fisher, I. P. *Trans. Faraday Soc*. **1967**, 684-692.

(21) (a) Karton, A.; Parthiban, S.; Martin, J. M. L. *J. Phys. Chem. A* **2009**, *113*, 4802-4816. (b) Gutowski, K. E.; Rogers, R. D.; Dixon, D. A. *J. Phys. Chem. A* **2006**, *110*, 11890-11897. (c) Martin, J. M. L. *J. Mol. Struct. (Theochem)* **2006**, *771*, 19-26. (d) Sicre, J. E.; Cobos, C. J. *J. Mol. Struct. (Theochem)* **2003**, *620*, 215-226. (e) Xu, Z. F.; Lin, M. C. *J. Chem. Phys*. **2003**, *119*, 8897-8904. (f) Workman, M. A.; Francisco, J. S. *Chem. Phys. Lett*. **1997**, *279*, 158-164. (g) Francisco, J. S. *J. Phys. Chem*. **1995**, *99*, 13422-13425. (h) Rohlfing, C. M. *Chem. Phys. Lett*. **1995**, *245*, 665-670.

(22) Tian, Z.; Radom, L.; Sullivan, M. B.; Chan, B.; Kass, S. R. *Proc. Natl. Acad. Sci*. **2008**, *105*, 7647-7651.

(23) Meyer, M. M.; Wang, X. B.; Reed, C. A.; Wang, L. S.; Kass, S. R. *J. Am. Chem. Soc.* **2009**, *131*, 18050-18051.

(24) Vianello, R.; Maksic, Z. B. *J. Phys. Chem. A* **2007**, *111*, 11718-11724.

(25) (a) Turco, R. P. J. *Geophys. Res*. **1977**, *82*, 3585-3592. (b) Prasad, S. S. *Ann. Geophys*. **1995**, *13*, 296-304.

(26) Wang, X. B.; Wang, L. S. *J. Chem. Phys*. **2000**, *113*, 10928-10933.

(27) Curtiss, L. A.; Raghavachari, K.; Redfern, P. C.; Rassolov, V.; Pople, J. A. *J. Chem. Phys.* **1998**, *109*, 7764-7776.

(28) Baboul, A. G.; Curtiss, L. A.; Redfern, P. C.; Raghavachari, K. *J. Chem. Phys.* **1999**, *110*, 7650-7657.

(29) (a) Becke, A. D. *J. Chem. Phys.* **1993**, *98*, 5648-5652. (b) Lee, C.; Yang, W.; Parr, R. G. *Phys. Rev. B* **1988**, *37*, 785-789.

(30) (a) Zhao, Y.; Truhlar, D. G. *J. Phys. Chem. A* **2008**, *112*, 1095-1099. (b) Zhao, Y.; Truhlar, D. G. *Theor. Chem. Acc.* **2008**, *120*, 215-241. (c) Zhao, Y.; Truhlar, D. G. *Acc. Chem. Res.* **2008**, *41*, 157-167.

(31) Frisch, M. J.; Trucks, G. W.; Schlegel, H. B.; Scuseria, G. E.; Robb, M. A., et al. *Gaussian 03*, Gaussian, Inc., Wallingford CT, 2004.

(32) Dunning, Jr., T. H. *J. Chem. Phys.* **1989**, *90*, 1007-1023.

(33) (a) Schultz, N. E.; Zhao, Y.; Truhlar, D. G. *J. Phys. Chem. A* **2005**, *109*, 11127-11143. (b) Zheng, J.; Zhao, Y.; Truhlar, D. G. *J. Phys. Chem. A* **2007**, *111*, 4632-4642.

(34) Burkholder, J. B.; Hammer, P. D.; Howard, C. J.; Maki, A. G.; Thompson, G.; Chackerian, Jr., C. *J. Mol. Spectrosc*. **1987**, *124*, 139-161.

(35) Miyazaki, K.; Tanoura, M.; Tanaka, K.; Tanaka, T. *J. Mol. Spectrosc*. **1986**, *116*, 435-449.

(36) Kopitzky, R.; Grothe, H.; Willner, H. *Chem. Eur. J.* **2002**, *8*, 5601-5621.

(37) Deeley, C. M. *J. Mol. Spectrosc*. **1987**, *122*, 481-489.

(38) Casper, B.; Mack, H. G.; Mueller, H. S. P.; Willner, H.; Oberhammer, H. *J. Phys. Chem*. **1994**, *98*, 8339-8342.

(39) Lee, T. J.; Taylor, P. R. *Int. J. Quantum Chem. Symp.* **1989**, *23*, 199-207.

(40) Nickolaisen, S. L.; Friedl, R. R.; Sander, S. P. *J. Chem. Phys.* **1994**, *98*, 155-169.

(41) M06 and M06-2X were also explored in ref 21a, but a smaller triple zeta basis set was used and this accounts for the qualitatively different results that were obtained.

(42) Su, T.; Bowers, M. T. *Int. J. Mass Spectrom. Ion Phys*. **1973**, *12*, 347-356.

(43) Ervin, K. M.; DeTuri, V. F. *J. Phys. Chem. A* **2002**, *106*, 9947-9956.

(44) The average of the computed B3LYP/6-311+G(d,p) and HF/6-31G(d) entropies reported by Koppel et al. affords TDS_{acid} = 7.9 kcal mol^{-1}, and this value was used to convert their DG°_{acid} to DH°_{acid}. For further details, see: Leito, I.; Raamat, E.; Kutt, A.; Saame, J.; Kipper, K.; Koppel, I. A.; Koppel, I.; Zhang, M.; Mishima, M.; Yagupolskii, L. M.; Garlyauskayte, Y. R.; Filatov, A. A. *J. Phys. Chem. A* **2009**, *113*, 8421-8424.

(45) Some of the acids near the bottom of the gas-phase acidity scale recently were revised. We applied the 5.3 kcal mol^{-1} revision for the acidity of $(CF_3SO_2)_2NH$ to the larger perfluorobutyl derivative to estimate its deprotonation enthalpy. Also, see: Koppel, I. A.; Taft, R. W.; Anvia, F.; Zhu, S. Z.; Hu, L. Q., et al. *J. Am. Chem. Soc*. **1994**, *116*, 3047-3057.

(46) (a) Gilles, M. K.; Polak, M. L.; Lineberger, W. C. J. Chem. Phys. **1992**, *96*, 8012-8020. (b) Distelrath, V.; Boesl, U. *Faraday Discuss*. **2000**, *115*, 161-174.

(47) (a) Otto, A. H.; Schrader, S.; Steiger, T.; Schneider, M. *J. Chem. Soc. Faraday Trans.* **1997**, *93*, 3927-3930. (b) Boily, J. F. *J. Phys. Chem. A* **2003**, *107*, 4276-4285.

(48) Fattahi, A.; Kass, S. R. *J. Org. Chem*. **2004**, *69*, 9176-9183.

(49) (a) Masschelein, W. J., *Chlorine Dioxide Chemistry and Environmental Impact of Oxychlorine Compounds*, Ann Arbor Science: MI, 1979; pp 1-200. (b) Van Huis, T. J.; Schaefer III, H. F. *J. Chem. Phys*. **1997**, *106*, 4028-4037.

Chapter 3.

(1) a) S. Gil, M. Parra, *Curr. Org. Chem*. **2002**, *6*, 283-302; b) S. Gil, M. Parra, *Recent Res. Develop. Org. Chem.* **2002**, *6*, 449-481; c) C. M. Thompson, *Dianion Chemistry in Organic Synthesis*, CRC Press: Boca Raton (Florida), 1994, pp. 1-250.

(2) V. Grignard, *Bull. Soc. Chim. Fr.* **1904**, *31*, 751-757.

(3) a) D. Ivanoff, A. Spassoff, *Bull. Soc. Chim. Fr.* **1931**, *49*, 19-23; b) B. Blagoev, D. Ivanov, *Synthesis* **1970**, 615-627; c) D. Ivanov, G, Vassilev, I. Panayotov, *Synthesis* **1975**, 83-98.

(4) For fundamental solution phase properties such as pKa and oxidation potentials, see: a) S. Gronert, A. Streitwieser, *J. Am. Chem. Soc.* **1988**, *110*, 4418-4419; b) P. Renaud, M. A. Fox, *J. Am. Chem. Soc.* **1988**, *110*, 5702-5705; c) P. Renaud, M. A. Fox, *J. Am. Chem. Soc.* **1988**, *110*, 5705-5709.

(5) a) J. Kaneti, P. v. R. Schleyer, A. J. Kos, *J. Chem. Soc. Chem. Commun.* **1985**, 1014-1016; b) A. Streitwieser, M. Husemann, Y. -J. Kim, *J. Org. Chem*. **2003**, *68*, 7937-7942.

(6) Theoretical calculations indicate that double deprotonation of acetic acid in the gas phase is highly unlikely due to the very large endothermicity of the second deprotonation step. See: D. W. Deerfield, L. G. Pedersen, THEOCHEM **1996**, *368*, 163-171.

(7) a) S. M. Bachrach, M. Hare, S. R. Kass, *J. Am. Chem. Soc.* **1998**, *120*, 12646-12649; b) R. A. J. O'Hair, *Chem. Comm.* **2002**, 20-21; c) R. A. J. O'Hair, A. K. Vrkic, P. F. James, *J. Am. Chem. Soc.* **2004**, *126*, 12173-12183; d) P. F. James, R. A. J. O'Hair, *Org. Lett.* **2004**, *6*, 2761-2764; e) A. P. Jacob, P. F. James, R. A. J. O'Hair, *Int. J. Mass Spectrom.* **2006**, *255-256*, 45-52; f) R. A. J. O'Hair, T. Waters, B. Cao, *Angew. Chem. Int. Ed*. **2007**, *46*, 7048-7051; *Angew. Chem*. **2007**, *119*, 7178-7181; g) N. Rijs, T. Waters, G. N. Khairallah, R. A. J. O'Hair, *J. Am. Chem. Soc.* **2008**, *130*, 1069-1079; h) C. C. L. Thum, G. N. Khairallah, R. A. J. O'Hair, *Angew. Chem. Int. Ed*. **2008**, *47*, 9118-9121; *Angew. Chem*. **2008**, *120*, 9258-9261.

(8) a) R. A. J. O'Hair, S. Gronert, C. H. DePuy, J. H. Bowie, *J. Am. Chem. Soc.* **1989**, *111*, 3105-3106; b) J. J. Grabowski, X. Cheng, *J. Am. Chem. Soc.*, **1989**, *111*, 3106-3108.

(9) For reviews on the use of CID to generate reactive metal containing ions see: a) R. A. J. O'Hair, *Chem. Comm.* **2006**, 1469-1481; b) R. A. J. O'Hair, "Gas Phase Ligand Fragmentation to Unmask Reactive Metallic Species.", in "MS investigations of reactive intermediates in solution." (L.S. Santos, Ed.), Wiley-VCH, in press.

(10) a) A. D. Becke, *J. Chem. Phys.* **1993**, *98*, 5648-5652; b) C. T. Lee, W. T. Yang, R. G. Parr, *Phys. Rev. B* **1988**, *37*, 785-789.

(11) L. A. Curtiss, K. Raghavachari, P. C. Redfern, V. Rassolov, J. A. Pople, *J. Chem. Phys.* **1998**, *109*, 7764-7776.

(12) Z. Tian, B. Chan, M. B. Sullivan, L. Radom, S. R. Kass, *Proc. Natl. Acad. Sci. USA* **2008**, *105*, 7647-7651.

(13) All thermodynamic values come from J. E. Bartmess, NIST Chemistry WebBook, NIST Standard Reference Database Number 69, W. G. Mallard, P. J. Linstrom, Eds.; National Institute of Standards and Technology: Gaithersburg, MD 20899 (http://webbook.nist.gov).

(14) This value is the average of the two acidities given in ref. (13).

(15) Pathway 4d is not available for ketones, but 4a – 4c were observed for acetone.

(16) M. J. Frisch, G. W. Trucks, H. B. Schlegel, G. E. Scuseria, M. A. Robb, J. R. Cheeseman, J. A. Montgomery, T. Vreven, K. N. Kudin, J. C. Burant, J. M. Millam, S. S. Iyengar, J. Tomasi, V. Barone, B. Mennucci, M. Cossi, G. Scalmani, N. Rega, G. A. Petersson, H. Nakatsuji, M. Hada, M. Ehara, K. Toyota, R. Fukuda, J. Hasegawa, M. Ishida, T. Nakajima, Y. Honda, O. Kitao, H. Nakai, M. Klene, L. X., J. E. Knox, H. P. Hratchian, J. B. Cross, C. Adamo, J. Jaramillo, R. Gomperts, R. E. Stratmann, O. Yazyev, A. J. Austin, R. Cammi, C. Pomelli, J. W. Ochterski, P. Y. Ayala, K. Morokuma, G. A. Voth, P. Salvador, J. J. Dannenberg, V. G. Zakrzewski, S. Dapprich, A. D. Daniels, M. C. Strain, O. Farkas, D. K. Malick, A. D. Rabuck, K. Raghavachari, J. B. Foresman, J. V. Ortiz, Q. Cui, A. G. Baboul, S. Clifford, J. Cioslowski, B. B. Stefanov, G. Liu, A. Liashenko, P. Piskorz, I. Komaromi, R. L. Martin, D. J. Fox, T. Keith, M. A. Al-Laham, C. Y. Peng, A. Nanayakkara, M. Challacombe, P. M. W. Gill, B. Johnson, W. Chen, M. W. Wong, C. Gonzalez, J. A. Pople, Gaussian, Inc., Pittsburgh, PA, 2003.

Chapter 4.

(1) a) S. Gil, M. Parra, *Curr. Org. Chem*. **2002**, *6*, 283-302; b) S. Gil, M. Parra, *Recent Res. Develop. Org. Chem.* **2002**, *6*, 449-481; c) C. M. Thompson, *Dianion Chemistry in Organic Synthesis*, CRC Press: Boca Raton (Florida), 1994, pp. 1-250.

(2) a) H. Moissan, *C. R. Hebd. Seances Acad. Sci.* **1896**, *122*, 362-363; b) H. Moissan, in "The Electric Furnace," (translated by V. Lenher), The Chemical Publishing Co.: Easton (PA), 1904, pp. 1-305.

(3) Y. Apeloig, P. v. R. Schleyer, J. S. Binkley, J. A. Pople, W. L. Jorgensen, *Tetrahedron Lett.* **1976**, *17*, 3923-3926.

(4) a) R. Juza, V. Werhe, *Naturwissenschaften*, **1965**, *52*, 537; b) R. Juza, V. Wehle, H. U. Schuster, *Z. Anorg. Allg. Chem.* **1967**, *352*, 252-257; c) U. Ruschewitz, R. Pöttgen, *Z. Anorg. Allg. Chem.* **1999**, *625*, 1599-1603.

(5) a) E. R. Swart, *Experientia* **1964**, *20*, 47-48; b) B. Matvienko, F. Gessner, Int. J. Appl Radiat. Isot. **1980**, *31*, 718-721.

(6) J. Mortier, M. Vaultier, F. Carreaux, J. M. Douin, *J. Org. Chem*. **1998**, *63*, 3515-3516.

(7) A. V. R. Rao, in "e-EROS Encyclopedia of Reagents for Organic Synthesis," John Wiley and Sons: Chichester (UK), 2001.

(8) S. M. Bachrach, M. Hare, S. R. Kass, *J. Am. Chem. Soc.* **1998**, *120*, 12646-12649.

(9) a) K. M. Broadus, S. R. Kass, *J. Phys. Org. Chem*. **2002**, *15*, 461-468; b) B. B. Kirk, D. G. Harman, S. J. Blanksby, *J. Phys. Chem. A* **2010**, *114*, 1446-1456; c) D. G. Harman, S. J. Blanksby, *Org. Bio. Chem*. **2007**, *5*, 3495-3503; d) D. G. Harman, S. J. Blanksby, *Chem. Comm*. **2006**, 859-861.

(10) a) M. M. Meyer, G. N. Khairallah, S. R. Kass, R. A. J. O'Hair, *Angew. Chem. Int. Ed*. **2009**, *48*, 2934-2936; *Angew. Chem*. **2009**, *121*, 2978-2980; b) R. A. J. O'Hair, *Chem. Comm.* **2002**, 20-21; c) R. A. J. O'Hair, A. K. Vrkic, P. F. James, *J. Am. Chem. Soc.* **2004**, *126*, 12173-12183; d) P. F. James, R. A. J. O'Hair, *Org. Lett.* **2004**, *6*, 2761-2764; e) A. P. Jacob, P. F. James, R. A. J. O'Hair, *Int. J. Mass Spectrom.* **2006**, *255-256*, 45-52; f) R. A. J. O'Hair, T. Waters, B. Cao, *Angew. Chem. Int. Ed*. **2007**, *46*, 7048-7051; *Angew. Chem*. **2007**, *119*, 7178-7181; g) N. Rijs, T. Waters, G. N. Khairallah, R. A. J. O'Hair, *J. Am. Chem. Soc.* **2008**, *130*, 1069-1079; h) C. C. L. Thum, G. N. Khairallah, R. A. J. O'Hair, *Angew. Chem. Int. Ed*. **2008**, *47*, 9118-9121; *Angew. Chem*. **2008**, *120*, 9258-9261.

(11) Z. Tian, B. Chan, M. B. Sullivan, L. Radom, S. R. Kass, *Proc. Natl. Acad. Sci. USA* **2008**, *105*, 7647-7651.

(12) All of the given gas-phase acidities come from the following two references: a) J. E. Bartmess, NIST Chemistry WebBook, NIST Standard Reference Database Number 69, W. G. Mallard, P. J. Linstrom, Eds.; National Institute of Standards and Technology: Gaithersburg, MD 20899 (http://webbook.nist.gov); b) K. M. Ervin, V. F. DeTuri, *J. Phys. Chem. A* **2002**, *106*, 9947-9956.

(13) D. Schröder, H. Schwarz, *Angew. Chem. Int. Ed. Engl*. **1990**, *29*, 910-911; *Angew. Chem*. **1990**, *102*, 925-927.

(14) The ionic product in Eq. 6 could be the lithium enolate of 3-butynal.

(15) T. Su., M. T. Bowers, *Int. J. Mass Spectrom. Ion Phys*. **1973**, *12*, 347-356.

(16) G. Bouchoux, J. Y. Salpin, D. Leblanc, *Int. J. Mass Spectrom. Ion Processes* **1996**, *153*, 37-48.

(17) L. A. Curtiss, K. Raghavachari, P. C. Redfern, V. Rassolov, J. A. Pople, *J. Chem. Phys.* **1998**, *109*, 7764-7776.

(18) L. A. Curtiss, P. C. Redfern, K. Raghavachari, *J. Chem. Phys.* **2007**, *126*, 084108-084108-12.

(19) a) J. M. L. Martin, G. de Oliveria, *J. Chem. Phys.* **1999**, *111*, 1843-1856; b) S. Parthiban, J. M. L. Martin, *J. Chem. Phys.* **2001**, *114*, 6014-6029.

(20) "Lithium Chemistry: A Theoretical and Experimental Overview" A. M. Sapse, P. v. R. Schleyer, Eds.; Wiley-Interscience: New York, 1995, pp. 1-595.

Chapter 5

(1) Hayes, C. J.; Simpkins, N. S.; Kirk, D. T.; Mitchell, L.; Baudoux, J.; Blake, A. J.; Wilson, C. *J. Am. Chem. Soc.* **2009**, *131*, 8196-8210.

(2) Nickon, A.; Lambert, J. L. S. J. *J. Am. Chem. Soc.* **1962,** *84*, 4604-4605.

(3) Werstiuk, N. H. *Tetrahedron* **1983**, *39*, 205-268.

(4) Spitz, U. P.; Eaton, P. E. *Angewandte Chemie-International Edition in English* **1994**, *33*, 2220-2222.

(5) Stothers, J. B.; Tan, C. T. *Journal of the Chemical Society, Chemical Communications* **1974**, , 738.

(6) Ma, Y.; Lobkovsky, E.; Collum, D. B. *J. Org. Chem.* **2005**, *70*, 2335-2337.

(7) Kass, S. R.; DePuy, C. H. *J. Org. Chem.* **1985**, *50*, 2874 <last_page> 2877.

(8) Baschky, M. C.; Peterson, K. C.; Kass, S. R. *J. Am. Chem. Soc.* **1994**, *116*, 7218-7224.

(9) Vodicka, L.; Triska, J.; Hajek, M. *COLLECT CZECH CHEM COMMUN* **1980**, *45*, 2670-2674.

(10) Duddeck, H.; Islam, M. R. *Chemische Berichte-Recueil* **1984**, *117*, 554-564.

(11) ALEKSANDROVICH, N. I.; SEMENOVICH, O. B.; NIKOLAEVICH, S. E. RU2319688 (C1), 2008.

(12) Papajak, E.; Truhlar, D. G. *Journal of Chemical Theory and Computation* **2010**, , 100216124608062.

(13) M. J. Frisch, G. W. Trucks, H. B. Schlegel, G. E. Scuseria, M. A. Robb, J. R. Cheeseman, J. A. Montgomery, T. Vreven, K. N. Kudin, J. C. Burant, J. M. Millam, S. S. Iyengar, J. Tomasi, V. Barone, B. Mennucci, M. Cossi, G. Scalmani, N. Rega, G. A. Petersson, H. Nakatsuji, M. Hada, M. Ehara, K. Toyota, R. Fukuda, J. Hasegawa, M. Ishida, T. Nakajima, Y. Honda, O. Kitao, H. Nakai, M. Klene, L. X., J. E. Knox, H. P. Hratchian, J. B. Cross, C. Adamo, J. Jaramillo, R. Gomperts, R. E. Stratmann, O. Yazyev, A. J. Austin, R. Cammi, C. Pomelli, J. W. Ochterski, P. Y. Ayala, K. Morokuma, G. A. Voth, P. Salvador, J. J. Dannenberg, V. G. Zakrzewski, S. Dapprich, A. D. Daniels, M. C. Strain, O. Farkas, D. K. Malick, A. D. Rabuck, K. Raghavachari, J. B. Foresman, J. V. Ortiz, Q. Cui, A. G. Baboul, S.

Clifford, J. Cioslowski, B. B. Stefanov, G. Liu, A. Liashenko, P. Piskorz, I. Komaromi, R. L. Martin, D. J. Fox, T. Keith, M. A. Al-Laham, C. Y. Peng, A. Nanayakkara, M. Challacombe, P. M. W. Gill, B. Johnson, W. Chen, M. W. Wong, C. Gonzalez, J. A. Pople, Gaussian, Inc., Pittsburgh, PA, 2003.

(14) Gaussian 09, Revision **A.1**, Frisch, M. J.; Trucks, G. W.; Schlegel, H. B.; Scuseria, G. E.; Robb, M. A.; Cheeseman, J. R.; Scalmani, G.; Barone, V.; Mennucci, B.; Petersson, G. A.; Nakatsuji, H.; Caricato, M.; Li, X.; Hratchian, H. P.; Izmaylov, A. F.; Bloino, J.; Zheng, G.; Sonnenberg, J. L.; Hada, M.; Ehara, M.; Toyota, K.; Fukuda, R.; Hasegawa, J.; Ishida, M.; Nakajima, T.; Honda, Y.; Kitao, O.; Nakai, H.; Vreven, T.; Montgomery, Jr., J. A.; Peralta, J. E.; Ogliaro, F.; Bearpark, M.; Heyd, J. J.; Brothers, E.; Kudin, K. N.; Staroverov, V. N.; Kobayashi, R.; Normand, J.; Raghavachari, K.; Rendell, A.; Burant, J. C.; Iyengar, S. S.; Tomasi, J.; Cossi, M.; Rega, N.; Millam, N. J.; Klene, M.; Knox, J. E.; Cross, J. B.; Bakken, V.; Adamo, C.; Jaramillo, J.; Gomperts, R.; Stratmann, R. E.; Yazyev, O.; Austin, A. J.; Cammi, R.; Pomelli, C.; Ochterski, J. W.; Martin, R. L.; Morokuma, K.; Zakrzewski, V. G.; Voth, G. A.; Salvador, P.; Dannenberg, J. J.; Dapprich, S.; Daniels, A. D.; Farkas, Ö.; Foresman, J. B.; Ortiz, J. V.; Cioslowski, J.; Fox, D. J. Gaussian, Inc., Wallingford CT, 2009.

Chapter 6

(1) Babcock, N. G. A.,L.M. In *Advances in Gas Phase Ion Chemistry, Volume 4 (Advances in Gas Phase Ion Chemistry)* Elsevier Science: , pp 320.

(2) Gronert, S. *Chem. Rev.* **2001**, *101*, 329-360.

(3) Van der Hart, W. J. *Mass Spectrom. Rev.* **1989**, *8*, 237-268.

(4) Bailey, C. *Chemical Physics Letters* **1997**, *269*, 122-127.

(5) Stearns, J. A.; Seaiby, C.; Boyarkin, O. V.; Rizzo, T. R. *Phys. Chem. Chem. Phys.* **2009**, *11*, 125-132.

(6) Eyler, J. R. *Mass Spectrom. Rev.* **2009**, *28*, 448-467.

(7) Bosenberg, W. R.; Guyer, D. R. *Journal of the Optical Society of America B* **1993; 1993**, *10*, 1716.

(8) Sorokina, I. T.; Vodopyanov, K. L. In *Solid-State Mid-Infrared Laser Sources (Topics in Applied Physics)* Springer: .

(9) AnonymousNETComm Information Page http://home.comcast.net/~hardandsoftware/NETCommOCX.htm (accessed 2/7/2010, 2010).

(10) McLafferty, F.W., Et al. *J. Am. Chem. Society.* **2005,** 127, 4076-4083

Appendix 1

Molecular Structure Calculations Energies and XYZ coordinates

Chapter 1

$H(CHB_{11}Cl_{11})$

Energy = -5375.674669 (B3LYP/aug-cc-pVDZ); -5375.890250 (B3LYP/aug-cc-pVTZ// B3LYP/aug-cc-pVDZ); ZPE = 0.090697 (unscaled); Thermal correction to 298 K = 0.111518; -5375.772808 (B3LYP/6-311+G(d,p); ZPE = 0.091433 (unscaled); Thermal correction to 298K = 0.112226; G3(MP2) = -5369.930917 (0 K), -5369.909345 (298 K).

B	0.54754400	0.42532700	1.48617400
Cl	1.22836500	1.14293300	2.97933200
Cl	2.01973500	-2.36809400	1.79666900
B	0.99978300	-1.20902300	0.91172400
B	-0.69083600	-0.85162300	1.46565700
Cl	-1.34266900	-1.67728800	2.90018900
Cl	3.24529100	0.93887300	0.00000000
B	1.56768000	0.20380100	0.00000000
B	0.25857800	1.37853800	0.00000000
Cl	0.95678700	3.13934200	0.00000000
H	2.23897000	2.53646000	0.00000000
Cl	-2.21836100	1.88632800	1.85324300
B	-1.14207700	0.80642500	0.91915600
B	-1.72872500	-0.61802100	0.00000000
C	-0.37637200	-1.70557500	0.00000000
H	-0.60617100	-2.76937800	0.00000000
B	0.99978300	-1.20902300	-0.91172400
Cl	2.01973500	-2.36809400	-1.79666900
B	0.54754400	0.42532700	-1.48617400
B	-1.14207700	0.80642500	-0.91915600
B	-0.69083600	-0.85162300	-1.46565700
Cl	-1.34266900	-1.67728800	-2.90018900
Cl	-3.40012400	-1.22634200	0.00000000
Cl	1.22836500	1.14293300	-2.97933200
Cl	-2.21836100	1.88632800	-1.85324300

$CHB_{11}Cl_{11}^-$

Energy = -5375.289591 (B3LYP/aug-cc-pVDZ); -5375.501993 (B3LYP/aug-cc-pVTZ// B3LYP/aug-cc-pVDZ)

ZPE = 0.083528 (unscaled); Thermal correction to 298K = 0.104086; -5375.388559 (B3LYP/6-311+G(d,p); ZPE = 0.083831 (unscaled); Thermal correction to 298 K = 0.104330; G3(MP2) = -5369.552856 (0 K), -5369.531915 (298 K).

B	0.00004700	1.54206000	0.59445700
Cl	0.00007600	3.16548300	1.37162400
Cl	-1.79134700	2.46557700	-1.87961400
B	-0.89935300	1.23786200	-0.92322000
B	0.89936100	1.23785600	-0.92322000
Cl	1.79134700	2.46557700	-1.87961400
Cl	-3.01053000	0.97826000	1.37162400
B	-1.46657200	0.47656700	0.59445700
B	0.00000000	0.00000000	1.53787900
Cl	0.00000000	0.00000000	3.33843300
Cl	3.01057700	0.97811600	1.37162400
B	1.46660100	0.47647900	0.59445700
B	1.45518900	-0.47282400	-0.92322000
C	0.00000000	0.00000000	-1.70821700
H	0.00000000	0.00000000	-2.79520900
B	-1.45519200	-0.47281600	-0.92322000
Cl	-2.89846000	-0.94176700	-1.87961400
B	-0.90643800	-1.24752600	0.59445700
B	0.90636300	-1.24758000	0.59445700
B	-0.00000500	-1.53007800	-0.92322000
Cl	0.00000000	-3.04762100	-1.87961400
Cl	2.89846000	-0.94176700	-1.87961400
Cl	-1.86068500	-2.56088500	1.37162400
Cl	1.86056300	-2.56097400	1.371624000

$CHB_{11}Cl_{11}^{\bullet}$

Energy = -5375.065941 (B3LYP/aug-cc-pVDZ); -5375.279907 (B3LYP/aug-cc-pVTZ// B3LYP/aug-cc-pVDZ)

ZPE = 0.080125 (unscaled); Thermal correction to 298K = 0.101447; -5375.165025 (B3LYP/6-311+G(d,p); ZPE = 0.080348 (unscaled); Thermal correction to 298 K = 0.101625; G3(MP2) = -5369.320093 (0 K), -5369.298264 (298 K).

B	-0.93034300	1.21805300	0.64050300
Cl	-1.86895400	2.48775000	1.43665100
Cl	-2.89435600	1.01152700	-1.84416100
B	-1.45478600	0.52804000	-0.93152600
B	-0.00077200	1.56112100	-0.91492600
Cl	-0.00291200	3.10917300	-1.78092500
Cl	-2.99738700	-1.04769400	1.32626300
B	-1.46530300	-0.53052100	0.58878900
B	-0.00270400	-0.04720200	1.55322800
Cl	-0.00483200	-0.08299600	3.33904200
Cl	1.84775200	2.49769800	1.44415200
B	0.91836900	1.22414400	0.64469400
B	1.45542700	0.53351200	-0.92837200
C	0.00302300	0.05164200	-1.72509700
H	0.00438600	0.07310600	-2.81309900
B	-0.91679300	-1.20676200	-0.97243000
Cl	-1.78173200	-2.39790200	-1.94551100
B	0.00090000	-1.56598900	0.57008000
B	1.46577500	-0.52395700	0.59306900
B	0.92987600	-1.20033100	-0.96889500
Cl	1.80370600	-2.38882700	-1.93834100
Cl	2.89667800	1.02679000	-1.83403000
Cl	0.00404500	-3.20281700	1.27117500
Cl	2.99677100	-1.03231800	1.33701400

Note – B3LYP/aug-cc-pVDZ geometries are provided above; the exact energy of $H^{\cdot}$ (-0.5 H) was used in computing DFT BDES.

Chapter 2

ClO

M06/aug-cc-pVD(+d)Z = -535.268549,
ZPE = 0.0020300, TC to the enthalpy = 0.0053900
M06/aug-cc-pVT(+d)Z = -535.295707,
ZPE = 0.002061, TC to the enthalpy = 0.005418
M06/aug-cc-pVQ(+d)Z = -535.309582,
ZPE = 0.002065, TC to the enthalpy = 0.005422
M062X/aug-cc-pVD(+d)Z = -535.270607,
ZPE = 0.002018, TC to the enthalpy = 0.005380
M062X/aug-cc-pVT(+d)Z = -535.309881,
ZPE = 0.002064, TC to the enthalpy = 0.005421
M062X/aug-cc-pVQ(+d)Z = -535.315598,
ZPE = 0.0020663, TC to the enthalpy = 0.005424
G3 (298 K) = -535.116854
G3B3 (298 K) = -535.118790

Cl	0.000000	0.000000	0.498860
O	0.000000	0.000000	-1.060077

ClO^-

M06/aug-cc-pVD(+d)Z = -535.354431, ZPE = 0.001514, TC to the enthalpy = 0.004946
M06/aug-cc-pVT(+d)Z = -535.375755, ZPE = 0.001571, TC to the enthalpy = 0.004993
M06/aug-cc-pVQ(+d)Z = -535.387849, ZPE = 0.001575, TC to the enthalpy = 0.004995
M062X/aug-cc-pVD(+d)Z = -535.354401, ZPE = 0.001627, TC to the enthalpy = 0.005039
M062X/aug-cc-pVT(+d)Z = -535.3394470, ZPE = 0.001656, TC to the enthalpy = 0.005063
M062X/aug-cc-pVQ(+d)Z = -535.398986, ZPE = 0.001660, TC to the enthalpy = 0.005066
G3 (298 K) = -535.201999
G3B3 (298 K) = -535.202753

Cl	0.000000	0.000000	0.530785
O	0.000000	0.000000	-1.127917

HOCl

M06/aug-cc-pVD(+d)Z = -611.0210373, ZPE = 0.016861, TC to the enthalpy = 0.021489
M06/aug-cc-pVT(+d)Z = -611.069939, ZPE = 0.016861, TC to the enthalpy = 0.021489
M06/aug-cc-pVQ(+d)Z = -611.091639, ZPE = 0.017191, TC to the enthalpy = 0.021760
M062X/aug-cc-pVD(+d)Z = -535.929439, ZPE = 0.01344, TC to the enthalpy = 0.017309
M062X/aug-cc-pVT(+d)Z = -535.969193, ZPE = 0.013505, TC to the enthalpy = 0.017370
M062X/aug-cc-pVQ(+d)Z = -535.975068, ZPE = 0.0135192, TC to the enthalpy = 0.017383699
G3 (298 K) = -535.767519
G3B3 (298 K) = -535.770376

Cl	0.035937	-0.588337	0.000000
O	0.035937	1.085642	0.000000
H	-0.898422	1.316591	0.000000

ClO_2

M06/aug-cc-pVD(+d)Z = -610.396604,
ZPE = 0.005887, TC to the enthalpy = 0.009990
M06/aug-cc-pVT(+d)Z = -610.450798,
ZPE = 0.006170, TC to the enthalpy = 0.010241
M06/aug-cc-pVQ(+d)Z = -610.472515,
ZPE = 0.006182, TC to the enthalpy = 0.010251
M062X/aug-cc-pVD(+d)Z = -610.394717,
ZPE = 0.005968, TC to the enthalpy = 0.010057
M062X/aug-cc-pVT(+d)Z = -610.465466,
ZPE = 0.006239, TC to the enthalpy = 0.010300
M062X/aug-cc-pVQ(+d)Z = -610.474916,
ZPE = 0.006247, TC to the enthalpy = 0.010306
G3 (298 K) = -610.238709
G3B3 (298 K) = -610.242093

O	0.000000	1.245300	-0.394015
Cl	0.000000	0.000000	0.370838
O	0.000000	-1.245300	-0.394015

ClO_2^-

M06/aug-cc-pVD(+d)Z = -610.478944,
ZPE = 0.004719, TC to the enthalpy = 0.008968
M06/aug-cc-pVT(+d)Z = -610.523455,
ZPE = 0.004954, TC to the enthalpy = 0.009161
M06/aug-cc-pVQ(+d)Z = -610.543312,
ZPE = 0.004967, TC to the enthalpy = 0.009173
M062X/aug-cc-pVD(+d)Z = -610.480461,
ZPE = 0.004738, TC to the enthalpy = 0.008975
M062X/aug-cc-pVT(+d)Z = -610.548119,
ZPE = 0.004930, TC to the enthalpy = 0.009132
M062X/aug-cc-pVQ(+d)Z = -610.556222,
ZPE = 0.004944, TC to the enthalpy = 0.009142756
G3 (298 K) = -610.321237
G3B3 (298 K) = -610.322733

O	0.000000	1.291793	-0.440114
Cl	0.000000	0.000000	0.414225
O	0.000000	-1.291793	-0.440114

HOClO

M06/aug-cc-pVD(+d)Z = -611.0210373, ZPE = 0.016861, TC to the enthalpy = 0.021489
M06/aug-cc-pVT(+d)Z = -611.069939, ZPE = 0.016861, TC to the enthalpy = 0.021489
M06/aug-cc-pVQ(+d)Z = -611.091639, ZPE = 0.017191, TC to the enthalpy = 0.021760
M062X/aug-cc-pVD(+d)Z = -611.022738, ZPE = 0.016952, TC to the enthalpy = 0.021577
M062X/aug-cc-pVT(+d)Z = -611.089223, ZPE = 0.017209, TC to the enthalpy = 0.021784
M062X/aug-cc-pVQ(+d)Z = -611.098585, ZPE = 0.017229, TC to the enthalpy = 0.021802
G3 (298 K) = -610.852975
G3B3 (298 K) = -610.856595

O	1.252592	0.540079	-0.013543
Cl	0.134424	-0.441022	0.017537
O	-1.344178	0.316665	-0.119399
H	-1.552527	0.643420	0.765406

ClO_3

M06/aug-cc-pVD(+d)Z = -685.489887, ZPE = 0.010488, TC to the enthalpy = 0.015063
M06/aug-cc-pVT(+d)Z = -685.571640, ZPE = 0.011168, TC to the enthalpy = 0.015645
M06/aug-cc-pVQ(+d)Z = -685.602161, ZPE = 0.011201, TC to the enthalpy = 0.015674
M062X/aug-cc-pVD(+d)Z = -685.487414, ZPE = 0.010666, TC to the enthalpy = 0.015202
M062X/aug-cc-pVT(+d)Z = -685.589418, ZPE = 0.011287, TC to the enthalpy = 0.015744
M062X/aug-cc-pVQ(+d)Z = -685.602648, ZPE = 0.011349, TC to the enthalpy = 0.15796
G3 (298 K) = -685.32784, G3B3 (298 K) = -685.329513

Cl	0.000000	0.000000	0.208229
O	0.000000	1.391251	-0.147495
O	1.204858	-0.695625	-0.147495
O	-1.204858	-0.695625	-0.147495

ClO_3^-

M06/aug-cc-pVD(+d)Z = -685.643502,
ZPE = 0.010160, TC to the enthalpy = 0.014745
M06/aug-cc-pVT(+d)Z = -685.717668,
ZPE = 0.010762, TC to the enthalpy = 0.015253
M06/aug-cc-pVQ(+d)Z = -685.746004,
ZPE = 0.010796, TC to the enthalpy = 0.015281
M062X/aug-cc-pVD(+d)Z = -685.643199,
ZPE = 0.010242, TC to the enthalpy = 0.014804
M062X/aug-cc-pVT(+d)Z = -685.744950,
ZPE = 0.010647, TC to the enthalpy = 0.015136
M062X/aug-cc-pVQ(+d)Z = -685.756676,
ZPE = 0.010661, TC to the enthalpy = 0.015146
G3 (298 K) = -685.482706, G3B3 (298 K) = -685.484894

Cl	0.000000	0.000000	0.310496
O	0.000000	1.377523	-0.219935
O	1.192970	-0.688761	-0.219935
O	-1.192970	-0.688761	-0.219935

$HOClO_2$

M06/aug-cc-pVD(+d)Z = -686.157582,
ZPE = 0.021230, TC to the enthalpy = 0.026516
M06/aug-cc-pVT(+d)Z = -686.235051,
ZPE = 0.021870, TC to the enthalpy = 0.027048
M06/aug-cc-pVQ(+d)Z = -686.265039,
ZPE = 0.021835, TC to the enthalpy = 0.027007
M062X/aug-cc-pVD(+d)Z = -686.156473,
ZPE = 0.021801, TC to the enthalpy = 0.026937
M062X/aug-cc-pVT(+d)Z = -686.255698,
ZPE = 0.021399, TC to the enthalpy = 0.026625
M062X/aug-cc-pVQ(+d)Z =-686.268689,
ZPE = 0.021798, TC to the enthalpy = 0.026934
G3 (298 K) = -685.983245, G3B3 (298 K) = -685.986965

O	0.210569	1.338302	-0.256970
Cl	0.170668	0.033329	0.333478
O	-1.354098	-0.520636	-0.113647
O	1.011920	-0.923381	-0.295606
H	-1.848487	0.279133	-0.339341

ClO_4

M06/aug-cc-pVD(+d)Z = -760.595725,
ZPE = 0.013647, TC to the enthalpy = 0.019176
M06/aug-cc-pVT(+d)Z = -760.703110,
ZPE = 0.014706, TC to the enthalpy = 0.020103
M06/aug-cc-pVQ(+d)Z = -760.742310,
ZPE = 0.014743, TC to the enthalpy = 0.020129
M062X/aug-cc-pVD(+d)Z = -760.596463,
ZPE = 0.0143035, TC to the enthalpy = 0.0197069
M062X/aug-cc-pVT(+d)Z = -760.725653,
ZPE = 0.015078, TC to the enthalpy = 0.020304
M062X/aug-cc-pVQ(+d)Z = -760.742520,
ZPE = 0.015092, TC to the enthalpy = 0.020318
G3 (298 K) = -760.422912, G3B3 (298 K) = -760.431188

1	17	0	0.000000	0.000000	0.077085
2	8	0	0.000000	1.082328	-0.920441
3	8	0	0.000000	-1.082328	-0.920441
4	8	0	-1.174890	0.000000	0.838538
5	8	0	1.174890	0.000000	0.838538

ClO_4^-

M06/aug-cc-pVD(+d)Z = -760.792939,
ZPE = 0.015876, TC to the enthalpy = 0.020800
M06/aug-cc-pVT(+d)Z = -760.894953,
ZPE = 0.016697, TC to the enthalpy = 0.021497
M06/aug-cc-pVQ(+d)Z = -760.933072,
ZPE = 0.014743, TC to the enthalpy = 0.020129
M062X/aug-cc-pVD(+d)Z = -760.796421,
ZPE = 0.015741, TC to the enthalpy = 0.020663
M062X/aug-cc-pVT(+d)Z = -760.9299438,
ZPE = 0.016507, TC to the enthalpy = 0.021312
M062X/aug-cc-pVQ(+d)Z = -760.945522,
ZPE =0.016532, TC to the enthalpy = 0.021329
G3 (298 K) = -760.626146, G3B3 (298 K) = -760.628189

1	17	0	0.000000	0.000000	0.000000
2	8	0	0.831628	0.831628	0.831628
3	8	0	-0.831628	-0.831628	0.831628
4	8	0	-0.831628	0.831628	-0.831628
5	8	0	0.831628	-0.831628	-0.831628

$HOClO_3$

M06/aug-cc-pVD(+d)Z = -761.279584,
ZPE = 0.027390, TC to the enthalpy = 0.032977
M06/aug-cc-pVT(+d)Z = -761.386965,
ZPE = 0.028337, TC to the enthalpy = 0.033784
M06/aug-cc-pVQ(+d)Z = -761.426367,
ZPE = 0.028392, TC to the enthalpy = 0.033832
M062X/aug-cc-pVD(+d)Z = -761.282754,
ZPE = 0.027496, TC to the enthalpy = 0.033042
M062X/aug-cc-pVT(+d)Z = -761.413933,
ZPE = 0.028326, TC to the enthalpy = 0.033752
M062X/aug-cc-pVQ(+d)Z = -761.430919,
ZPE = 0.028369, TC to the enthalpy = 0.033788
G3 (298 K) = -761.100895, G3B3 (298 K) = -761.103854

H	1.795770	-0.829306	0.000000
O	1.482081	0.086618	0.000000
Cl	-0.138497	0.009588	0.000000
O	-0.470749	1.366051	0.000000
O	-0.470749	-0.684690	1.176114
O	-0.470749	-0.684690	-1.176114

All geometries are at the M06/aug-cc-pVQ(+d)Z level

Chapter 3

$^{-}CH_2CO_2Li$ (2a)

DH°_{298K} = -235.504827
G3 (298 K) = -235.303775

C	-0.15136031	0.10750428	1.53144621
H	-0.33688478	1.08111721	1.96418572
H	-0.11142010	-0.76270683	2.17233807
C	0.03318052	-0.02356660	0.17052440
O	0.26531774	-1.20583832	-0.41089820
O	-0.00716369	1.02248335	-0.66245711
Li	0.30833062	-0.21899309	-1.85860810

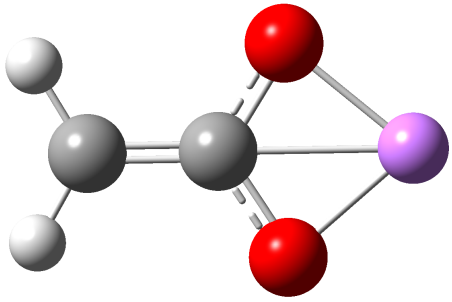

$^{-}CH_2CO_2Li$ (2b)

DH°_{298K} = -235.495094
G3 (298 K) = -235.295050

C	0.685780	1.139168	-0.046835
H	1.346935	1.155432	-0.919600
H	0.224232	2.106340	0.126450
C	-0.257847	-0.013732	-0.070058
O	0.342698	-1.190441	-0.200878
O	-1.482557	0.105749	0.131393
Li	1.660036	-0.445618	0.683463

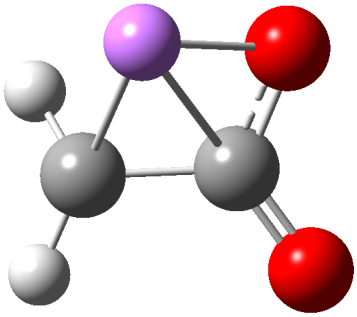

CH_3CO_2Li (C-protonation)

DH°_{298K} = -236.118149
G3 (298 K) = -235.920164

C	0.00000000	0.04701000	0.00000000
O	-1.17881500	-0.42537200	0.00000000
O	1.01473300	-0.71843500	0.00000000
C	0.21273500	1.54245000	0.00000000
H	0.79700600	1.82287000	0.87661000
H	0.79700600	1.82287000	-0.87661000
Li	-0.27421500	-2.03495700	0.00000000
H	-0.73511800	2.07282600	0.00000000

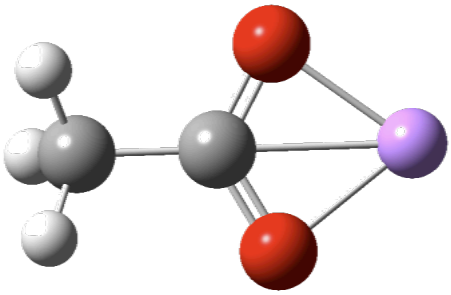

$LiCH_2CO_2H$ (O-protonation)

ΔH°_{298K} = -236.064419

C	0.789688	1.094171	-0.077845
H	1.697406	0.996359	-0.663701
H	0.442036	2.095516	0.116365
C	-0.101826	0.034962	-0.115723
O	0.255262	-1.189439	-0.243607
O	-1.417573	0.279765	0.140113
H	-1.844174	-0.584993	0.191186
Li	1.625350	-0.668095	0.781838

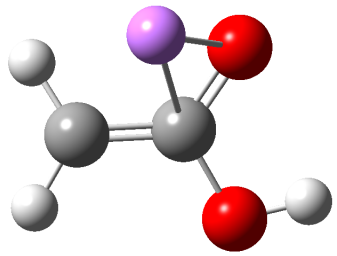

$^{\cdot}CH_2CO_2Li$

ΔH°_{298K} = -235.465367
G3 (298 K) = -235.264168

C	-0.00142600	1.56458600	0.00000000
H	-0.93904600	2.09876500	0.00000000
H	0.93579400	2.09937200	0.00000000
C	0.00000000	0.11211400	0.00000000
O	1.11323600	-0.51614500	0.00000000
O	-1.11162800	-0.51940400	0.00000000
Li	-0.00035000	-1.99131400	0.00000000

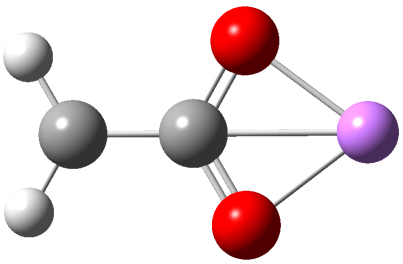

$^{\cdot}CH_2CO_2Li$

ΔH°_{298K} = -235.431367

H	0.093799	1.863360	-0.910566
C	-0.118349	1.314287	0.000197
H	0.088381	1.862108	0.912982
C	0.209496	-0.167708	0.000021
Li	-2.048086	0.159059	-0.001986
O	-0.743060	-1.012368	0.000609
O	1.419960	-0.372897	-0.000330

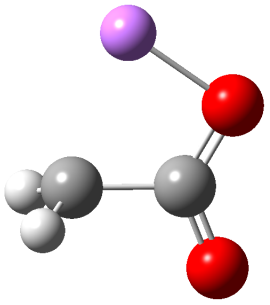

Chapter 4

C_2Li_2 (D_{2h})

G3 (0 K) = -91.116228, G3 (298 K) = -91.110668
W1 (0 K) = -91.179436 , W1 (298 K) = -91.173991

C	0.000000	0.628018	-0.000058
C	0.000000	-0.628018	-0.000058
Li	0.000000	0.000000	-1.881323
Li	0.000000	0.000000	1.881554

C_2Li_2 ($D_{\infty h}$)

G3 (0 K) = -91.102992, G3 (298 K) = -91.097489
W1 (0 K) = -91.167079 , W1 (298 K) = -91.161626

C	0.000000	0.000000	0.621756
C	0.000000	0.000000	-0.621756
Li	0.000000	0.000000	-2.489889
Li	0.000000	0.000000	2.489889

C_2LiH ($C_{\infty v}$)

G3 (0 K) = -84.197869, G3 (298 K) = -84.193249
G4 (0 K) = -84.212795, G4 (298 K) = -84.208253
W1 (0 K) = -84.254643, W1 (298 K) = -84.250016

C	0.000000	0.000000	-0.247508
C	0.000000	0.000000	0.972852
H	0.000000	0.000000	2.036445
Li	0.000000	0.000000	-2.129503

C_2Li^- (C_{2v})

G3 (0 K) = -83.579900, G3 (298 K) = -83.575610
G4 (0 K) = -83.594634, G4 (298 K) = -83.590430
W1 (0 K) = -83.634400, W1 (298 K) = -83.630171

C	0.000000	0.630871	-0.363196
C	0.000000	-0.630871	-0.363196
Li	0.000000	0.000000	1.452782

C_2Li (C_{2v})

G3 (0 K) = -83.516349, G3 (298 K) = -83.511904
G4 (0 K) = -83.530235, G4 (298 K) = -83.525863
W1 (0 K) = -83.572575, W1 (298 K) = -83.568197

C	0.000000	0.628131	-0.384117
C	0.000000	-0.628131	-0.384117
Li	0.000000	0.000000	1.536468

C_2H_2 ($D_{\infty h}$)

G3 (0 K) = -77.275963, G3 (298 K) = -77.272275
W1 (0 K) = -77.325379, W1 (298 K) = -77.321614

C	0.000000	0.000000	0.598022
C	0.000000	0.000000	-0.598022
H	0.000000	0.000000	-1.659577
H	0.000000	0.000000	1.659577

C_2H ($C_{\infty v}$)

G3 (0 K) = -76.564682, G3 (298 K) = -76.560925
W1 (0 K) = -76.616789, W1 (298 K) = -76.612615

C	0.000000	0.000000	-0.471846
C	0.000000	0.000000	0.727636
H	0.000000	0.000000	-1.534738

C_2H^- ($C_{\infty v}$)

G3 (0 K) = -76.674752, G3 (298 K) = -76.671128
W1 (0 K) = -76.724337, W1 (298 K) = -76.720664

C	0.000000	0.000000	-0.489359
H	0.000000	0.000000	-1.556926
C	0.000000	0.000000	0.748847

All geometries are from the W1 calculations (B3LYP/cc-pVT(+d)Z)

Chapter 5

Adamantanone Neutral

B3LYP/aug-cc-pVDZ =	-464.789050	ZPE =	0.223099	TC =	0.231700118
M06/aug-cc-pVDZ =	-464.6049176	ZPE =	0.225368	TC =	0.233900589
M06/maug-cc-pVT(+d)Z =	-464.7037536				
G3 0K =	-464.353393	G3 298K=	-464.344232		

0 1

C	1.259733	1.253060	-0.226510
H	2.161845	1.272083	0.400624
H	1.270184	2.159861	-0.848312
C	0.000000	1.266625	0.663675
H	0.000000	2.127313	1.341361
C	1.255636	0.000000	-1.113947
H	2.152731	0.000000	-1.747185
C	1.259733	-1.253060	-0.226510
H	2.161845	-1.272083	0.400624
H	1.270184	-2.159861	-0.848312
C	0.000000	-1.266625	0.663675
H	0.000000	-2.127313	1.341361
C	-1.259733	-1.253060	-0.226510
H	-1.270184	-2.159861	-0.848312
H	-2.161845	-1.272083	0.400624
C	-1.259733	1.253060	-0.226510
H	-1.270184	2.159861	-0.848312
H	-2.161845	1.272083	0.400624
C	0.000000	0.000000	-1.997628
H	0.000000	0.886345	-2.648461
H	0.000000	-0.886345	-2.648461

Enol

M06/aug-cc-pVDZ = -464.5110228 ZPE = 0.223839 TC = 0.232592098

0 1

C	0.484311	-1.716882	-0.039783
H	1.478621	-2.024020	0.300515
H	-0.060189	-2.618301	-0.352777
C	0.493877	-0.616112	-1.104323
C	-0.278798	-0.994123	1.136565
H	-0.307709	-1.671765	2.002111
C	0.413233	0.322215	1.559355
H	1.418375	0.136849	1.951869
H	-0.180370	0.801007	2.350317
C	0.488041	1.336982	0.339714
H	1.042105	2.239448	0.624384
C	-0.950814	1.650893	-0.079955
H	-1.454724	2.146241	0.762090
H	-0.961831	2.349907	-0.926652
C	-0.900815	-0.285238	-1.606436
H	-1.393529	-1.206686	-1.947140
H	-0.847943	0.388773	-2.470050
C	-1.713721	-0.641109	0.707573
H	-2.252217	-1.549813	0.401007
H	-2.256962	-0.211412	1.561936
C	-1.688507	0.357020	-0.461865
H	-2.715784	0.598806	-0.768227
C	1.221792	0.424300	-0.600230
O	2.525788	0.259804	-0.231697
H	2.874262	-0.485144	-0.739510

Cyclopropanol

M06/aug-cc-pVDZ = -464.5637415 ZPE = 0.22437 TC = 0.233122405

M06/maug-cc-pVT(+d)Z = -464.6617041

0 1

C	0.010043	-1.873053	0.061615
H	-0.849996	-2.480862	-0.246645
H	0.781181	-2.532456	0.483843
C	-0.445565	-0.764702	1.028762
H	-1.098937	-1.128066	1.829893
C	0.513325	-1.020451	-1.120270
H	0.656588	-1.604398	-2.036115
C	-0.637544	-0.010642	-1.279786
H	-1.293662	-0.075150	-2.144289
C	-0.553742	1.325229	-0.554488
H	-1.235917	2.080802	-0.944627
C	0.775821	1.816174	-0.029480
H	1.323223	2.337905	-0.827373
H	0.617580	2.535303	0.787072
C	0.801757	-0.070448	1.599379
H	1.429359	-0.820587	2.100756
H	0.518294	0.677958	2.353284
C	1.829961	-0.343275	-0.705595
H	2.556231	-1.117982	-0.421582
H	2.258292	0.216286	-1.549080
C	1.590085	0.619671	0.471614
H	2.553635	0.973957	0.859846
C	-1.246903	0.153039	0.082646
O	-2.643079	0.149936	0.190784
H	-2.894676	0.748554	0.902369

Adamantanone a anion (C1)

B3LYP/aug-cc-pVDZ =	-464.1345528	ZPE =	0.205386	TC =	0.214082
M06/aug-cc-pVDZ =	-463.9533502	ZPE =	0.208296	TC =	0.216859
M06/maug-cc-pVT(+d)Z =	-464.0509499				
G3 0K =	-463.712605	G3 298K=	-463.703253		

-1 1

C	0.212788	-1.741234	-0.084286
H	1.107554	-2.221358	0.341744
H	-0.427290	-2.545499	-0.495310
C	0.603136	-0.730306	-1.180981
C	-0.573609	-1.029018	1.059595
H	-0.832801	-1.751764	1.854288
C	0.273949	0.105040	1.666062
H	1.193741	-0.298440	2.112791
H	-0.296304	0.618077	2.460531
C	0.653784	1.128177	0.557550
H	1.319680	1.901282	0.968088
C	-0.636898	1.732641	-0.004261
H	-1.173600	2.262694	0.803583
H	-0.407649	2.473725	-0.786074
C	-0.689171	-0.079983	-1.690251
H	-1.312772	-0.862612	-2.159952
H	-0.467604	0.651349	-2.486547
C	-1.860633	-0.410874	0.492312
H	-2.492399	-1.202117	0.055452
H	-2.441485	0.067167	1.301133
C	-1.510661	0.618108	-0.592538
H	-2.440323	1.054538	-1.000826
C	1.436308	0.211124	-0.415155
O	2.652162	0.128863	-0.227149

A anion (cs) transition state

-1 1

C	0.577225	-1.153873	1.233199
H	1.070610	-0.826003	2.165241
H	0.572363	-2.259555	1.254287
C	1.372054	-0.683466	0.000000
C	-0.889859	-0.658791	1.254934
H	-1.413435	-1.024781	2.156900
C	-0.889859	0.875028	1.253714
H	-0.387590	1.249993	2.159570
H	-1.923528	1.265573	1.262714
C	-0.157507	1.387530	0.000000
H	-0.103418	2.486019	0.000000
C	-0.889859	0.875028	-1.253714
H	-1.923528	1.265573	-1.262714
H	-0.387590	1.249993	-2.159570
C	0.577225	-1.153873	-1.233199
H	0.572363	-2.259555	-1.254287
H	1.070610	-0.826003	-2.165241
C	-1.613937	-1.165900	0.000000
H	-1.623014	-2.268497	0.000000
H	-2.665104	-0.825997	0.000000
C	-0.889859	-0.658791	-1.254934
H	-1.413435	-1.024781	-2.156900
C	1.284796	0.814576	0.000000
O	2.209021	1.616652	0.000000

Alpha radical

B3LYP/aug-cc-pVDZ =	-464.1170534	ZPE =	0.209597	TC =	0.218229736
M06/aug-cc-pVDZ =	-463.9334571	ZPE =	0.211768	TC =	0.220333363
M06/maug-cc-pVT(+d)Z =	-464.0307822				
G3 0K =	-463.688606	G3 298K=	-463.679437		

0 2

C	0.587128	-1.167722	1.260107
H	1.109981	-0.807451	2.156109
H	0.606798	-2.266318	1.266124
C	1.222103	-0.634830	0.000000
C	-0.879883	-0.660605	1.259593
H	-1.393252	-1.029925	2.157522
C	-0.879883	0.875786	1.260543
H	-0.381611	1.255359	2.163266
H	-1.913093	1.251710	1.272183
C	-0.166178	1.410341	0.000000
H	-0.120910	2.505414	0.000000
C	-0.879883	0.875786	-1.260543
H	-1.913093	1.251710	-1.272183
H	-0.381611	1.255359	-2.163266
C	0.587128	-1.167722	-1.260107
H	0.606798	-2.266318	-1.266124
H	1.109981	-0.807451	-2.156109
C	-1.591274	-1.177360	0.000000
H	-1.603156	-2.276777	0.000000
H	-2.637110	-0.837858	0.000000
C	-0.879883	-0.660605	-1.259593
H	-1.393252	-1.029925	-2.157522
C	1.261982	0.863096	0.000000
O	2.251924	1.558186	0.000000

Beta anion up

B3LYP/aug-cc-pVDZ =	-464.1380508	ZPE =	0.205196	TC =	0.214096
M06/aug-cc-pVDZ =	-463.9528982	ZPE =	0.208031	TC =	0.217332
M06/maug-cc-pVT(+d)Z =	-464.0502315				
G3 0K =	-463.723195	G3 298K=	-463.714011		

-1 1

C	0.322823	-1.759566	-0.316844
H	-0.249347	-2.345422	-1.045596
H	0.977960	-2.440342	0.259121
C	-0.635491	-1.059424	0.663417
H	-1.313053	-1.771074	1.154793
C	1.123340	-0.678390	-1.062978
H	1.789607	-1.169083	-1.790597
C	0.135083	0.223156	-1.797879
H	0.646946	0.909952	-2.496677
C	-0.670753	1.026036	-0.767707
H	-1.363419	1.724740	-1.255957
C	0.183407	1.770790	0.296186
H	0.796407	2.524904	-0.221286
H	-0.449446	2.293312	1.038545
C	0.203370	-0.293101	1.709874
H	0.832908	-1.010133	2.262047
H	-0.458955	0.199430	2.439347
C	1.997934	0.057075	-0.011653
H	2.672355	-0.642873	0.520181
H	2.623330	0.804847	-0.521871
C	1.086838	0.754997	1.011625
H	1.696974	1.267558	1.772254
C	-1.494263	-0.025310	-0.065498
O	-2.714499	-0.055424	-0.008197

Beta Anion Down

B3LYP/aug-cc-pVDZ =	-464.1470472	ZPE =	0.206387	TC =	0.21502933
M06/aug-cc-pVDZ =	-463.9606293	ZPE =	0.208775	TC =	0.217331604
M06/maug-cc-pVT(+d)Z =	-464.058192				
G3 0K =	-463.723332	G3 298K=	-463.714202		

-1 1

C	1.465456	0.143934	0.131143
C	0.590627	-0.792521	0.974363
H	1.251746	-1.304718	1.686349
C	0.682053	1.026420	-0.790104
H	1.370550	1.714151	-1.298145
C	-0.423204	1.793107	-0.055926
H	0.002735	2.517277	0.659631
H	-1.008215	2.341808	-0.809574
C	-0.489157	0.023002	1.709060
H	-1.133517	-0.659988	2.287417
H	-0.018800	0.719449	2.421420
C	-1.331413	0.805433	0.690617
H	-2.120995	1.359607	1.223824
C	-1.966051	-0.175995	-0.306627
H	-2.557127	0.378722	-1.048626
H	-2.638973	-0.862152	0.237856
C	-0.095053	-1.790318	0.021352
H	0.671532	-2.398490	-0.478910
H	-0.755012	-2.476416	0.594127
C	0.064428	0.010799	-1.776037
H	0.862839	-0.545496	-2.294695
C	-0.857178	-0.955717	-1.034760
H	-1.325917	-1.643987	-1.757399
O	2.694513	0.041421	0.149780

Beta cyclized

B3LYP/aug-cc-pVDZ =	-464.1429356	ZPE =	0.206235	TC =	0.21480627
M06/aug-cc-pVDZ =	-463.9630091	ZPE =	0.208738	TC =	0.21719588
M06/maug-cc-pVT(+d)Z =	-464.0613778				
G3 0K =	-463.722267	G3 298K=	-463.713482		

-1 1

C	-0.077446	-1.858701	0.032086
H	-0.963465	-2.422180	-0.289715
H	0.673022	-2.562260	0.436461
C	-0.503652	-0.759491	1.013375
H	-1.168844	-1.114816	1.807810
C	0.451362	-1.001704	-1.136455
H	0.590066	-1.584815	-2.058483
C	-0.663236	0.039644	-1.290336
H	-1.287211	0.017387	-2.183226
C	-0.555428	1.347987	-0.510928
H	-1.213015	2.137514	-0.879063
C	0.800810	1.793602	-0.015683
H	1.378157	2.291336	-0.817371
H	0.688072	2.520197	0.806036
C	0.762446	-0.110203	1.594084
H	1.380108	-0.875558	2.096205
H	0.490061	0.642771	2.349553
C	1.795166	-0.388280	-0.703093
H	2.490504	-1.194377	-0.414960
H	2.254276	0.166240	-1.536837
C	1.579486	0.571163	0.481026
H	2.555612	0.890985	0.878170
C	-1.360125	0.198270	0.102436
O	-2.655455	0.261732	0.300793

Beta anion epimerization TS
M06/aug-cc-pVDZ = -463.951288

-1 1

C	0.234372	-1.820158	-0.019517
H	-0.441827	-2.503347	-0.546484
H	0.953311	-2.412939	0.582211
C	-0.577102	-0.886882	0.889800
H	-1.243593	-1.445215	1.560196
C	0.920640	-0.897330	-1.045985
H	1.426994	-1.500488	-1.815046
C	-0.166968	-0.056267	-1.677103
H	-0.149594	0.124416	-2.753030
C	-0.697091	1.034460	-0.769989
H	-1.404257	1.690081	-1.292322
C	0.352901	1.830373	0.020873
H	0.943839	2.442590	-0.680602
H	-0.124385	2.503905	0.755211
C	0.413543	-0.022791	1.699858
H	1.065925	-0.679091	2.300107
H	-0.133942	0.629895	2.398053
C	1.978803	-0.065358	-0.274491
H	2.693392	-0.723098	0.254513
H	2.546565	0.556198	-0.983047
C	1.270007	0.837778	0.751613
H	2.017842	1.387550	1.344282
C	-1.474929	0.043756	0.045395
O	-2.709416	-0.006992	0.144153

Beta anion cyclization TS

M06/aug-cc-pVDZ = -463.9546952

-1 1

C	0.234388	-1.820162	-0.019536
H	-0.441796	-2.503358	-0.546513
H	0.953330	-2.412935	0.582196
C	-0.577104	-0.886901	0.889781
H	-1.243598	-1.445244	1.560167
C	0.920655	-0.897314	-1.045988
H	1.427015	-1.500456	-1.815057
C	-0.166950	-0.056248	-1.677103
H	-0.149567	0.124450	-2.753027
C	-0.697093	1.034464	-0.769986
H	-1.404266	1.690079	-1.292317
C	0.352889	1.830378	0.020890
H	0.943830	2.442600	-0.680579
H	-0.124402	2.503906	0.755228
C	0.413524	-0.022807	1.699857
H	1.065905	-0.679104	2.300110
H	-0.133976	0.629870	2.398049
C	1.978805	-0.065345	-0.274473
H	2.693391	-0.723086	0.254533
H	2.546571	0.556220	-0.983018
C	1.269993	0.837778	0.751630
H	2.017818	1.387547	1.344314
C	-1.474928	0.043743	0.045384
O	-2.709415	-0.007001	0.144147

Beta radical

B3LYP/aug-cc-pVDZ =	-464.1240726	ZPE =	0.208828	TC =	0.217694934
M06/aug-cc-pVDZ =	-463.940244	ZPE =	0.211086	TC =	0.219868344
M06/maug-cc-pVT(+d)Z =	-464.0374422				
G3 0K =	-463.6958	G3 298K=	-463.686455		

0 2

C	0.264796	-1.776465	0.045000
H	-0.364812	-2.475919	-0.520117
H	0.931389	-2.368203	0.690245
C	-0.613098	-0.862799	0.922198
H	-1.264817	-1.450089	1.578204
C	1.100610	-0.906884	-0.925749
H	1.711478	-1.554655	-1.565785
C	0.152448	-0.085784	-1.747584
H	-0.175521	-0.419459	-2.729839
C	-0.694013	0.860871	-0.948466
H	-1.396216	1.428039	-1.566889
C	0.211640	1.789168	-0.102124
H	0.800921	2.420991	-0.780184
H	-0.411293	2.447660	0.519101
C	0.289418	0.087658	1.735241
H	0.939084	-0.508466	2.391998
H	-0.325927	0.733669	2.376625
C	2.004692	0.029201	-0.098249
H	2.678833	-0.568887	0.531857
H	2.624489	0.635296	-0.772630
C	1.137140	0.941230	0.781372
H	1.784273	1.606888	1.367989
C	-1.498885	-0.015640	0.018651
O	-2.707547	-0.036274	0.049711

Gama anion

B3LYP/aug-cc-pVDZ =	-464.1425572	ZPE =	0.205463	TC =	0.214171958
M06/aug-cc-pVDZ =	-463.955983	ZPE =	0.207691	TC =	0.216314797
M06/maug-cc-pVT(+d)Z =	-464.053652				
G3 0K =	-463.717993	G3 298K=	-463.70878		

-1 1

C	-0.547397	-1.161887	1.252720
H	-1.577994	-1.548843	1.307933
H	-0.015910	-1.515716	2.153571
C	-0.547397	0.378431	1.248619
H	-1.080585	0.787275	2.120000
C	0.166867	-1.686860	0.000000
H	0.142389	-2.791574	0.000000
C	-0.547397	-1.161887	-1.252720
H	-1.577994	-1.548843	-1.307933
H	-0.015910	-1.515716	-2.153571
C	-0.547397	0.378431	-1.248619
H	-1.080585	0.787275	-2.120000
C	0.976296	0.859232	-1.213994
H	1.429422	0.495580	-2.153923
H	0.969997	1.961555	-1.253342
C	0.976296	0.859232	1.213994
H	1.429422	0.495580	2.153923
H	0.969997	1.961555	1.253342
C	1.630759	-1.174849	0.000000
H	2.139822	-1.592093	0.889310
H	2.139822	-1.592093	-0.889310
C	1.700691	0.344326	0.000000
C	-1.182118	0.912706	0.000000
O	-2.043387	1.791852	0.000000

Gama Radical

B3LYP/aug-cc-pVDZ =	-464.1224752	ZPE =	0.209746	TC =	0.218352264
M06/aug-cc-pVDZ =	-463.9389418	ZPE =	0.211884	TC =	0.220423225
M06/maug-cc-pVT(+d)Z =	-464.0362769				
G3 0K =	-463.693693	G3 298K=	-463.684546		

0 2

C	-0.510660	-1.147397	1.254495
H	-1.544782	-1.518575	1.275248
H	-0.010373	-1.517365	2.161128
C	-0.510660	0.395746	1.270386
H	-1.060239	0.790513	2.132166
C	0.208481	-1.666828	0.000000
H	0.202887	-2.765122	0.000000
C	-0.510660	-1.147397	-1.254495
H	-1.544782	-1.518575	-1.275248
H	-0.010373	-1.517365	-2.161128
C	-0.510660	0.395746	-1.270386
H	-1.060239	0.790513	-2.132166
C	0.965123	0.903111	-1.251413
H	1.476481	0.539512	-2.153199
H	0.980656	2.001001	-1.262447
C	0.965123	0.903111	1.251413
H	1.476481	0.539512	2.153199
H	0.980656	2.001001	1.262447
C	1.672922	-1.149544	0.000000
H	2.197090	-1.521409	0.891208
H	2.197090	-1.521409	-0.891208
C	1.582976	0.348866	0.000000
C	-1.185068	0.889603	0.000000
O	-2.160255	1.608458	0.000000

Ring opened at Gama position neutral

M06/aug-cc-pVDZ = -464.57103 ZPE = 0.22172 TC = 0.231191777

0 1

C	0.381173	0.970017	1.439485
H	1.300734	1.549968	1.599958
H	-0.186520	0.989043	2.381192
C	0.727560	-0.483188	1.085137
H	1.343274	-0.946035	1.864450
C	-0.439708	1.589265	0.304629
H	-0.699564	2.621936	0.575046
C	0.416990	1.646446	-0.968557
H	1.228126	2.367634	-0.795404
H	-0.179063	2.034730	-1.805197
C	1.037768	0.294752	-1.367097
H	1.865734	0.421740	-2.072249
C	-2.197378	-1.388228	-0.965132
H	-2.908880	-0.919312	-1.644309
H	-2.038012	-2.461246	-1.066960
C	-0.573579	-1.302238	0.925075
H	-1.043503	-1.341723	1.920933
H	-0.347090	-2.332911	0.626359
C	-1.756919	0.810754	0.133874
H	-2.354413	0.969272	1.046607
H	-2.336577	1.210099	-0.708413
C	-1.550726	-0.675198	-0.039750
C	1.552980	-0.518186	-0.193090
O	2.560806	-1.186967	-0.274124
H	0.280350	-0.332639	-1.856471

Gama anion ring open

M06/aug-cc-pVDZ =	-463.955983	ZPE =	0.207691	TC =	0.216314797
M06/maug-cc-pVT(+d)Z =	-464.0810809				
G3 0K =	-463.742645	G3 298K=	-463.732286		

-1 1

C	0.235883	1.107675	1.394517
H	1.087333	1.789288	1.535446
H	-0.364654	1.117754	2.322311
C	0.747967	-0.301068	1.096638
H	1.419403	-0.648306	1.893978
C	-0.609168	1.582715	0.210810
H	-1.028514	2.577769	0.433151
C	0.284935	1.698970	-1.034869
H	0.771084	2.696839	-0.995466
H	-0.376705	1.739698	-1.922276
C	1.299159	0.588627	-1.168238
H	1.839805	0.513887	-2.114316
C	-1.894713	-1.638044	-1.010557
H	-2.584853	-1.270727	-1.771325
H	-1.578303	-2.678840	-1.073078
C	-0.433532	-1.282651	0.988799
H	-0.962133	-1.334442	1.958862
H	-0.048422	-2.280551	0.746977
C	-1.804797	0.626609	0.029031
H	-2.454925	0.740928	0.915351
H	-2.395083	0.914334	-0.852847
C	-1.408235	-0.825608	-0.067404
C	1.558578	-0.376656	-0.215408
O	2.352439	-1.370132	-0.302086

Gama Ring opening transition state

B3LYP/aug-cc-pVDZ =	-464.133941
M06/aug-cc-pVDZ =	-463.9444676
M06/maug-cc-pVT(+d)Z =	-464.0438661

-1 1

C	0.024022	-0.164596	1.845437
H	-0.936704	-0.499122	2.247741
H	0.560643	0.544200	2.486342
C	-0.710174	1.234925	0.526242
H	-1.309386	1.951727	1.097389
C	0.763762	-1.047182	1.047530
C	-0.099144	-1.761828	0.056039
H	-0.974580	-2.229407	0.530008
H	0.451144	-2.535892	-0.506393
C	-0.645502	-0.706137	-1.004326
H	-1.306492	-1.221486	-1.714201
C	0.563924	-0.076319	-1.708666
H	1.151312	-0.866259	-2.210646
H	0.235050	0.630599	-2.486617
C	0.624885	1.748832	0.003974
H	1.219777	2.158131	0.842661
H	0.485894	2.584578	-0.706073
C	1.946882	-0.391792	0.367756
H	2.586149	0.129775	1.100749
H	2.576401	-1.136587	-0.152852
C	1.443943	0.637435	-0.674822
H	2.313458	1.091983	-1.179938
C	-1.475973	0.293545	-0.227815
O	-2.709053	0.099558	-0.092033

Gama ring open radical

M06/aug-cc-pVDZ = -463.924491 ZPE = 0.208184 TC = 0.217592383

0 2

C	0.134210	1.166744	1.363324
H	0.914040	1.936273	1.454262
H	-0.435105	1.164290	2.303689
C	0.774858	-0.208305	1.143038
H	1.468730	-0.459900	1.953245
C	-0.793502	1.495143	0.187679
H	-1.283322	2.460518	0.369540
C	0.030950	1.616229	-1.104996
H	0.469883	2.627921	-1.162307
H	-0.622003	1.533680	-1.988114
C	1.146425	0.631461	-1.219932
H	1.705526	0.557142	-2.152363
C	-1.571646	-1.783287	-1.056133
H	-2.271678	-1.498510	-1.841348
H	-1.104885	-2.764838	-1.129225
C	-0.314918	-1.300141	1.050370
H	-0.839729	-1.343958	2.017535
H	0.149711	-2.275492	0.866339
C	-1.892345	0.419895	0.076594
H	-2.506684	0.469649	0.989729
H	-2.548197	0.628790	-0.778296
C	-1.299367	-0.960395	-0.040457
C	1.574287	-0.234666	-0.152686
O	2.521251	-1.011454	-0.297937

Delta anion

B3LYP/aug-cc-pVDZ =	-464.1335926	ZPE =	0.205882	TC =	0.214556812
M06/aug-cc-pVDZ =	-463.9503076	ZPE =	0.20826	TC =	0.216838831
M06/maug-cc-pVT(+d)Z =	-464.0474222				
G3 0K =	-463.711311	G3 298K=	-463.7024029		

-1 1

C	0.536867	-1.145496	1.265459
H	1.070573	-0.779147	2.163648
H	0.576364	-2.244723	1.275662
C	1.261629	-0.632148	0.000000
H	2.324134	-0.910113	0.000000
C	-0.944809	-0.685529	1.233461
H	-1.433781	-1.050661	2.151695
C	-0.944809	0.853068	1.266173
H	-0.425630	1.243057	2.158998
H	-1.983657	1.208200	1.276931
C	-0.242841	1.395692	0.000000
H	-0.203972	2.493651	0.000000
C	-0.944809	0.853068	-1.266173
H	-1.983657	1.208200	-1.276931
H	-0.425630	1.243057	-2.158998
C	0.536867	-1.145496	-1.265459
H	0.576364	-2.244723	-1.275662
H	1.070573	-0.779147	-2.163648
C	-1.708665	-1.171146	0.000000
H	-1.720782	-2.280558	0.000000
C	-0.944809	-0.685529	-1.233461
H	-1.433781	-1.050661	-2.151695
C	1.179595	0.880056	0.000000
O	2.160949	1.605540	0.000000

Delta radical

B3LYP/aug-cc-pVDZ =	-464.1216733	ZPE =	0.208526	TC =	0.217447422
M06/aug-cc-pVDZ =	-463.938482	ZPE =	0.210805	TC =	0.219641993
M06/maug-cc-pVT(+d)Z =	-464.0357441				
G3 0K =	-463.693806	G3 298K=	-463.6900295		

0 2

C	0.523877	-1.163961	1.264810
H	1.039796	-0.800962	2.165111
H	0.551694	-2.262157	1.281851
C	1.247370	-0.656135	0.000000
H	2.300393	-0.958857	0.000000
C	-0.943019	-0.669119	1.256345
H	-1.462620	-1.044818	2.145950
C	-0.943019	0.873299	1.263171
H	-0.434606	1.246797	2.163053
H	-1.975197	1.248347	1.278894
C	-0.230530	1.399426	0.000000
H	-0.183145	2.494012	0.000000
C	-0.943019	0.873299	-1.263171
H	-1.975197	1.248347	-1.278894
H	-0.434606	1.246797	-2.163053
C	0.523877	-1.163961	-1.264810
H	0.551694	-2.262157	-1.281851
H	1.039796	-0.800962	-2.165111
C	-1.601036	-1.155257	0.000000
H	-2.232932	-2.040954	0.000000
C	-0.943019	-0.669119	-1.256345
H	-1.462620	-1.044818	-2.145950
C	1.189843	0.862071	0.000000
O	2.173699	1.568517	0.000000

Appendix 2

PERL Scripts for Recalculating Temperature Corrections

The temperature correction generated in the Gaussian output of a frequency calculation has been shown to overestimate the contribution of energy from the low frequency vibrational modes to the predicted enthalpy of a molecule. This overestimation can be corrected by replacing any the contribution that is more 1/2RT with 1/2RT for a given mode. In an effort to avoid the arduous task of making this correction by hand, a series of PERL script were developed to read in the output files directly, and compute the adjusted temperature correction.

2.1 General Frequency Jobs

This script allow for the user to vary the temperature, the vibrational scale factor, and the scale factor for the ZPE independently through a series of input options listed below with the default value in parentheses

-t temperature in Kelvin (298.15)
-s vibrational scale factor (1)
-z scale factor for ZPE (if no input present –z = -s)

User input

$ freq.pl –t 289.15 –s 1 –z 1 outputfile.out

Code saved in file freq.pl

```
#!/usr/bin/perl -w
# User Input information #
use strict; use Getopt::Std; our $opt_t; our $opt_s; our $opt_z;
getopts('t:s:z:');
# Defining Constants and Variables #
my @line; my @zpe; my @zpesum; my @freqs; my @scaledfreqs;
my @energies; my @int; my @freqint; our $scale_factor=1;
our $T=298.15; my $R=8.314472; my $h=6.62608E-34;
my $N=6.02214E23; my $k=1.38066E-23; my $c=29979250000;
my $oneHalfRT=$R*$T/(2*$N*$h*$c); my $totalE=0;
my $totalEcor=0; my $zpecor=1; my $zpesum=1; my $tempcorE=1;
my $scaledzpe; my $electronicE; my $tempcor;
# input options #
if ($opt_t) { $T=$opt_t;}
if ($opt_s) { $scale_factor=$opt_s;}
my $z=$scale_factor;
```

```
if ($opt_z) { $z=$opt_z;}
# finding Freqs and calculating contribution of vibration #
while (<>) { if (/Frequencies/){ @line=split;
foreach (@line){ if (/\d+\.\d+/){ push @freqs, $_;
$_=$_*$scale_factor; push @scaledfreqs, $_;
$_=$_/(exp($h*$c*$_/($k*$T))-1);
if (1) { if ($_ > $oneHalfRT){ $_=$oneHalfRT;}
push @energies, $_;}        }           }           }
# Finding ZPE from File #
if (/Zero-point/){ @zpe=split;
foreach (@zpe){ if (/\d+\.\d+/) { $zpecor=$_; }  }      }
# finding Electronic Energy #
if (/SCF Done/){ @zpesum=split;
foreach (@zpesum){ if (/\d+\.\d+/) { $electronicE=$_;} }  }   }
# Summing contribution of each frequency #
foreach (@energies){ $totalE=$totalE+$_;}
# Calculating output quantities #
$scaledzpe= $zpecor*$z;
$zpesum= $electronicE + $scaledzpe;
$totalEcor=($totalE*$N*$h*$c+4*$R*$T)/2625501;
$tempcorE=$electronicE + $scaledzpe + $totalEcor;
$tempcor=$scaledzpe + $totalEcor;
# Printing data #
print "\n\ Scale Factor $scale_factor\n";
print "ZPE scale factor is $z\n";
print "Electronic Energy\n";
print "Scaled ZPE\n";
print "Temperature correction at $T\n";
print "$electronicE\n";
print "$scaledzpe\n";
print "$tempcor\n";
```

2.2 Correcting G3 Jobs

User input

$ freqg3.pl –t 289.15 output_file.out

Code saved in file freqg3.pl

```
#!/usr/bin/perl -w
use strict; use Getopt::Std;
our $opt_t; getopts('t:');
my @line; my @g3e; my @zpe; my @freqs; my @scaledfreqs;
my @energies; our $scale_factor=.89285; our $T=298.15;
my $R=8.314472; my $h=6.62608E-34; my $N=6.02214E23;
my $k=1.38066E-23; my $c=29979250000;
my $oneHalfRT=$R*$T/(2*$N*$h*$c); my $totalE=0;
my $totalEcor=0; my $zpecor=.8982; my $zpesum=1;
my $tempcorE=1; my $scaledzpe; my $electronicE;
my $tempcor; my $tempcorzpe; my $zpecorE; my $EnergyG3;
# Change value for G3X dervaties #
our $scale_factor=.89285;
my $z=$scale_factor;
# input options #
if ($opt_t) { $T=$opt_t;}
# finding Freqs and calculating vibration contributions #
while (<>) { if (/Frequencies/){ @line=split;
foreach (@line){ if (/\d+\.\d+/){ push @freqs, $_;
$_=$_*$scale_factor;
push @scaledfreqs, $_;
$_=$_/(exp($h*$c*$_/($k*$T))-1);
if (1) { if ($_ > $oneHalfRT){ $_=$oneHalfRT; }
push @energies, $_; }       }           }           }
# Finding ZPE and G3 energy #
if (/ZPE/){@zpe=split;
$zpecor=$zpe[1]; }
if (/G3\sEnergy/){ @g3e=split;
$EnergyG3="$g3e[2]";}    }
# Summing Contributions of each fequency #
foreach (@energies){ $totalE=$totalE+$_; }
# Calculating output data #
$totalEcor=($totalE*$N*$h*$c+3*$R*$T)/2625501;
$tempcorzpe=$totalEcor+$zpecor;
$tempcorE=$EnergyG3+$totalEcor+($R*$T/2625501);
# printing Data #
print "\n\ Scale Factor $scale_factor\n";
print "ZPE scale factor is $z\n";
print "G3 OK\n";
print "E(ZPE)\n";
print "E(Thermal)";
print "G3 298K\n";
print "$EnergyG3\n";
print "$zpecor\n";
print "$tempcorzpe\n";
print "$tempcorE\n";
```

2.3 Correcting W1 Jobs

User input

$ freqw1.pl –t 289.15 output_file.out

Code saved in file freqw1.pl

```
#!/usr/bin/perl -w
use strict; use Getopt::Std;
our $opt_t;
getopts('t:');
my @line; my @W1e; my @zpe; my @freqs;
my @scaledfreqs; my @energies;
our $scale_factor=.985; our $T=298.15;
my $R=8.314; my $h=6.62608E-34;
my $N=6.02214E23; my $k=1.38066E-23;
my $c=29979250000; my $oneHalfRT=$R*$T/(2*$N*$h*$c);
my $totalE=0; my $totalEcor=0; my $zpecor=.985;
my $zpesum=1; my $tempcorE=1;my $scaledzpe;
my $electronicE; my $tempcor; my $tempcorzpe;
my $zpecorE; my $EnergyW1;
# input options #
if ($opt_t) { $T=$opt_t;}
my $z=$scale_factor;
# finding Freqs #
while (<>) { if (/Frequencies/){ @line=split;
foreach (@line){ if (/\d+\.\d+/){ push @freqs, $_;
$_=$_*$scale_factor;
push @scaledfreqs, $_;
$_=$_/(exp($h*$c*$_/($k*$T))-1);
if (1) { if ($_ > $oneHalfRT){ $_=$oneHalfRT; }
push @energies, $_; } } }  }
if (/ZPE/){@zpe=split; $zpecor=$zpe[1]; }
if (/W1\s\s\sEnergy/){ @W1e=split;
$EnergyW1=$W1e[3];}   }
foreach (@energies){ $totalE=$totalE+$_; }
$totalEcor=($totalE*$N*$h*$c+3*$R*$T)/2625501;
$tempcorzpe=$totalEcor+$zpecor;
$tempcorE=$EnergyW1+$totalEcor+($R*$T/2625501);
# Printing output #
print "\n\ Scale Factor $scale_factor\n";
print "ZPE scale factor is $z\n";
print "W1 OK\n";
print "E(ZPE)\n";
print "E(Thermal)";
print "W1 298K\n";
print "$EnergyW1\n";
print "$zpecor\n";
print "$tempcorzpe\n";
print "$tempcorE\n";
```

Appendix 3

PERL Scripts for Predicting IR Spectra from Gaussian Output Files

This script numerically predicts a vibrational spectrum from the output of a Gaussian frequency calculation by generating a Loretzian function for each vibration and summing the individual functions to yield a composite spectrum. The user has input controls for the scale factor, range, linewidth and resolution of the spectra. The default for each variable is seen if parenthesis.

-p interval between predicted points (1 cm^{-1})
-w half width at half height (10)
-s vibrational scale factor (1)
-l starting point for predicted spectra (500 cm^{-1})
-h ending point for predicted spectra (4000 cm^{-1})

User input

$ spectra.pl <output_file.out> output_spectra.txt

Code saved in file spectra.pl

```
#!/usr/bin/perl -w
# input options #
use strict;
use Getopt::Std;
our $opt_p; our $opt_s; our $opt_l;
our $opt_w; our $opt_h;
getopts('p:s:l:w:h:');
my @line; my @lineint; my @intensity;
my @freqs; my @scaledfreqs; my @freqint;
our $scale_factor=1; our $l; our $d=1 ;
our $min=500; our $max=4000; our $w=10;
our $absorbcon; our $total_intensity; our $output;
if ($opt_p) { $d=$opt_p;}
if ($opt_s) { $scale_factor=$opt_s;}
if ($opt_w) { $w=$opt_w;}
if ($opt_l) {$min = $opt_l;}
if ($opt_h) {$max = $opt_h;}
# finding frequencies
while (<>) { if (/Frequencies/){ @line=split;
foreach (@line){if (/\d+\.\d+/){push @freqs, $_;
$_=$_*$scale_factor; push @scaledfreqs, $_; } } }
# finding intensities #
if (/Inten/){ @lineint=split;
foreach (@lineint){ if (/\d+\.\d+/){
push @intensity, $_;    }       }       }           }
# printing list of frequencies and intensities #
for (my $j=0;$j<=$#freqs;$j++) {
print  "\t$scaledfreqs[$j]\t$intensity[$j]\n";}
```

```
# Calculating at regular intervals #
for ($l=$min ; $l<= $max ; $l += $d) {$total_intensity = 0;
for (my $j=0;$j<$#freqs;$j++) {
$absorbcon = $intensity[$j]*($w**2/(($l-
($scaledfreqs[$j]))**2)+$w**2)) ;
$total_intensity = $absorbcon + $total_intensity;
$output = sprintf("%.1f",$total_intensity ); }
print "\t$l\t$output\n"; }
```

Appendix 4
VBScript for Control of Laser Vision OPO from Omega

In order for script to run properly NETCOMOCX.OCX must be installed.
Sleep.exe should be present in script folder and check that com port is correctly assigned .

```
Sub main
	Dim Step_num
	Dim Scans
	Dim oDoc
	Dim file_name
	Dim wavelength
	Dim int_wave
	Dim Step_size
	Dim Sfname
	Dim bProg
	Dim xmlname
	Dim path
	Dim com
	Dim oApp
	Dim Reg
	Dim bufferdata
	Dim strBuffer
	Dim i, x
	Dim yag
	Dim yagwavelength
	Dim laserdelay
	yag=9398.4

Const MY_COMPUTER = &H11&
Const WINDOW_HANDLE = 0
Const OPTIONS = 0
Const comNone = 0
Const comInputModeText = 0
Const comInputModeBinary = 1

'collects input parameters
	file_name = InputBox("What is the File Name")
	int_wave = InputBox("What wavelengths would you like to start")
	Step_size =InputBox("Step Size")
	Step_num = InputBox("Number of Steps")
	Scans = inputbox("Number of Scans per Spectra")

'destination folder script
```

```
Set objShell = CreateObject("Shell.Application")
Set objFolder = objShell.Namespace(MY_COMPUTER)
Set objFolderItem = objFolder.Self
strPath = objFolderItem.Path

Set objShell = CreateObject("Shell.Application")
Set objFolder = objShell.BrowseForFolder _
   (WINDOW_HANDLE, "Select a folder:", OPTIONS, strPath)
Set objFolderItem = objFolder.Self
path = objFolderItem.Path 'selected path

Set com = CreateObject("NETCommOCX.NETComm")
Set oApp = Omega.ExternalAppControl
Set Reg = New RegExp
        Reg.Pattern="DONE"

For N=1 to Step_num
        wavelength = int_wave + (N-1) * Step_size              'steps wave lengths count
                yagwavelength = wavelength + yag                'laser input
        Sfname =  path & "\" & file_name & wavelength & "matt.trans"  'sets file name
        xmlname =  path & "\" & file_name & wavelength & "matt.xml" 'sets xml name

        com.CommPort = 2
        com.Settings = "9600,N,8,1"
        com.RThreshold = 1 'Generates an event after this many characters
        com.InputLen = 0 '0 Reads the entire buffer
        com.Handshaking = comNone
        com.DTREnable = False
        com.RTSEnable = False
        com.InputMode = comInputModeText
        com.PortOpen = True
        com.Output = "GOTO " & yagwavelength & vbCrLf

        For i=1 To 2 Step 1 '10 sec delay before time out
        strBuffer = ""
        strBuffer = com.InputData
        bufferdata= strBuffer + bufferdata
   oApp.RunApplication "C:\Program Files\Omega8\Scripts\sleep.exe" 'call delay exe
to allow for spacing out signal
   oApp.WaitForCompletion 5

        Next
com.PortOpen = False 'Close Comm port
If i = 99 Then Exit For
bProg = False      'Tells omega not transfer setup file
```

```
If N=1 Then bProg = True 'transfer setup file on first scan
Set oDoc = Omega.Acquire.AcquireTransient ( Scans , bProg, True )
'               saves trans file
        brtn=Omega.FileIO.WriteTransientFile( Sfname , wavelength )
'               saves M/I table as XML for later searching
xmlname =  path & "\" & file_name & wavelength & "matt.xml"
Omega.FileIO.MakeFTDocOfTransient.MassIntensityTable.WriteXMLFile( xmlname )

        Next
End Sub
```